High temperature thermodynamic studies on the transuranium oxides and their solid solutions

Proefschrift

ter verkrijging van de graad van doctor
aan de Technische Universiteit Delft,
op gezag van de Rector Magnificus Prof.ir. K.C.A.M. Luyben,
voorzitter van het College voor Promoties,
in het openbaar te verdedigen
op woensdag 15 juni 2011 om 10.00 uur
door

Petronela GOTCU-FREIS

Magister in de chemie van de Faculteit Chemie
van de „Alexandru Ioan Cuza" Universiteit van Iaşi, Roemenië
geboren te Iaşi, Roemenië

Dit proefschrift is goedgekeurd door de promotoren:
Prof.dr. H.Th. Wolterbeek
Prof.dr. R.J.M. Konings

Samenstelling promotiecommissie:

Rector Magnificus,	voorzitter
Prof.dr. H.Th. Wolterbeek,	Technische Universiteit Delft, promotor
Prof.dr. R.J.M. Konings,	Technische Universiteit Delft, promotor
Prof.dr.ir. A. Verkooijen,	Technische Universiteit Delft
Prof.dr.ir. E. Bruck,	Technische Universiteit Delft
Prof.dr. K. Hack,	RWTH Aachen University, Duitsland
Prof.dr. D. Haas,	VU Brussels, België
Dr. Ch. Guéneau,	CEA Saclay, Frankrijk
Prof.dr.ir. C. Pappas,	Technische Universiteit Delft, reservelid

The research described in this thesis was performed within a cooperation of the Institute of Transuranium Elements of the Joint Research Centre (JRC) of the European Commission, P.O. Box 2340, 76125 Karlsruhe, Germany and the Section of Radiation and Isotopes for Health of the Department of Radiation, Radionuclides and Reactors, Faculty of Applied Sciences, Delft University of Technology, Melkeweg 15, 2629 JB Delft, The Netherlands.

ISBN 978-1-60750-779-6
Keywords: actinide oxides, americium, heat capacity, high temperature mass spectrometry, Knudsen cell, neptunium, phase diagram, plutonium, thermodynamic modelling, vapour pressure.

Published and distributed by IOS Press under the imprint Delft University Press Publisher
IOS Press
Nieuwe Hemweg 6b
1013 BG Amsterdam
The Netherlands
tel: +31-20-688 3355
fax: +31-20-687 0019
email: info@iospress.nl
www.iospress.nl
www.dupress.nl

PRINTED IN THE NETHERLANDS

High temperature thermodynamic studies on the transuranium oxides and their solid solutions

Contents

Chapter 1

Introduction

The growing demand for energy supply worldwide and the necessity to reduce emission of the greenhouse gases led to a renewed interest into the renewal of nuclear energy in the last years. Due to its low contribution to the greenhouse effect, nuclear power is a suitable alternative to fossile fuels for electricity production. However, studies have shown that the limited resources of economically accessible fissile material on earth used nowadays in thermal spectrum reactors, would be enough for a maximum 100 years of operation (static range) [1]. Furthermore, thermal reactors have a limited capability to burn minor actinides (MAs: Np, Am, Cm, formed by neutron capture under irradiation), the primary contributors to the long term radiotoxicity of the spent fuel. Although the MAs blended with plutonium isotopes (which all constitute the so-called transuranium elements) make up only about 1% of the spent fuel, they represent the main source of today's nuclear waste problem. Currently, two waste management options are available: either the spent fuel is conditioned for the final storage (once-through then out fuel cycle), or it is recycled to extract the re-usable materials like uranium and plutonium (recycling or reprocessing fuel cycle) and all remaining materials are vitrified for storage.

In order to minimise the radiotoxic inventory, partitioning and transmutation has been proposed as a third option: long-lived minor actinides are separated (partitioned) from the spent fuel and then fissioned (transmuted) in order to produce short-lived fission products. The time during which the material remains hazardous can be considerably reduced if the plutonium and MAs could be removed from the spent fuel [2]. However, the impact of removing only plutonium from the spent fuel is not enough to decrease the radiotoxicity on an acceptable timescale (< 1000 years) [3]. Therefore the MAs recovering process is the first step in actinide recycling. In the next step, MAs need to be destroyed by fission. Transmutation of minor actinides is foreseen to be performed preferably in fast neutron systems: fast nuclear reactors (FNR, where the fission reaction is induced by fast neutrons), which can operate as breeders or burners, or Accelerator-Driven Systems (ADS). This can be done by incorporating small amounts of MAs (up to 5%) in uranium plutonium mixed oxide fuels, or

larger amounts in MA-bearing blankets (e.g. $(U,Am)O_{2-x}$) or dedicated transmutation fuels or special targets (e.g. $(Pu,Am)O_{2-x}$ in MgO or Mo matrices).

Historically, the first fast breeder reactors existed since the early 1950s. These facilities used metallic fuels with a high heavy-metal density to achieve optimal neutronic performance for breeding. Later, the high swelling rates led engineers to use mixed uranium and plutonium oxide $(U,Pu)O_2$ which became the reference fuel for fast reactors worldwide. The favourable physical properties especially the high melting point (which together with the thermal conductivity give the margin between operating and melting temperature) and the good chemical stability were the criteria which triggered oxides into the most studied and developed fuels.

Nowadays there are only few fast breeding reactors used for electricity production (e.g. BN-600 built in Russia). Most of the reactors of this type currently under operation are either prototypes, such as Monju in Japan or BN-600 in Russia, or test reactors, such as Joyo in Japan, FBTR in India or BOR-60 in Russia.

In order to improve all the key aspects of nuclear power generation such as safety, economics, sustainability and availability, the Generation IV International Forum [4] proposed six reactor types for further research and evaluation. Among them, three systems are fast reactors: Gas Cooled Fast Reactor (GFR), Sodium cooled Fast Reactor (SFR) and Lead cooled Fast Reactor (LFR). However, their designs are generally not expected to be available for commercial construction before 2030.

Most fast breeder designs use fuel in the form of fuel pins. A fuel pin is a long cylinder (1 to 3 m long, 5 to 10 mm diameter), clad in a steel tube (~0.4 to 0.6 mm thick) and closed at both ends by plugs welded in identical steel [5]. The oxide fissile column is a stack of pressed and sintered pellets with an outer diameter slightly smaller than the inner diameter of the cladding, providing a radial gap between the fuel and cladding. The cladding is the first safety barrier between the highly radioactive inventory and the coolant and it is intended to keep its integrity during the irradiation process.

The power density in a fast breeder reactor, such as the SFR, is much higher than in a conventional light water reactor. Thus, compared to the

conventional reactors, a fast reactor fuel pin will experience a much higher temperature, above 2300 K in the centre, and a steep radial temperature gradient. This occurs especially during the first phase of irradiation when the fuel cladding gap is still open and the fuel structure is not modified. During irradiation, the fuel material suffers significant structure modifications also called fuel restructuring. Due to the thermal expansion installed in the fuel pin its outer radius increases and thus, the pellet cladding gap is minimised. The strong thermal stress induced by the temperature gradient leads to cracking of the pellet into several fragments. Post-irradiation examinations (PIE) revealed both radial and circumferential cracks, and particularly a central void present in the centre of the initially solid pellet (Figure 1). In fact, typical effects are the three distinct radial zones in the fuel [6-9]: the fuel with original microstructure, adjacent to the cladding, for which the temperature is too low to cause major restructuring, followed by the mid radius region with equiaxed grains, and the large columnar grains region next to the central void (Figure 1).

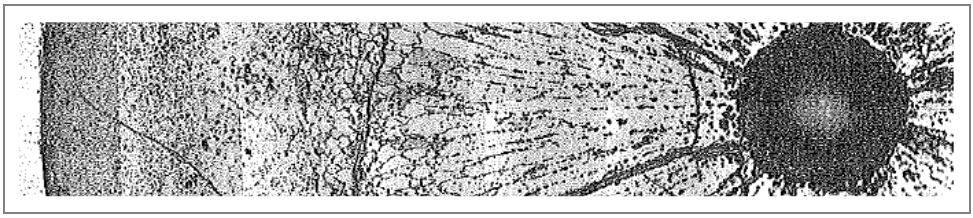

Figure 1. Photomosaic section of a mixed oxide fuel pellet showing the fuel restructuring after irradiation performed in Dounreay Fast Reactor (DS 1 experiment). @European Atomic Energy Communities [1968], reproduced with permission.

It has been shown that the restructuring is related to the redistribution of the porosity, initially present in the fuel pellet to accommodate for fission product swelling [10]. The pores take the shape of disks, therefore called lenticular pores, with their axis oriented in the direction of the thermal gradient. Between the hot and cold walls of a lenticular pore, a thermal gradient occurs, that is much higher than the gradient in the surrounding fuel. The pressure of the fuel vapour in equilibrium with the oxide is higher on the hot wall of the lenticular pore than on its cold wall. Therefore, pores migrate toward the centre part of the pellet, up the temperature gradient by a complex mechanism known as vaporisation-condensation: the matter vaporised at the hot wall would condense on the cold wall.

All the lenticular pores accumulate in the centre of the pellet and lead to the formation of the central void. Furthermore on their way towards the centre of the pellet, the lenticular pores destroy the initial structure of the fuel and leave behind new formed grains, the columnar grains. These grains form usually at temperatures above 2100 K. Metallographic pictures have revealed that the grain boundaries were marked by a string of small bubbles released at the periphery of the lenticular pores during their migration [5,9] (Figure 2). Below this temperature the equiaxed grain growth region is formed, as a result of the repeated growth of the fine grains in the initial fuel, until a limiting equilibrium size is attained. Generally, the dimensions of the columnar region and the diameter of the central hole increases with temperature. A short irradiation experiment on (U,Pu) mixed oxide containing 3-5% Am in the Joyo fast reactor showed the formation of the central void after ten minutes irradiation at full power [11,12].

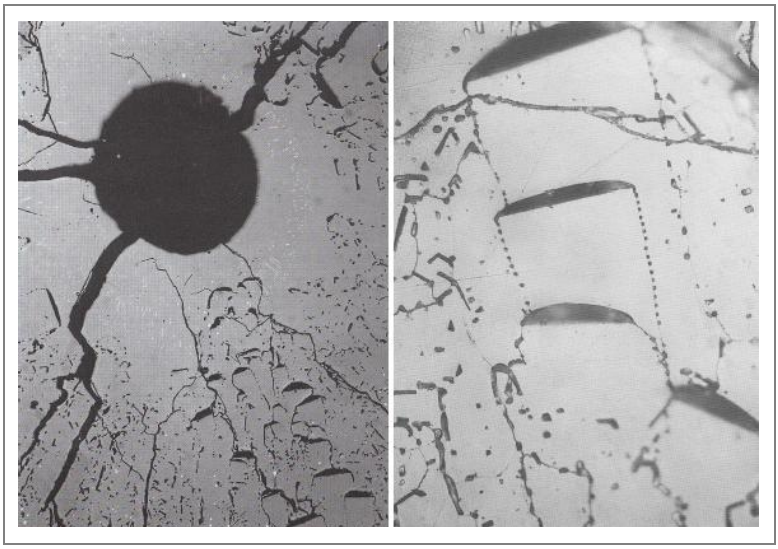

Figure 2. Lenticular pores observed in irradiated fast reactor mixed oxide fuel. @European Atomic Energy Communities [1968], reproduced with permission.

As a result of the thermal gradient in the fuel pin, the restructuring is accompanied by a radial migration of certain fuel constituents. Fast reactor fuel is usually hypostoichiometric at the beginning of irradiation. At increased power, oxygen redistributes and migrates radially along the

thermal gradient. As a result, the composition of the oxide the periphery of the pellet becomes close to stoichiometric composition and the oxide region around the central void, where the temperature reaches high values, shifts to lower hypostoichiometry.

In view of this, the oxygen redistribution influences the thermal conductivity which is improved at the periphery of the fuel. The matter redistribution in the fuel pin under thermal gradient has been described by processes of thermal diffusion and/or vapour transport [13]. The experimental redistribution observed recently in the post-irradiation examinations of the (U,Pu) mixed fuel with low americium content [11] was analysed using the models for pore migration by the two processes and a good agreement was found for the pore migration model [12]. It has been suggested that the vapour transported to the colder side of the lenticular pore is enriched in uranium and the hotter side in plutonium and americium. Therefore the oxide area around the central hole will have an increased plutonium and americium concentration.

However, the experience with MAs fuel for fast reactors is limited. The SUPERFACT irradiation in the Phénix reactor (1986-1988) demonstrated the feasibility of MAs (Am or Np) incorporation into the $(U,Pu)O_2$ fuels up to 2%. The impact of larger amounts of MAs in the fuel material (blankets, transmutation fuels or special targets) has to be evaluated in the frame of the reactor safety and fuel performance issues. The behaviour of the high MAs content fuel is very complex due to the helium production and the fission gas release. This will affect the restructuring and redistribution of the MAs. Lately the inert matrix concepts were explored intensively. The increased concentration of the MAs in the fuel material is necessary to be evaluated also from the perspective of the influence of the matrix material under irradiation. Studies are ongoing in order to develop such suitable fuels for transmutation.

In order to describe such high temperature processes and to predict critical behaviour at even higher temperatures, which could occur during off-normal conditions, reliable thermodynamic data for the solid and gaseous phases are fundamental. With respect to the mass transport phenomenon explained by vaporisation-condensation processes a highly relevant property of the reactor fuel is the vapour pressure. Another important property that determines how much heat can be accumulated in a material

before it reaches a defined critical temperature value is the heat capacity. Furthermore the knowledge of the temperature dependence of vapour pressure and heat capacity is essential in calculation of the thermodynamic functions in order to predict stable phases in any multi-component system.

Thesis outline

The aim of the research described in this thesis is to present the high temperature thermodynamic studies of the transuranium oxides and their solid solutions. For this purpose vapour pressure measurements at high temperatures have been performed on actinide oxide samples using a Knudsen cell coupled with a mass spectrometer.

The systems described in this thesis focused on the binaries Np-O, Pu-O, Am-O and their ternary solid solutions. Data on total vapour pressure was obtained above several samples prepared in order to correspond to different phase regions of interest. The partial pressures of gaseous species involved in the vaporisation process were assessed from ionisation efficiency measurements recorded at constant temperature. Different experimental conditions were applied for samples in order to derive the solid-gas phase relations. Additionally, heat capacity data on neptunium dioxide was derived using drop calorimetry.

Each chapter is dedicated to a systematic study on actinide oxides and constitutes of a paper accepted or already published in a peer reviewed scientific journal.

Chapters 2 and 3 present investigations on two of the most important thermophysical properties on NpO_2, the vapour pressure and heat capacity high temperature data. The mass spectrometric measurements have been also performed on samples containing very small amounts of neptunium. In these samples, americium dioxide and plutonium-americium mixed oxide, neptunium was produced by alpha-decay from americium and the results were discussed in the view of extreme dilution of neptunium in the samples.

Chapter 4 describes the results of a new study on the vaporisation behaviour and phase relations in the Pu-O system. Plutonium oxide samples corresponding to different phase fields were prepared and

measured. The results were discussed in the frame of the available literature data with regard to the controversy about the congruent partial pressures above plutonia at high temperature.

In Chapter 5 it is reported the first experimental results for the vapour pressure of pure americium oxide samples. These results are jointly discussed with the literature data limited to studies of plutonium dioxide containing small amounts of americium. Additional information is included from measurements performed on a mixed dioxide sample of plutonium containing 6.1 wt% americium.

Chapter 6 presents the variation of the total pressure of plutonium and americium bearing species over the $(Pu,Am)O_2$ solid solutions. Mass spectrometric measurements were performed on a sample with an initial Am content of 24.4% in order to evaluate the congruent vapour composition. The results were combined with the assessment of the Pu-Am-O system using the CALPHAD method. In this chapter a section is dedicated to the description of the ternary model, for which the data on the binaries have been evaluated and assessed. A consistent thermodynamic description of the ternary was obtained which allow calculating the ternary phase diagram, the oxygen potential for $(Pu,Am)O_{2\pm x}$ and the equilibrium partial vapour pressures.

Chapter 7 deals with the mass spectrometric investigations of candidate fuels and targets for transmutation of MAs. This chapter made use of the results obtained on the pure plutonium oxide and americium oxide samples presented in the previous chapters and appeals the technological use of the study in this thesis. The thermal stability and high temperature behaviour of zirconia-based solid solution, MgO-based CERamic-CERamic (CERCER) and molybdenum-based CERamic-METalic (CERMET) fuels containing Am and/or Pu in various concentrations was discussed based on their vapour pressure results and vaporisation behaviour. The samples described here have all been prepared as part of fuel irradiation campaigns in the Phénix fast neutron reactor in France and in the High Flux Reactor in the Netherlands.

This thesis concludes with a chapter summarising the most important findings.

References

[1] World Nuclear Association public information. Available online at http://www.world-nuclear.org/.
[2] W.M. Stacey, Nuclear Reactor Physics. John Wiley & Sons, 2001.
[3] International Atomic Energy Agency, Status of Minor Actinide Fuel Development, No. NF-T-4.6, Vienna 2009.
[4] U.S. DOE Nuclear Energy Research Advisory Committee and the Generation IV International Forum. A technology roadmap for Generation IV nuclear energy systems, December 2002. Available online at http://gif.inel.gov/roadmap/.
[5] The nuclear fuel of pressurised water reactors and fast reactors design and behaviour, H. Bailly, D. Menessier, C. Prunier (Eds.) Paris, France: Lavoisier Publishing, 1999.
[6] D.R. de Halas, G.R. Horn, J. Nucl. Mater. 2 (1963) 207.
[7] D.R. O'Boyle, F.L. Brown, J.E. Sanecki, J. Nucl. Mater. 29 (1969) 27.
[8] D.R. Olander, Fundamental aspects of nuclear reactor fuel elements, Technical Information Center, Energy Research and Development Administration, Oak Ridge, Tenn. and Springfield, Va., 1976.
[9] R.J.M. Konings, T. Wiss, C. Guéneau, Chemistry of the Actinide and Transactinide Elements, Chapter 34, L.R. Morss, N.M. Edelstein, J. Fuger (Eds), Springer, The Netherlands, 2011.
[10] W. J. Lackley, F. J. Homan, A. R. Olsen, Nucl. Technol. 16 (1972) 120.
[11] K. Tanaka, S. Miwa, I. Sato, T. Hirosawa, H. Obayashi, S.I. Yoshimochi, K. Tanaka, J. Nucl. Mater. 385 (2009) 407.
[12] K. Maeda, S. Sasaki, M. Kato, Y. Kihara, J. Nucl. Mater. 389 (2009) 78.
[13] M. Bober, G. Schumacher in: Advances in Nuclear Science and Technology, Vol. 7, Academic Press, New York, 1973, p. 495.

Chapter 2

(Solid+gas) equilibrium studies for neptunium dioxide

Abstract

*Knudsen cell high temperature mass spectrometric measurements have been performed on neptunium dioxide. Several samples have been analysed for vaporisation in vacuum and oxidative conditions and different behaviours have been observed. The results for the vapour pressure of pure neptunium dioxide samples are discussed together with the data on americium dioxide and plutonium-americium mixed oxide samples containing very small amounts of neptunium, in which neptunium is produced by alpha-decay from americium. In the view of extreme dilution of neptunium in the sample, Raoult's law has been applied. The ionisation efficiency curves for Np^+, NpO^+ and NpO_2^+ were recorded for constant temperature. The dissociative ionisation contribution was evaluated with respect to the composition of the gaseous phase which under Knudsen conditions is in equilibrium with the condensed phase.**

*This chapter is reprinted with kind permission of Elsevier: "(Solid+gas) equilibrium studies for neptunium dioxide. P. Gotcu-Freis, J.-Y. Colle, J.-P. Hiernaut, R.J.M. Konings. The Journal of Chemical Thermodynamics 43 (2011) 492-498".

2.1 Introduction

As member of the minor actinide series, ^{237}Np is one of the important long lived isotopes. It is formed during irradiation in conventional nuclear fuel, predominantly from ^{235}U by nuclear reactions. During storage its concentration further increases from the alpha-decay of ^{241}Am ($t_{1/2}$ = 432.2 years). In order to reduce the high level radiotoxicity of the spent fuel, ^{237}Np can be partitioned and incorporated in mixed oxide fuel, e.g. (U,Pu,Np)O_2. As a result, transmutation of the advanced minor actinides bearing fuels in next generation nuclear reactors is foreseen to decrease the long term environmental burden. Therefore better knowledge of the thermophysical properties of advanced fuel materials containing neptunium is required for analysing and predicting their behaviour under normal operational and accidental conditions. Mass spectrometric data are of particular interest to determine the thermodynamic stability of neptunium bearing mixed oxides at high temperature phases.

The actinide oxides show a complex vaporisation behaviour that is reasonably well characterised for the (uranium+oxygen) system (see e.g. the assessment by Guéneau *et al.* [1]) but poorly for the oxides of the transuranium elements. The vapour pressure data of neptunium dioxide are restricted to an experimental determination by means of the Knudsen effusion method combined with collection on platinum targets [2]. In the same study appearance potential measurements were performed using mass spectrometry. Recent results on the ionisation energies for the neptunium oxygen gaseous binary species were reported by Gibson *et al.* [3] using the electron-transfer bracketing technique employing Fourier transform ion cyclotron resonance mass spectrometry (FTICR MS). The latter study presented a larger value for the ionisation energy of NpO_2 than the one found by Ackermann *et al.* [2], which is in agreement with the ionisation energy trends for the early actinide dioxides. Estimations of the values for the dissociative ionisation processes have been made from the same kind of FTICR mass spectrometric measurements on atomic and molecular actinide ions and neutrals [4-5].

High temperature mass spectrometric measurements of the vapour pressure of neptunium dioxide are reported in this study. A Knudsen cell mass spectrometer assembly was used to analyse the behaviour of the

samples in vacuum and in oxidative conditions. Results of vapour pressure data for pure neptunium dioxide samples and mixed oxide samples with low content of neptunium will be discussed. In addition, ionisation efficiency curves for Np^+, NpO^+ and NpO_2^+ were recorded to provide insight into the dissociative ionisation processes and the composition of the gaseous phase, which under Knudsen conditions, is in equilibrium with the condensed phase.

2.2 Experimental method

2.2.1 Sample preparation

For the present study NpO_2 samples in the form of disks were prepared by pressing and sintering neptunium dioxide powder, which was fired in air. The ICP-MS analysis of the initial powder showed that the mass fraction of impurities in the sample was less than 0.0013; the highest amount of impurity was represented by P (with a mass fraction of $504 \cdot 10^{-6}$) followed by W (with a mass fraction of $279 \cdot 10^{-6}$), Pb (with a mass fraction of $152 \cdot 10^{-6}$), the rest of the impurities were found with a mass fraction less than $100 \cdot 10^{-6}$. Alpha spectroscopy analysis showed that the ^{237}Np to (^{241}Am+^{238}Pu) mass ratio is in the order of 50,400. The uncertainties of the two investigation methods are the total combined uncertainties with a coverage factor of 2. The sintering was performed as described in a recent publication [6] under flowing air at about 300 $cm^3 \cdot min^{-1}$ at T = 1723 K for 7.5 h. The X-ray diffraction analysis with Cu Kα radiation performed on the disks after sintering indicated a single fluorite-type phase. The lattice parameter of the NpO_2 sample was found 0.5434 ± 0.0001 nm, consistent with the results from the earlier studies [7-12].

Additionally measurements were made on a of few-years old pure americium dioxide sample and on two plutonium-americium mixed oxides samples ($Pu_{0.80}Am_{0.20}O_{2-x}$ and $Pu_{0.76}Am_{0.24}O_{2-x}$) to assess the vapour pressure of neptunium oxide produced by alpha-decay of americium. The amount of neptunium accumulated in these samples by alpha-decay of ^{241}Am was calculated from the initial analysis reports as 5.65 wt% for pure americium dioxide, and (0.63 and 0.94) wt%, respectively, for the above mentioned mixed oxide samples at the time of the measurement. The pure americium dioxide sample was in form of powder which was prior to the

measurements fired for few hours in air to $AmO_{2.00}$ at about 1200 K as was previously reported by Sari and Zamorani [13]. The mixed oxide samples were fabricated by a combination of external gelation, also known as gel supported precipitation (GSP), and infiltration routes, followed by compaction and sintering under Ar/H_2 atmosphere, at 1873 K [14]. An americium nitrate solution with a concentration of (300 ± 1) $g{\cdot}Am{\cdot}dm^{-3}$ has been used for the infiltration step. After infiltration, the obtained spheres were dried at room temperature overnight and thereafter calcined under an air atmosphere to convert the nitrate into oxide. These two last procedures were repeated to obtain the desired concentrations. The final Am content (in wt%) was determined by gravimetric analysis before and after the infiltration step, with an absolute accuracy of about 1%. The O/Am ratio of americium oxide samples is expected to be close to 2.0, the O/(Pu+Am) ratio of the mixed oxide samples is estimated to be between 1.75 and 1.85, typical for these sintering conditions. It should, however, be noted that these values are not representative for the temperatures at which the mass spectrometric measurements in this study have been made.

2.2.2 Mass spectrometric measurements

The experimental facility consists of a Knudsen cell coupled with a mass spectrometer designed to study radioactive materials (actinides compounds and irradiated material) at high temperature, and has been built in a 5 cm thick lead shielded glove box. The mass spectrometer is a quadrupole QMG422 from Pfeiffer Vacuum GmbH which offers a mass range of (1 to 512) amu. The mass filter is made of molybdenum rods of 8 mm in diameter and 200 mm in length. It is equipped with a cross beam electron bombardment ion source, an axial Faraday cup and a SEM (Secondary Electron Multiplier) located at 90° to the filter axis. The sintered samples {ca. (30 to 50) mg} were loaded in the cell which is centred in a high temperature furnace made of a tungsten coil-heating element surrounded by seven cylindrical thermal shields. The whole system is placed in a high vacuum chamber.

The behaviour of the NpO_2 samples was studied under different conditions: mass spectrometric measurements have been conducted in vacuum using a tungsten cell or in oxidative conditions using a ThO_2 cell, having a small

orifice at the bottom for the oxygen gas inlet. Compatibility tests between actinide oxides and several cell materials proposed for the oxidative condition measurements like Al_2O_3, ZrO_2, MgO, or ThO_2, revealed ThO_2 as the best material with non-reactive properties. Moreover ThO_2 can be used up to very high temperature; has a pre-melting transition at 3090 K [15] and a melting point of 3663 K. A detailed description of the cell is given in another publication [16]. Pure oxygen gas (mass fraction purity 0.99999) was introduced in the cell and the gas flow was controlled. In order to avoid the direct contact between the solid dioxide sample and the tungsten cell material, because possible reactions at high temperature are suspected [17,18], iridium foils were placed at the bottom of the cells. During the measurements the temperature was increased at 10 $K \cdot min^{-1}$ up to about (2200 to 2300) K for the pure NpO_2 samples. One of the dioxide samples was measured and analysed at 2500 K. The americium dioxide and plutonium-americium mixed oxide samples were analysed at higher temperature ranges up to 2400 K and only *in vacuo* non-oxidative conditions.

The Knudsen cell mass spectrometer assembly was calibrated by vaporising a known quantity of silver together with the sample, as described in another publication which we refer to for details [16]. Silver was used as a reference material because it is a metal with a well-known vapour pressure. It is relatively inert in this system and was vaporised completely at about 1500 K, before the sample evaporation started. By integration of the known effused mass of silver provided by the Hertz-Knudsen equation [19], a calibration factor is obtained, which is then applied to calculate the vapour pressure of the required species.

The temperature of the Knudsen cell assembly was calibrated by measurement of the melting points of standard materials (Zn, Cu, Fe, Pt, Al_2O_3). Temperature is a very important parameter in mass spectrometry as the vapour pressure function is directly dependant on it according to the basic mass spectrometry relation [19,20]:

$$P_i = I_i^+ \cdot T / K_i , \qquad (1)$$

where P_i is the vapour pressure of species i, T is the temperature at which the pressure is calculated, I_i^+ and K_i are the intensity of the molecular beam and the calibration factor, respectively, for a species i. The

calibration factor contains an instrumental term, which is independent of species i, and a term which is dependent of species i which includes the ionisation cross section, the ionisation potential, the efficiency of the secondary electron multiplier and the isotopic weight of species i. The measurements have been carried out using an ionisation energy of 40 eV. The atomic ionisation cross sections for the studied species were calculated using the program SIGMA [19,21,22]. For molecular cross sections calculations the additive postulate proposed by Otvos and Stevenson [23] was used.

Ionisation efficiency curves were measured at a selected temperature at which the signal of the oxide ions was sufficiently high. During the scan the energy of ionising electrons was increased stepwise by 0.5 eV while the temperature was kept constant. The offset between the applied cathodic voltage and the effective electron energy spectrum was solved as described in the previous study [24].

The first ionisation potentials of silver and a known gas composition of krypton, helium, argon, neon, and xenon have been taken as standards. The energy range covered by the calibration was from (7.5 to 24.5) eV. The results showed a good linear dependence (the regression coefficient is equal to 0.998) for extrapolation of the scale up to 40 eV. The errors quoted in this paper are 1σ standard deviations. The calibration does not apply to the measurements in an oxygen flow for which an internal calibration was made.

2.3. Experimental results and discussion

2.3.1 Ionisation efficiency curves

The mass spectrometric measurements of different neptunium oxide samples revealed the presence of the NpO_2^+, NpO^+ and Np^+ ions in the vapour. Measurements of the ionisation efficiencies were made for different isotherms for which, under Knudsen conditions, the gaseous phase is in equilibrium with the condensed phase. The following reactions must be considered at the temperatures of the measurements:

$$NpO_2(cr) = NpO_2(g), \quad (2)$$

$$NpO_2(cr) = NpO_{2-x}(g) + x/2\ O_2(g), \quad (3)$$

$$2\ NpO_{2-x}(cr) = NpO(g) + NpO_{2-x+y}(cr) + (1-x-y)/2\ O_2(g), \quad (4)$$

$$NpO(g) = Np(g) + 1/2\ O_2(g). \quad (5)$$

Figure 1 shows the mass spectrometric signals of the NpO_2^+, NpO^+ and Np^+ ions as a function of the energy of the ionising electrons. From these results the appearance and dissociation potentials of the key molecular species were determined.

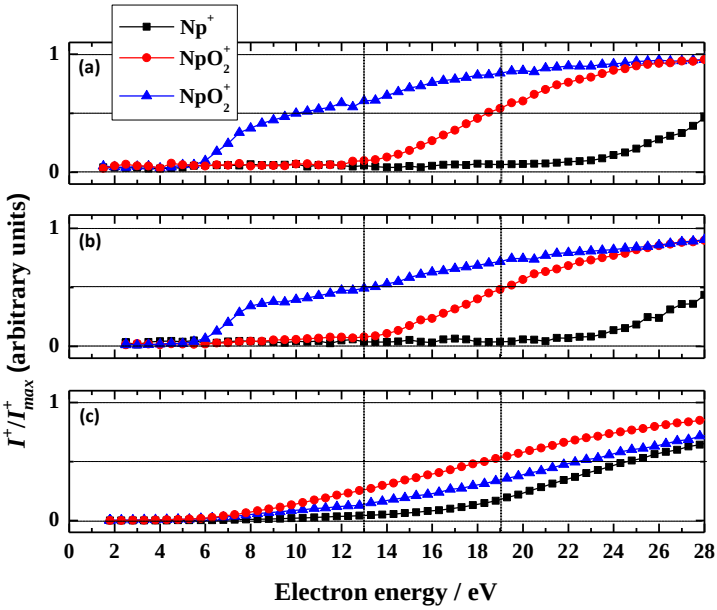

Figure 1. Ionisation efficiency curves of (■) Np^+, (●) NpO^+ and (▲) NpO_2^+ from molecules coming from neptunium dioxide sample. **(a)** Measurements on NpO_2 sample in oxidative conditions at T = 2200 K. **(b)** Measurements on NpO_2 sample under vacuum at T = 2260 K. **(c)** Measurements on reduced NpO_2 sample at T = 2500 K.

The appearance potential is defined as the minimum energy required to produce a given ion and its accompanying neutral fragments from a given molecule, ion or radical [25], considering both ionisation and dissociation processes. When only ionisation occurs, the appearance potential is called the ionisation potential, essentially given by the minimum energy required to remove an electron from the neutral molecules, atoms or radicals. The

values obtained in this study are given in Tables 1 and 2 together with available literature data. Good agreement is generally found especially for the dissociative ionisation processes. The appearance potential values of NpO and NpO_2 species found in this study are (6.0 and 5.6) eV respectively. These values are in good agreement with those reported by Ackermann *et al.* [2] who carried out a similar electron impact study by high temperature mass spectrometric measurements. Our value for the appearance potential of NpO_2 is slightly lower than the one given by Gibson *et al.* [3,5] measured by electron-transfer bracketing technique.

Table 1. Ionisation energy (IE) values for neptunium, neptunium monoxide and dioxide: comparison between this work and existing literature data.

Species	IE (this work); eV	IE (literature); eV
Np	6.1 ± 0.3	6.2 [29]
NpO	6.0 ± 0.3	5.5 [2]; 6.1 ± 0.2 [5]
NpO_2	5.6 ± 0.3	5 [2]; 6.3 ± 0.2 [4-5]

Table 2. Dissociation energy (DE) values for NpO_2 and NpO: comparison between this work and estimated values from literature. All the results are given in eV.

Dissociative ionisation process	DE (this work); eV	DE (literature); eV
$NpO_2+e^-\rightarrow NpO^+ + O + 2\cdot e^-$	12.5 ± 0.6	12.3 ± 0.7 [4-5]
$NpO_2+e^-\rightarrow Np^+ + 2\cdot O + 2\cdot e^-$	20.5 ± 1	20.3 ± 0.8 [4-5]
$NpO+e^-\rightarrow Np^+ + O + 2\cdot e^-$	13.0 ± 0.6	14.1 ± 0.5 [4-5]

Gibson *et al.* [3] extended the study of the ionisation energy of NpO_2 to the lighter actinide oxide species. Earlier high temperature electron impact measurements on uranium oxide samples [24] yielded lower values for the first ionisation energy of uranium monoxide and dioxide in comparison to the spectroscopic studies by Han *et al.* [26,27]. Possible explanations for the low value for the first ionisation energy of uranium dioxide by electron ionisation mass spectrometric method are discussed by Gagliardi *et al.* [28], who performed *ab initio* calculations. In the latter work [28] it has been suggested that the electron ionisation technique involves population

of the neutral excited states which would result in a lower ionisation appearance threshold than for the ground state NpO_2.

In this work, the ionisation efficiency curves for Np^+, NpO^+ and NpO_2^+ were primarily recorded to provide insight of the dissociative ionisation processes and the true composition of the gaseous phase. Figure 1(a) shows the ionisation efficiency curves measured on neptunium dioxide sample in oxidative conditions at 2200 K. Neptunium dioxide is the only gaseous species observed. Neptunium monoxide appears as a product of the dissociation process of the dioxide at about 12.5 eV whereas neptunium ion comes from the dissociation of the dioxide at about 20.5 eV.

Figure 1(b) shows measurements of neptunium dioxide in vacuum at 2260 K. Neptunium dioxide is still the major species in the vapour, but also neptunium monoxide is observed at a lower energy of the ionising electrons, which indicates a slight reduction of the initial sample. Amounts of metallic neptunium ion are noticeable only from the dissociation process of the dioxide. At 12 eV, NpO_2^+ is more than four times higher than NpO^+ whereas at a slightly higher temperature, T = 2300 K, a ratio equal to 2 was reported by Ackermann *et al.* [2].

Measurements of reduced neptunium dioxide obtained from high temperature treatment are shown in Figure 1(c). The ionisation efficiency curves for Np^+, NpO^+ and NpO_2^+ were recorded for a sample heated to about 2500 K, for which a significant reduction is expected. The low ionisation energy (IE) of Np, its monoxide and dioxide shows that simple ionisation processes can be assigned and all species are produced from the condensed sample. The observed appearance potential of Np is 6.1 eV consistent with the work of Trautmann [29], who found 6.2 eV. The signal of the dioxide significantly decreased whereas that of the other two gaseous species increased, indicating the initial sample was significantly reduced during heating at high temperature. At this stage the vaporisation is more complex and the equilibrium is represented by the equation (4). This is in agreement with the observations by Ackerman *et al.* [2] of a sample heated in a similar way at 2400 K, showing traces of Np_2O_3 in post-experimental X-ray diffraction.

2.3.2 Total and partial vapour pressure above NpO_2

Total vapour pressure above pure neptunium dioxide samples are plotted against the inverse temperature in Figure 2. The results of the measurements of samples in tungsten cell with or without additional iridium foil agree well and the total pressures from these measurements in the temperature range from (2000 to 2300) K can be represented by the equations:

$$\ln(P/\mathrm{Pa}) = (26.05 \pm 0.06) - (60534 \pm 139)\cdot(T/\mathrm{K})^{-1}, \quad (6)$$

$$\ln(P/\mathrm{Pa}) = (26.08 \pm 0.14) - (60704 \pm 307)\cdot(T/\mathrm{K})^{-1}, \quad (7)$$

for the measurements in tungsten and tungsten with additional iridium foil, respectively.

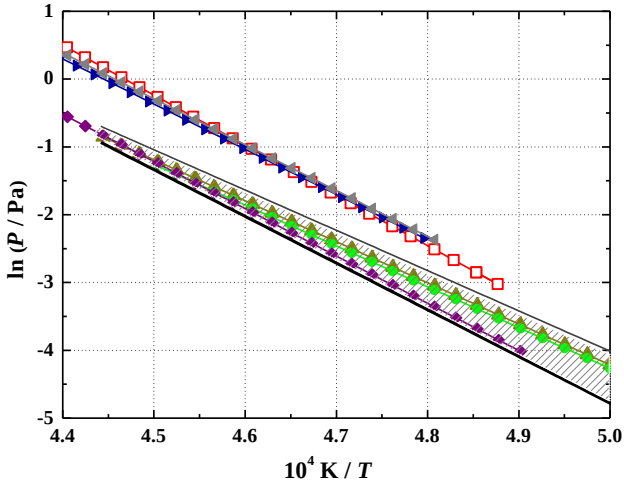

Figure 2. Total vapour pressure results above neptunium dioxide. (▲) and (●): this study - the vapour pressure measurements over NpO_2 in W and W/Ir cells under vacuum. (□): this study - the vapour pressure measurement over reduced NpO_2 sample. (►), (◄) and (◆): this study - the vapour pressure measurements of neptunium oxide bearing species from $Pu_{0.76}Am_{0.24}O_{2-x}$, $Pu_{0.80}Am_{0.20}O_{2-x}$ and AmO_2 respectively. (———) and (▬▬): literature data from Ackermann *et al.* [2] for vaporisation of 35 and 300 mg, respectively, of NpO_2 sample.

Further measurements were performed with the aim of examining the dependence of the vapour pressure on composition. For that purpose the sample was placed in the thoria cell and was heated in “quasi vacuum”, i.e.

an oxygen flow was directed into the cell. Since the oxygen pressure applied (*ca.* 100 Pa) is above the equilibrium pressure for NpO_2 (for T = 2200 K, $P(O_2) = 1.12 \cdot 10^{-3}$ Pa, assessed from calculations performed with the FactSage 5.5© software [30] using evaluated data by Konings *et al.* [31]) we can assume that the results refer to a near stoichiometric composition. The temperature was increased stepwise 10 K·min^{-1} up to 2200 K. At that temperature the measurement was stopped, the sample was cooled down and then reheated in vacuum using the same heating rate. These conditions approach those of measurements in W cell (*in vacuo*) and we thus assume that the results refer to almost identical substoichiometric composition. The mass spectrometric results at 40 eV are given in Figure 3, which shows no significant difference between vacuum and oxygen conditions, indicating that the variation of the NpO_2 pressure with temperature is independent of the composition of the condensed phase in the range studied. The curves can be represented by the equations:

$$\ln(I \cdot T) = (17.55 \pm 0.19) - (72150 \pm 420) \cdot (T/\mathrm{K})^{-1}, \quad (8)$$

for the first annealing in ThO_2 cell in oxygen flow and

$$\ln(I \cdot T) = (16.49 \pm 0.54) - (69358 \pm 839) \cdot (T/\mathrm{K})^{-1}, \quad (9)$$

for the annealing in ThO_2 cell under vacuum.

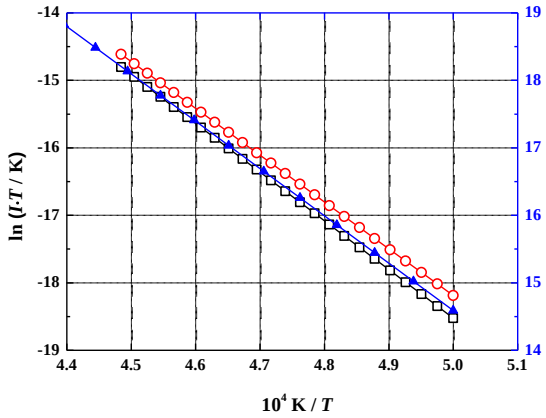

Figure 3. The mass spectrometric results of NpO_2^+ species expressed in ln ($I \cdot T$/K). (□) and (○): this study, the measurements of NpO_2 in ThO_2 cell. (□): annealing in oxidative conditions. (○): annealing under vacuum. (▲): literature data from Ackermann *et al.* [2] for vaporisation of a 300 mg NpO_2 sample, shown on the right y-scale.

Figure 3 is relevant for evaluating the value of the slope of the ln(*I*·*T*) versus 1/*T* curve (representing the enthalpy of sublimation, $\Delta_{sub}H$) over neptunium dioxide for the measurement in thoria cell for the both conditions. The enthalpy of sublimation between (2000 and 2200) K derived from equations (8) and (9) are very close, $\Delta_{sub}H$ = {(599.8 ± 3.5) and (576.6 ± 6.9)} kJ·mol^{-1}, respectively, and are in agreement with the result from the work by Ackermann *et al.* [2] for the vaporisation of a 300 mg NpO_2 sample, 595.3 kJ·mol^{-1}. The latter data [2] are plot on right y-scale, with the same range and increment as the left y-scale.

The partial pressures were derived for the neptunium dioxide sample measured in vacuum using the ionisation efficiency curves measured at *T* = 2260 K for information on the fragmentation patterns of NpO_2 and NpO. The signal intensities were corrected for dissociation processes and the real partial pressure of the oxide species as function of temperature were obtained. The vapour was found to be composed of 93% gaseous NpO_2^+, about 6% NpO^+ and 1% Np^+. Furthermore the fraction of NpO_2^+ observed at 40 eV represents only 52% of the total amount of neptunium dioxide, considering all the fragmentation processes involved when increasing the electron energy. Figure 4 shows the derived partial pressure of NpO_2, NpO, and Np measured at 40 eV as a function of the inverse temperature, as well as the corrections for dissociation processes. As discussed before, no neptunium metal is present in the vapour, the observed ions coming from the dissociation of NpO_2.

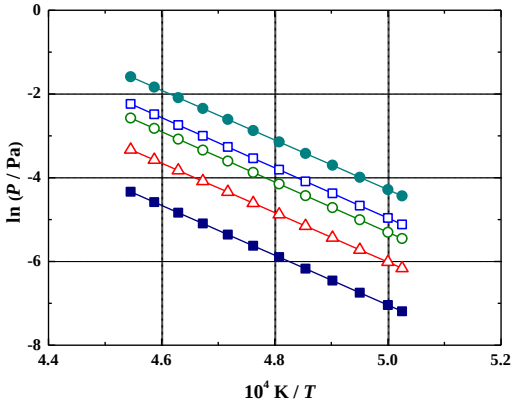

Figure 4. The mass spectrometric partial vapour pressure curves above NpO_2 measured under vacuum in tungsten Knudsen cell, against the inverse of the temperature: (Δ), (○),

(□) - of neptunium, neptunium monoxide and neptunium dioxide observed at 40 eV; (■), (●) - of neptunium monoxide and dioxide, corrected for the dissociation processes.

The available literature data on the vapour pressure of NpO_2 are restricted to measurements by Ackermann *et al.* [2], who carried out experimental work using the Knudsen effusion method combined with collection on platinum targets for a 300 mg and a 35 mg neptunium dioxide sample. These two samples showed similar behaviour except that for the 35 mg sample the steady state conditions were reached in much shorter time. Our results for the total pressure are in very good agreement with these measurements (Figure 2). However, our observations are in disagreement with Ackermann *et al.* [2] with respect to the vapour composition. They estimated the partial pressure of NpO_2 as two-thirds of the total pressure measured at 2300 K from the ionisation curves, whereas our results for slightly lower temperature show that the NpO_2(g) contributes a little more than 90% to the total pressure.

Considering congruent vaporisation of neptunium dioxide at T = 2260 K, the stoichiometry of the condensed phase is given by the atomic flow ratio between oxygen and neptunium, $\phi_{\mathrm{O}} / \phi_{\mathrm{Np}}$ [32]:

$$\phi_{\mathrm{O}} = F_{\mathrm{O}} + F_{\mathrm{NpO}} + 2 \cdot F_{\mathrm{NpO_2}} + 2 \cdot F_{\mathrm{O_2}}, \tag{10}$$

$$\phi_{\mathrm{Np}} = F_{\mathrm{Np}} + F_{\mathrm{NpO}} + F_{\mathrm{NpO_2}}, \tag{11}$$

where F_i is the molecular flow of the species i. In vacuum F_i is a function of the ratio between the partial pressure, P_i and molar mass, M_i, of species i and can be calculated using the Hertz-Knudsen relation [24,32]:

$$F_i = (\alpha_i \cdot P_i) / (2 \cdot \pi \cdot \mathrm{M}_i \cdot R \cdot T)^{1/2}, \tag{12}$$

where α_i is the evaporation coefficient of the species i, which at equilibrium is taken equal to unity, $\alpha_i = 1$, and R is the ideal gas constant, R = 8.314472 J·K^{-1}·mol^{-1}. Using equation (12), the atomic flow of oxygen from (10) becomes:

$$\phi_{\mathrm{O}} = P_{\mathrm{O}} / (\mathrm{M}_{\mathrm{O}} \cdot T)^{1/2} + P_{\mathrm{NpO}} / (\mathrm{M}_{\mathrm{NpO}} \cdot T)^{1/2} + 2 \cdot P_{\mathrm{NpO_2}} / (\mathrm{M}_{\mathrm{NpO_2}} \cdot T)^{1/2} + 2 \cdot P_{\mathrm{O_2}} / (\mathrm{M}_{\mathrm{O_2}} \cdot T)^{1/2}, \tag{13}$$

and the atomic flow of Np from (11) becomes:

$$\phi_{\mathrm{Np}} = P_{\mathrm{Np}} / (\mathrm{M}_{\mathrm{Np}} \cdot T)^{1/2} + P_{\mathrm{NpO}} / (\mathrm{M}_{\mathrm{NpO}} \cdot T)^{1/2} + P_{\mathrm{NpO_2}} / (\mathrm{M}_{\mathrm{NpO_2}} \cdot T)^{1/2}. \quad (14)$$

Since P_{O}, $P_{\mathrm{O_2}}$ and P_{Np} are marginally low, the O/Np ratio depends only on the NpO and NpO_2 partial pressures and their molar masses for the given temperature when congruency is attained. As a result, at 2260 K the calculated nonstoichiometry of the reduced neptunium dioxide equals O/Np = (1.939 ± 0.003). This result, corresponding to the congruent composition at 2260 K, is consistent with the findings of Bartscher and Sari [33] who reported O/Np = 1.97 at 1900 K.

2.3.3 Total pressure from diluted samples

In the view of extreme dilution of the neptunium in the pure americium dioxide and americium-plutonium mixed oxide samples ($Pu_{0.80}Am_{0.20}O_{2-x}$ and $Pu_{0.76}Am_{0.24}O_{2-x}$), Raoult's law can be used to estimate the vapour pressure of pure neptunium dioxide. The total pressure derived from these measurements is shown in Figure 2, and compared to the measurements on NpO_2 under vacuum. It can be seen that the total pressure of the diluted neptunium oxide in americium dioxide sample is close to the total pressure measured by Ackermann *et al.* [2] for vaporisation of the 300 mg NpO_2 sample which shows the ideal behaviour of the solute neptunium oxide in the americium oxide solvent. The total pressure of the mixed oxide samples is higher than the measurements in vacuum (W/Ir) but is close to the result for the reduced neptunium dioxide obtained from high temperature treatment. This is due to the increase of the NpO partial pressure with decreasing of O/Np ratio, according to the reaction: $NpO_{2-x}(cr) = NpO(g) + NpO_{2-x+y}(g)$. As a result the vapour pressure for diluted samples refers to different thermodynamic conditions compared to the NpO_2 sample for which: $NpO_2(cr) = NpO_2(g)$. Under these conditions the PuO_2 will tend to reach the congruent vaporisation composition around O/M = 1.85 [34], whereas AmO_{2-x} will be reduced even further. The oxygen potential in the actinide series indicates an important decrease of the oxide stability from uranium to americium [33]. Thus our measurements

qualitatively indicate an increase of the total pressure above NpO_{2-x} with decreasing O/Np ratio, similar to the behaviour of PuO_2 [34].

2.3.4 Thermodynamic evaluation

The enthalpy of sublimation of NpO_2(g) can be derived from the vapour pressure data using the second- and third- law analysis assuming the measured pressures to be representative for the NpO_2(cr) = NpO_2(g) equilibrium, neglecting the deviation from stoichiometry of the solid phase, which seems justified in view of the current results. For the analysis we have used the thermodynamic data for the solid phase from Huber and Holley [35] and Benes *et al.* [36] for the standard entropy and the high temperature heat capacity, respectively. The entropy and heat capacity of the gaseous species were calculated from the molecular parameters assessed by Gorokhov *et al.* [37].

The vapour pressure methods to determine thermodynamic data are based on the relation:

$$\Delta_r G_T^{\circ} = -R \cdot T \cdot \ln K_p , \qquad (15)$$

where $\Delta_r G_T^{\circ}$ is the standard Gibbs energy of the reaction involved (i.e. vaporisation process), R is the ideal gas constant, R = 8.314472 J·mol^{-1}·K^{-1}, T is the absolute temperature, and $K_p = \prod_i P_i^{n_i}$ is the equilibrium constant of the reaction, with P_i the partial pressure of the species i and n_i the stoichiometric coefficients of the reaction. Since the standard Gibbs free energy for an isothermal reaction is given by

$$\Delta_r G_T^{\circ} = \Delta_r H_T^{\circ} - T \cdot \Delta_r S_T^{\circ} , \qquad (16)$$

where $\Delta_r H_T^{\circ}$ and $\Delta_r S_T^{\circ}$ are the standard enthalpy and entropy, respectively, of the reaction, obtained by a comparison of the coefficients of the equations (15) and (16). Generally there are two ways to interpret the experimental results: by second- and third- law analysis. The methods were described, interpreted and discussed in many publications [19,38,39].

The second-law is based on the variation of the equilibrium constant with temperature and is given by the following relation:

$$\mathrm{d}(\ln K_p) / \mathrm{d}(1/T) = -\Delta_r H_T^{\circ} / R\,. \qquad (17)$$

According to equation (1), the pressure P_i is directly depending on the mass spectrometric intensity of the signal I_i^+ and the temperature, T, and thus of the product ($I{\cdot}T$), the equation (17) becomes:

$$\mathrm{d}(\ln K_{I\cdot T}) / \mathrm{d}(1/T) = -\Delta_r H_T^{\circ} / R\,. \qquad (18)$$

The major advantage of the second-law method is that it does not require entropy data. Following this method the standard enthalpy of the reaction is determined for an average temperature along the measurement (from many measurements of the equilibrium constant) which is then derived to the standard enthalpy of the reaction for room temperature.

The third-law method involves the free energy function FEF, closely related to the entropy, based on third law of thermodynamics:

$$FEF_T^{\circ} = (G_T^{\circ} - H_{298.15\,K}^{\circ}) / T\,. \qquad (19)$$

For each measurement temperature the standard enthalpy of the reaction, $\Delta_r H_T^{\circ}$, is derived from equations (15) and (16), and thereafter to room temperature in a final equation:

$$\Delta_r H_{298.15\,K}^{\circ} = -R \cdot T \cdot \ln K_{p(T)} - T \cdot \Delta_r FEF_T^{\circ}\,. \qquad (20)$$

From our results performed in vacuum (W/Ir cell) we obtain $\Delta_{\mathrm{sub}} H^{\circ}$ (298.15 K) = 623 kJ·mol^{-1} by third-law analysis, however, with a poor agreement with the second-law value $\Delta_{\mathrm{sub}} H^{\circ}$ (298.15 K) = 546 kJ·mol^{-1}, which is probably due to the slight but continuous change of the O/Np ratio of the solid phase with temperature. From our results in the ThO_2 cell, which indicate almost 100% NpO_2 in the vapour, we obtain $\Delta_{\mathrm{sub}} H^{\circ}$ (298.15 K) = 637 kJ·mol^{-1} by second-law analysis. The second-law enthalpy of sublimation derived from the measurement under vacuum in the ThO_2 cell, is only slightly lower than this value, probably due to the less reducing conditions compared to the measurement in the W/Ir cell.

These values for the enthalpy of sublimation can be compared to the results of Ackermann *et al.* [2] which were re-analysed with the same auxiliary data for the solid and gas phase, yielding $\Delta_{\mathrm{sub}} H^{\circ}$ (298.15 K) =

628.5 kJ·mol^{-1} by third-law analysis, $\Delta_{sub}H^{o}$ (298.15 K) = 619.2 kJ·mol^{-1} by second-law.

Regarding our measurements in the W/Ir cell, the second/third law agreement is not as good as in the work of Ackermann *et al.* [2], which is most likely due to the larger sample size in that study. The change in the O/Np ratio was more modest compared to our work, which is confirmed by the analysis of the data for the 35 mg sample by Ackerman *et al.* For that sample the steady state conditions were reached in much shorter time, which yields almost identical results to the analysis of our measurement. The second-law value derived from the measurement in oxygen is in much better agreement with the results of Ackermann *et al.* [2].

2.4 Summary and Conclusions

Knudsen cell mass spectrometric measurements of neptunium dioxide and of americium dioxide and plutonium-americium mixed oxide samples containing very small amounts of neptunium as decay product have been performed. Using electron impact measurements the ionisation efficiency curves were recorded for Np^+, NpO^+ and NpO_2^+ to provide insight into the vapour composition. The partial vapour pressures of the observed neptunium oxide bearing species have been derived taking into account the dissociation processes occurred up to 40 eV, the energy at which the signals were recorded.

Our measurements of the equilibrium between solid and gaseous neptunium dioxide in ThO_2 cell have clearly revealed that the variation of NpO_2 vapour pressure with temperature is independent of the composition of the condensed phase for compositions not far from O/Np = 2.00. Our results are in agreement with the previous work of Ackermann *et al.* [2]. Our measurements performed on few tens of milligrams of neptunium dioxide in W/Ir Knudsen cells show similar results as a 35 mg sample in W cell by Ackermann *et al.* [2]. The results by Ackermann *et al.* on a 300 mg NpO_2 sample annealed in a W cell under vacuum are probably the most accurate done up to date, but our results show that these measurements can be interpreted to apply to the NpO_2(cr) = NpO_2(g) equilibrium and do not need to be corrected for the NpO(g) contribution, as suggested by Ackermann *et al.* [2].

The results for the reduced NpO_2 sample as well as for diluted neptunium oxide in americium dioxide and americium-plutonium mixed oxide samples assuming Raoult's law suggest that for O/Np ratios well below 1.9 the total pressure increases, similar to the behaviour of PuO_2.

2.5 References

[1] C. Guéneau, M. Baichi, D. Labroche, C. Chatillon, B. Sundman, J. Nucl. Mater. 304 (2002) 161.

[2] R.J. Ackermann, R.L. Faircloth, E.G. Rauh, R.J. Thorn, J. Inorg. Nucl. Chem. 28 (1966) 111.

[3] J.K. Gibson, R.G. Haire, J. Marçalo, M. Santos, A. Pires de Matos, J.P. Leal, J. Nucl. Mater. 344 (2005) 24.

[4] J.K. Gibson, J. Marçalo, Coord. Chem. Rev. 250 (2006) 776.

[5] J.K. Gibson, R.G. Haire, J. Marçalo, M. Santos, J.P. Leal, A. Pires de Matos, R. Tyagi, M.K. Mrozik, R.M. Pitzer, B.E. Bursten, Eur. Phys. D. D 45 (2007) 133.

[6] T. Nishi, A. Itoh, M. Takano, M. Numata, M. Akabori, Y. Arai, K. Minato, J. Nucl. Mater. 376 (2008) 78.

[7] J.A. Fahey, R.P. Turcotte, T.D. Chikalla, Inorg. Nucl. Chem. Lett. 10 (1974) 459.

[8] J.A.C. Marples, in: Plutonium and Other Actinides, H. Blank, R. Lindner (Eds), North-Holland, Amsterdam, 1976.

[9] D. Taylor, Br. Ceram. Trans. J. 83 (1984) 32.

[10] K. Richter, C. Sari, J. Nucl. Mater. 148 (1987) 266.

[11] T. Yamashita, N. Nitani, T. Tsuji, H. Inagaki, J. Nucl. Mater. 245 (1997) 72.

[12] H. Serizawa, Y. Arai, K. Nakajima, J. Chem. Thermodyn. 33 (2001) 615.

[13] C. Sari, E. Zamorani, J. Nucl. Mater. 37 (1970) 324.

[14] A. Fernández, R.J.M. Konings, J. Somers, D. Haas, J. Mat. Sci. Lett. 22 (2003) 119.

[15] C. Ronchi, J.-P. Hiernaut, J. Alloys Compd. 240 (1996) 179.

[16] P. Gotcu-Freis, J.-Y. Colle, J.-P. Hiernaut, F. Naisse, C. Guéneau, R.J.M. Konings, J. Chem. Thermodyn. 43 (2011) 1164.

[17] R.J. Ackermann, R.L. Faircloth, M.H. Rand, J. Phys. Chem. 70 (1966) 3698.

[18] J.E. Battles, J.W. Reihus, W.A. Shinn, USAEC, Argonne Nat. Lab., Rep. ANL 7575, 1969.

[19] J. Drowart, C. Chatillon, J. Hastie, D. Bonnell, Pure Appl. Chem. 77 (2005) 683.

[20] M.G. Inghram, J. Drowart, High Temperature Technology, McGraw-Hill, New York (1959) 219.

[21] J.B. Mann, Recent developments in Mass Spectrometry, in: Proceedings of the Conference on Mass Spectroscopy, Tokyo, K. Ogata, T. Hayakawa (Eds.), University Park Press , Baltimore , MD (1970) 814.

[22] D.W. Bonnell, J.W. Hastie Program SIGMA, A Fortran code for computing atomic ionisation cross-sections, NIST, Gaithersburg, MD, unpublished work, 1990-1997.

[23] J.W. Otvos, D.P. Stevenson, J. Amer. Chem. Soc. 8 (1956) 546.

[24] F. Capone, J.-Y. Colle, J.-P. Hiernaut, C. Ronchi, J. Phys. Chem. A 103 (1999) 10899.

[25] R.W. Kiser, in: Introduction to Mass Spectroscopy and its Applications, Prentice-Hall Inc., New York, 1965.
[26] J. Han, L.A. Kaledin, V. Goncharov, A.V. Komissarov, M.C. Heaven, J. Am. Chem. Soc. 125 (2003) 7176.
[27] J. Han, V. Goncharov, L.A. Kaledin, A.V. Komissarov, M.C. Heaven, J. Chem. Phys. 120 (2004) 5155.
[28] L. Gagliardi, B.O. Roos, P.A. Malmqvist, J.M. Dyke, J. Phys. Chem. 105 (2001) 10602.
[29] N. Trautmann, J. Alloys Comds. 213&214 (1994) 28.
[30] FactSage 5.5© 2007, Developed at the Facility for the Analysis of Chemical Thermodynamics (FACT), Centre for Research in Computational Thermochemistry (CRCT), École Polytechnique de Montréal, Canada, and GTT Technologies, Herzogenrath, Germany.
[31] R.J.M. Konings, O. Benes, D. Manara, D. Sedmidubsky, L. Gorokhov, V.S. Iorish, The thermodynamic properties of f-elements. Part II. The Lanthanide and Actinide Oxides, J. Phys. Chem. Ref. Data, (2010) submitted.
[32] L. Dumas, C. Chatillon, E. Quesnel, J. Crys. Growth 222 (2001) 215.
[33] W. Bartscher, C. Sari, J. Nucl. Mater. 140 (1986) 91.
[34] C. Guéneau, C. Chatillon, B. Sundman, J. Nucl. Mater. 378 (2008) 257.
[35] E.J.Jr. Huber, C.E.Jr. Holley, J. Chem. Eng. Data, 13 (1968) 545.
[36] O. Benes, P. Gotcu-Freis, F. Schworer, R.J.M. Konings, T. Fanghaenel, J. Chem. Thermodyn. 43 (2011) 651.
[37] L. Gorokhov, V.S. Iorish, V. Yungman, personal communication.
[38] I. Prigogine, R. Defay, translated by D.H. Everett, Chemical Thermodynamics, Longmans, London, 1965.
[39] G.N. Lewis, M. Randall, revised by K.S. Pitzer and L. Brewer, Thermodynamics, 3rd ed., McGraw-Hill, New York, 1995.

Chapter 3

The high temperature heat capacity of NpO_2

Abstract

The enthalpy increments of pure NpO_2 have been measured using drop calorimetery in the temperature range from (376 K to 1770) K. The heat capacity was derived using the obtained data constrained to 66.20 $J \cdot K^{-1} \cdot mol^{-1}$ at 298.15 K taken from published low temperature measurements. The heat capacity of NpO_2 determined in this study is given by the following equation:

$$C^{o}_{p,m} / (J \cdot K^{-1} \cdot mol^{-1}) = 71.608 + 0.015845 \cdot (T / K) - 900648 \cdot (T / K)^{-2}.$$ *

*This chapter is reprinted with kind permission of Elsevier: "The high temperature heat capacity of NpO_2. O. Benes, P. Gotcu-Freis, F. Schwörer, R. J. M. Konings, T. Fanghänel. The Journal of Chemical Thermodynamics 43 (2011) 651-655".

3.1 Introduction

In the actinide series ^{237}Np is one of the long lived nuclides ($t_{1/2}$ = 2.14·10^6 years) that accumulates in the nuclear fuel during irradiation processes in the nuclear reactors and is predominantly present in the form of oxide (NpO_{2-x}). In case the nuclear power plant operates in an open fuel cycle the spent fuel is not reprocessed and is put to a long-term storage where it decays to stable elements. If the power plant uses the so-called closed fuel cycle the spent fuel is reprocessed, significantly reducing the radiotoxicity of the waste that needs to be stored. In such a case ^{237}Np together with uranium and plutonium isotopes are partitioned and incorporated in the fresh mixed oxide fuel (MOX) and re-used for energy production in nuclear reactors. It is evident that besides the energy production the transmutation of the reprocessed actinides decreases the environmental burden.

In order to predict the behaviour of either nuclear waste or nuclear fuel, both containing NpO_2, knowledge of thermophysical properties of this compound is essential. One of the most important properties that determine how much heat can be accumulated in a material before it reaches a defined critical temperature value is the heat capacity. Moreover the knowledge of this quantity is of interest for the reactor safety analysis in order to predict the fuel behaviour under operational and/or accidental conditions. Furthermore the knowledge of the temperature function of heat capacity is essential in calculation of the Gibbs energy function in order to predict stable phases in any multi-component system.

The low temperature heat capacity of NpO_2 was determined from (5 to 300) K by Westrum Jr. *et al.* [1] using adiabatic calorimetry and from (0.7 to 300) K by Magnani *et al.* [2] using a relaxation method. The enthalpy increments of NpO_2 have been measured by Arkhipov *et al.* [3] and recently by Nishi *et al.* [4], both using a drop calorimetry technique and covering a temperature range from (300 to 1100) K. Furthermore several estimations of the high temperature heat capacity have been made: Sobolev [5] made an estimation based on the theoretical approach presented in his earlier study [6], Serizawa *et al.* [7] determined the heat capacity as a sum of phonon vibrations, dilatation contributions and Schottky specific heat whereas Kurosaki *et al.* [8] derived the heat capacity of NpO_2 using a molecular dynamic study. Since all these high temperature

results are not in adequate agreement, particularly the measurements deviate significantly, we present new experimental data of the enthalpy increments of NpO_2 measured using a drop calorimeter. Based on the obtained data the high temperature heat capacity is derived. Moreover the temperature range covered in this study is (376 to 1770) K thus higher than the two previous experimental studies which both had an upper limit of 1100 K.

3.2 Experimental work

Since NpO_2 is a radioactive material the sample preparation as well as all the measurements had to be performed in alpha-tight glove boxes. The initial material for our samples was pure NpO_2 which was delivered to the Institute for Transuranium Elements (ITU) in the framework of collaboration with the Lawrence Livermore and Los Alamos National Laboratories and the US Department of Energy. The ICP-MS analysis of the initial powder showed a mass fraction less than 0.0013 impurities in the sample.

For the drop calorimetry measurements it is required to have compacted pieces of the material. In the present case cylindrical pellets of 4 mm diameter and *ca.* 2 mm height were prepared using a hydraulic press (260 MPa). The mass of samples ranged from (140 to 190) mg. The prepared pellets were sintered in a furnace at 1800 K for 7.5 hours under the constant flow of air (300 $dm^{-3}\cdot min^{-1}$) which guaranteed that no hypostoichiometric NpO_{2-x} phase would be formed. Since NpO_2 is known not to become hyperstoichiometric (NpO_{2+x}) and hence can not be further oxidised, the oxygen rich atmosphere (air, pure oxygen) is required to condition the pure NpO_2 phase. After the sintering process a small batch of sample was analysed using a powder diffraction X-ray. NpO_2 crystallises in a body centered cubic structure and the cell parameter obtained in this study was 0.5434 nm compared to 0.5433 nm taken from the references [9], indicating that the NpO_2 phase we used for our measurements was pure and stoichiometric.

The measurements of the enthalpy increments of NpO_2 were performed on the Setaram Multi Detector High Temperature Calorimeter (MDHTC-96 type) with installed drop sensor. In order to measure actinide containing

samples the calorimeter was adapted by Setaram in such way that only the necessary parts were installed within the glove box. This modification is very important in the field of nuclear research as it minimises the contaminated waste which arises from the dismantling of the calorimeter after its operational lifetime. The following components were installed within the glove box: the supporting frame with hermetically closed graphite furnace and the experimental chamber consisting of upper and bottom detectors. In order to control the working conditions in the furnace and experimental chamber the front panel with various pressure gauges remained also within the box. All the other parts which are normally installed within the calorimeter frame were inserted in a separate closet which was put next to the glove box and was connected with the calorimeter through cables. This includes all electronics and the power sup ply which, due to its size and weight, would be the most expensive part to treat as a contaminated waste. An emergency button is placed on the outer panel of this closet so quick system shut down is possible if necessary. The experimental setup is shown in Figure 1.

Figure 1. A drop calorimeter installed in an alpha-tight glove box in ITU. The labelled box on the left contains electronic parts of the calorimeter that were excluded from the glove box.

The principle of drop calorimetry is the measurement of the enthalpy increment of a sample that is being dropped from the ambient temperature to the detector which is kept at constant (higher)

temperature. When a 'cold' sample reaches the detector an additional heat must be delivered to the system in order to maintain the programmed target temperature. This heat is proportional to the heat content of the sample. Through performing the experiment for several temperatures, enthalpy as a function of temperature is obtained and the heat capacity is calculated from its derivative according to:

$$C_p(T) = \left(\frac{\partial H}{\partial T} \right)_p . \quad (1)$$

The detector is an alumina tube which consists of 28 B-type thermocouples which provide an integrated heat exchange signal between vertically aligned sample and reference crucibles. Since the drop calorimetry used in this study is a relative technique it is necessary that during each experiment a standard material with known heat capacity is measured. In the present case high purity sapphire (Al_2O_3) has been used with the heat capacity data taken from [10]. From the heat exchange signal, $\int \phi_R d\tau$, of the standard material the sensitivity, s, of the calorimeter is calculated according to

$$s = \frac{\int \phi_R d\tau}{\int_{T_a}^{T_m} C_{p,R}(T) dT} \cdot \frac{M_R}{m_R}, \quad (2)$$

where T_a and T_m are, respectively, the ambient and detector temperatures, the latter being evaluated as an average from the stable values before and after the drop. m_R and M_R are the mass and the molar mass of the standard material respectively and $C_{p,R}(T)$ is the temperature function of its molar heat capacity. The sensitivity of the calorimeter varies with temperature as reported in Figure 2, showing the average sensitivity obtained in this study for each measuring sequence. The maximal sensitivity falls between 1300 K and 1500 K and it implies that in this range the ratio between the heat flow signal and the real enthalpy is the highest and the calorimeter should have the best accuracy here. On the other hand at low temperatures the sensitivity rapidly decreases and the experiment possesses large relative errors. However since small heat quantities are measured due to the small temperature increase of the dropped sample, on an absolute scale the

enthalpy error for this temperature range is acceptable (as shown in Figure 4) and these results can be considered in the heat capacity evaluation.

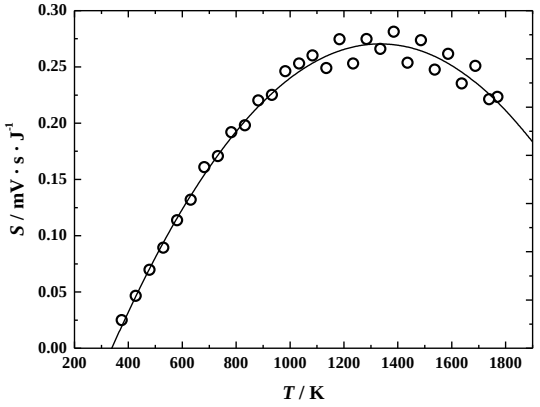

Figure 2. The average sensitivity of the calorimeter determined in this study. The line represents a polynomial fit of the obtained results indicating the maximum between 300 K and 1500 K.

Once the sensitivity of the calorimeter is defined the molar enthalpy increment of the measured NpO_2 sample corresponding to the heating from T_a to T_m is calculated according to

$$\Delta_{T_a}^{T_m} H_m = \frac{\int \phi_s d\tau}{s} \cdot \frac{M_s}{m_s}. \qquad (3)$$

where the sensitivity, s, is taken as an average value from the precedent and the consecutive drops of the reference material, while $\int \phi_s d\tau$ is the area of the heat flow peak of the sample and m_s and M_s are, respectively, its mass and molar mass.

Typical output of one measurement sequence is shown in Figure 3 consisting of four drops of NpO_2 samples and five drops of the sapphire reference. Each peak of the heat flow signal (the thick line in the Figure) was integrated individually using Origin Software [11] obtaining the $\int \phi_R d\tau$ and $\int \phi_s d\tau$ terms from equations (2) and (3), respectively. It is also evident that a slight variation of the temperature (thin line in the Figure) appears during the experiment which is due to the shock upon the drop of the 'cold'

material into the hot sensor. However, this phenomenon has no negative effect on the final enthalpy increment determination as the temperature always re-equilibrates at the programmed value.

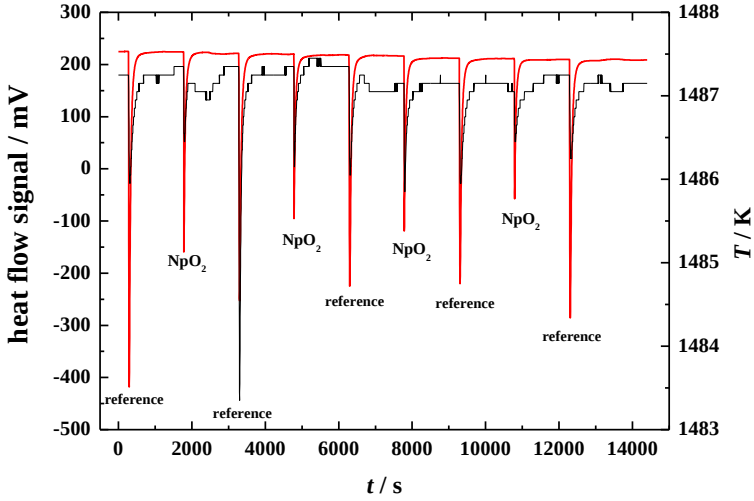

Figure 3. A typical output of the enthalpy increment measurement of the NpO_2 sample performed using the drop calorimeter. The thick line (red line in online version) is the heat flow signal, the thin line represents the temperature in the detector.

3.3 Results

The enthalpy increments of NpO_2 were measured for the temperature range from (376 to 1770) K and the obtained results are shown in Figure 4 where each point corresponds to the average value of the four NpO_2 drops performed for a given temperature. The error bars are calculated as a standard deviation of these data sets. The exact values are given in Table 1.

Using a simultaneous linear regression the heat capacity of NpO_2 was calculated taking into account all measured enthalpy data presented in Table 1 and the low temperature heat capacity data measured by Westrum Jr. *et al.* [1]. In total eleven low temperature data from the temperature range (210 to 310) K with assigned relative error of 1% were considered during the fitting procedure. This amount has been found as a good balance between the two sets of data in order to obtain a smooth transition between the low and the high temperature heat capacity. A

constraint at 298.15 K corresponding to a value of 66.2 $J \cdot K^{-1} \cdot mol^{-1}$ as determined by Westrum Jr. *et al.* has been kept.

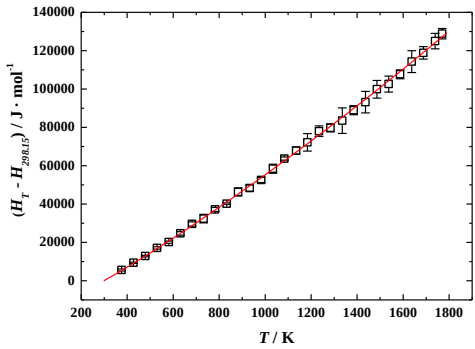

Figure 4. The enthalpy increments of NpO_2 measured in this study. The fit is obtained by a simultaneous linear regression taking into account the low temperature heat capacity data by Westrum Jr. *et al.* [1].

Table 1. The experimental data of the enthalpy increments of NpO_2 measured using a drop calorimeter.

T / K	$\Delta_{298.15}^{T} H_m^{o}$ / (J·mol^{-1})	T / K	$\Delta_{298.15}^{T} H_m^{o}$ / (J·mol^{-1})
375.9	5616± 576	1134.5	67,926 ± 1995
427.4	9406 ± 382	1184.2	72,190 ± 4932
478.8	12,888 ± 421	1234.4	78,019 ± 2978
529.9	17,130 ± 635	1284.3	79,734 ± 3124
580.8	20,148 ± 627	1335.3	83,527 ± 7333
631.4	24,705 ± 1011	1385.3	88,949 ± 2627
681.7	29,621 ± 1170	1436.2	93,132 ± 6204
732.7	32,406 ± 2351	1485.8	99,897 ± 5088
782.2	37,186 ± 1158	1536.9	102,600 ± 4591
833.0	40,195 ± 415	1586.8	107,695 ± 2585
882.3	46,330 ± 2245	1637.7	114,299 ± 6339
933.2	48,336 ± 1667	1688.1	118,824 ± 3635
982.8	52,563 ± 1433	1739.3	124,997 ± 4556
1033.6	58,403 ± 2543	1769.7	128,852 ± 3054
1083.5	63,711 ± 928		

The final high temperature heat capacity of NpO_2 has been described by a three coefficient polynomial of a general formula:

$$C^{\circ}_{p,m} / (\mathrm{J \cdot K^{-1} \cdot mol^{-1}}) = \mathrm{A} + \mathrm{B} \cdot (T / \mathrm{K}) + \mathrm{C} \cdot (T / \mathrm{K})^{-2}. \quad (4)$$

with the obtained coefficients*:*

$$A = 71.608 \pm 0.747,$$
$$B = 0.015845 \pm 0.001742, \quad (5)$$
$$C = -\,900648 \pm 23152.$$

The obtained heat capacity curve is shown in Figure 5 as a bold solid line and the corresponding temperature function of the enthalpy increments is given in Figure 4 indicating a very good fit to the experimental data.

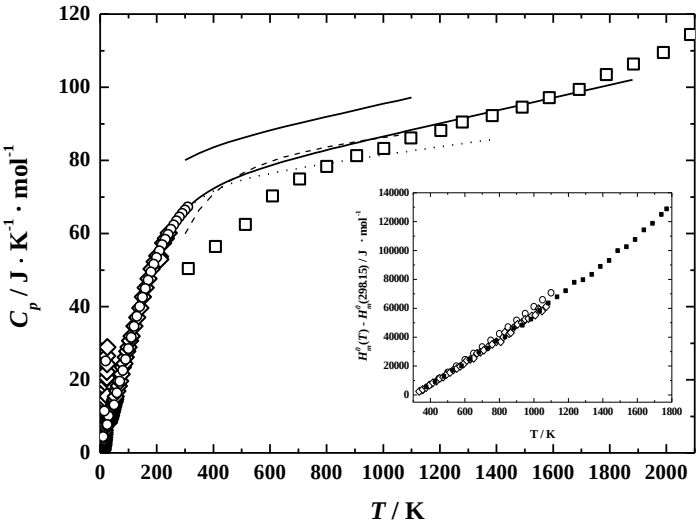

Figure 5. Results of the measurements of NpO_2: (○) data by Westrum Jr. *et al.* [1], [◊] data by Magnani *et al.* [2], (□) data by Kurosaki *et al.* [8], solid thin line- data by Arkhipov *et al.* [3], dashed line - data by Nishi *et al.* [4], dotted line- data by Serizawa *et al.* [7], solid thick line - this study. Inset graph: the enthalpy increment data: (■) measured in this study; (○) measured by Arkhipov *et al.* [3]; (◊) measured by Nishi *et al.* [4].

The values of the molar quantities of the heat capacity, enthalpy and entropy calculated based on equations (4) and (5) for the temperature range (298 to 1800) K are given in Table 2. In this table the entropy is given

in absolute values taking into account the value 80.3 $J \cdot K^{-1} \cdot mol^{-1}$ at 298.15 K derived by Westrum Jr. *et al.* [1] from their low temperature measurement.

Table 2. The thermodynamic functions of NpO_2 calculated in this study.

T / K	$C^{\circ}_{p,m}$ / ($J \cdot K^{-1} \cdot mol^{-1}$)	$\Delta^{T}_{298.15} H^{\circ}_{m}(T)$ / ($kJ \cdot mol^{-1}$)	$S^{\circ}_{m}(T)$ / ($J \cdot K^{-1} \cdot mol^{-1}$)
298.15	66.20 ± 0.66	0	80.3
300	66.35 ± 0.66	0.123 ± 0.00	80.71 ± 0.81
400	72.32 ± 0.72	7.087 ± 0.07	100.71 ± 1.01
500	75.93 ± 0.76	14.511 ± 0.15	117.26 ± 1.17
600	78.61 ± 0.79	22.243 ± 0.22	131.35 ± 1.31
700	80.86 ± 0.81	30.219 ± 0.30	143.64 ± 1.43
800	82.88 ± 0.83	38.408 ± 0.38	154.57 ± 1.55
900	84.76 ± 0.85	46.790 ± 0.47	164.44 ± 1.64
1000	86.55 ± 0.87	55.356 ± 0.55	173.46 ± 1.73
1100	64.099 ± 0.64	64.099 ± 0.64	181.79 ± 1.82
1200	90.00 ± 0.90	73.014 ± 0.73	189.55 ± 1.90
1300	91.67 ± 0.92	82.097 ± 0.82	196.82 ± 1.97
1400	93.33 ± 0.93	91.348 ± 0.91	203.67 ± 2.04
1500	95.98 ± 0.96	100.763 ± 1.01	210.17 ± 2.10
1600	97.61 ± 0.98	110.343 ± 1.10	216.35 ± 2.16
1700	98.23 ± 0.98	120.085 ± 1.20	222.26 ± 2.22
1800	99.85 ± 1.00	129.989 ± 1.30	227.92 ± 2.28

3.4 Discussion

As mentioned in Section 1 the high temperature heat capacity of pure NpO_2 has been experimentally determined in two previous studies, by Arkhipov *et al.* [3] and Nishi *et al.* [4]. Since the results of these two studies are in significant disagreement, we present new experimental data in this work. Moreover they extend the temperature range of the measurements by more than 650 K. A comparison of the NpO_2 heat capacities obtained in various studies is given in Figure 5 including the theoretically determined heat capacities [7, 8] as well.

Comparing the experimental results, our data are in excellent agreement with the data of Nishi *et al.*, only in their case the derived heat capacity curve does not fit to the low temperature data of Westrum Jr. *et al.* [1] and Magnani *et al.* [2] who measured nearly identical values. This is because no constraint to the low temperature values has been made when deriving their heat capacity curve and also, as the authors reported, due to an increased statistical error of the enthalpy increments at low temperatures. As shown in the figure, the data of Arkhipov *et al.* [3] are much higher than the ones obtained in this study or the ones of Nishi *et al.* and are probably incorrect as they significantly disagree with the low temperature data in the region of ambient temperature. The inset graph of Figure 5 shows that systematically higher values of the enthalpy increments with steeper slope have been determined by Arkhipov *et al.* compared to the data obtained in this study and in the work of Nishi *et al.*

Figure 6 shows a comparison of the obtained heat capacity of NpO_2 with other actinide dioxides which have been determined experimentally. For the major part of the measured temperature range the values for NpO_2 fit well between the data of the neighbouring actinide dioxides UO_2 and PuO_2, only between 450 K and 750 K is the reported heat capacity of UO_2 [12] slightly higher. Furthermore all three compounds having partial f-shell occupancy possess significantly higher heat capacity compared to ThO_2, in which Th^{4+} has a formal $[Rn]7s^0 6d^0$ configuration, indicating a contribution due to the electronic excitations.

Figure 6 also shows that the heat capacities of both PuO_2 and UO_2 compounds sharply increase at higher temperatures as a result of Frenkel pair formation [13] while in case of NpO_2 this behaviour is not evident. This can be explained by the fact that only experimental data up to 1800 K have been measured in case of NpO_2 that do not justify higher polynominal description than used in this work, whereas in case of PuO_2 and UO_2 data for higher temperatures were available [13,14]. It is concluded that in order to investigate this phenomena in NpO_2 more data from the higher temperature range are required.

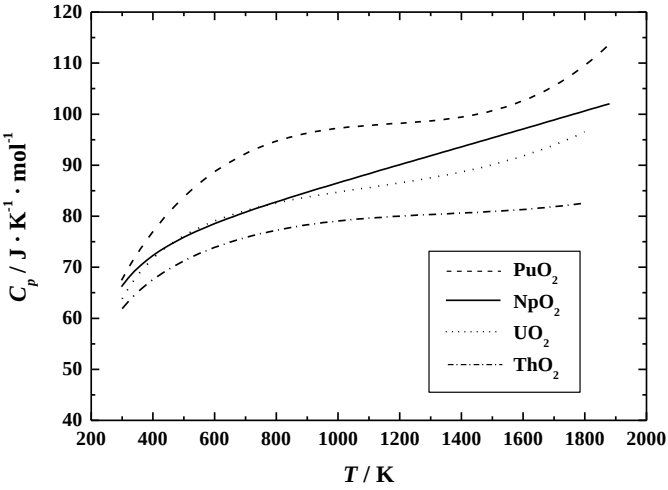

Figure 6. A comparison of the heat capacities of ThO_2 [12], UO_2 [12], NpO_2 (this study) and PuO_2 [12].

3.5 References

[1] E.F. Westrum Jr., J.B. Hatcher, D.W. Osborne, J. Chem. Phys. 21 (1953) 419.

[2] N. Magnani, P. Santini, G. Amoretti, R. Caciuffo, P. Javorsky, F. Wastin, J. Rebizant, G.H. Lander, Physica B 359-361 (2005) 1087.

[3] V.A. Arkhipov, E. A. Gutina, V. N. Dobretsov, V. A. Ustinov, Sov. Radiochem. 16 (1974) 123.

[4] T. Nishi, A. Itoh, M. Takano, M. Numata, M. Akabori, Y. Arai, K. Minato, J. Nucl. Mater. 376 (2008) 78.

[5] V. Sobolev, J. Nucl. Mater. 389 (2009) 45.

[6] V. Sobolev, J. Nucl. Mater. 344 (2005) 198.

[7] H. Serizawa, Y. Arai, K. Nakajima, J. Chem. Thermodyn. 33 (2001) 615.

[8] K. Kurosaki, M. Imamura, I. Sato, T. Namekawa, M. Uno, S. Yamanaka, J. Alloys Compd. 387 (2005) 9.

[9] J.A. Fahey, R. P. Turcotte, T. D. Chikalla, J. Inorg. Nucl. Chem. 38 (1976) 495.

[10] C. Bale *et al.*, ELEM – FACTSAGE 5.3 elements database, 2009

[11] OriginPro 7.5 SR4, Copyright 1991-2004 OriginLab Corporation, 236 <http://www.originlab.com>.

[12] R.J.M. Konings, O. Benes, D. Manara, D. Sedmidubsky, L. Gorokhov, V.S. Iorish, The thermodynamic properties of f-elements. Part II. The Lanthanide and Actinide Oxides, J. Phys. Chem. Ref. Data, (2010) submitted.

[13] C. Ronchi, M. Shiendlin, M. Musella, G. J. Hyland, J. Appl. Phys. 85 (1999) 776.

[14] A. E. Ogard, in: W.N. Miner (Ed.), Proceedings of the 4th International Conference on Plutonium and Other Actinides, Santa Fe, New Mexico, October 5-9, 1970, p. 78.

Chapter 4

Mass spectrometric studies of the vapour phase in the (Pu+O) system

Abstract

*Vapour pressure measurements at high temperatures have been performed on plutonium oxide samples using a Knudsen cell coupled with a mass spectrometer. Different experimental conditions were applied for the derivation of the solid-gas phase relations for three compositions in the Pu-O phase diagram: the (Pu_2O_3-PuO_{2-x}) two-phase domain, the congruent vaporisation composition and near stoichiometric $PuO_{2.00}$. The partial pressures of the gaseous species PuO_2, PuO and Pu were assessed from ionisation efficiency curves recorded at constant temperature. The vapour pressure results for different phase fields were discussed together with all the available literature data.**

*This chapter is reprinted with kind permission of Elsevier: "Mass spectrometric studies of the vapour phase in the (Pu+O) system. P. Gotcu-Freis, J.-Y. Colle, J.-P. Hiernaut, F. Naisse , C. Guéneau, R.J.M. Konings. The Journal of Chemical Thermodynamics 43 (2011) 1164-1173".

4.1 Introduction

The (Pu+O) system is of key importance for nuclear fuel applications. Mixed oxide (U,Pu)O_2 fuels have already been in use in thermal reactors, in fast reactors and space systems, for which a wide range of plutonium oxide concentrations are of interest. Whereas fuels for thermal reactors and space application operate at moderate temperature (below ~1500 K), fast reactor fuels can be exposed to temperatures above 2300 K during operation. The resulting steep temperature gradient existing in fast reactors fuel pins induces significant changes of the fuel material during operation, also called fuel restructuring. Typical effects are the formation of a central void and large columnar grains in the central part of the pellets and equiaxed grains in the mid radius region [1]. This process is accompanied by material transport along the temperature gradient. In particular, the composition of the restructured fuel, represented by the oxygen-to-metal (O/M, with M = U+Pu) ratio as well as the Pu/(Pu+U) ratio, varies considerably between the periphery and the centre of the fuel pellet. This requires knowledge of the phase equilibria, primarily in the binaries (U+O) and (Pu+O), and in the ternary (U+Pu+O) systems. A highly relevant property of the reactor fuel is the vapour pressure, i.e. the (solid+gas) equilibrium, as the mass transport in fast reactor fuel has been explained by vaporisation/condensation processes [1]. Reliable thermodynamic data for the solid and gaseous phases are fundamental to describe such high temperature processes and to predict critical behaviour at even higher temperature that could occur during off-normal conditions.

During the last decades several critical reviews and assessments of the phase behaviour, chemical and thermodynamical properties of plutonium oxides were published [2-5]. The most recent review for the (Pu+O) system [5] summarises the past literature and describes the vapour pressure data obtained for condensed plutonium oxide of various compositions. The experimental data were analysed with the CALPHAD method in which the Gibbs free energy of each phase was modelled and it was concluded that the (Pu+O) system is not well defined in the gaseous phase, in line with the earlier studies. A slight change of the model was made in [6] to improve the description of the small miscibility gap extent in the PuO_{2-x} fluorite phase. In the view of the further discussions, the calculated phase diagram is presented in Figure 1.

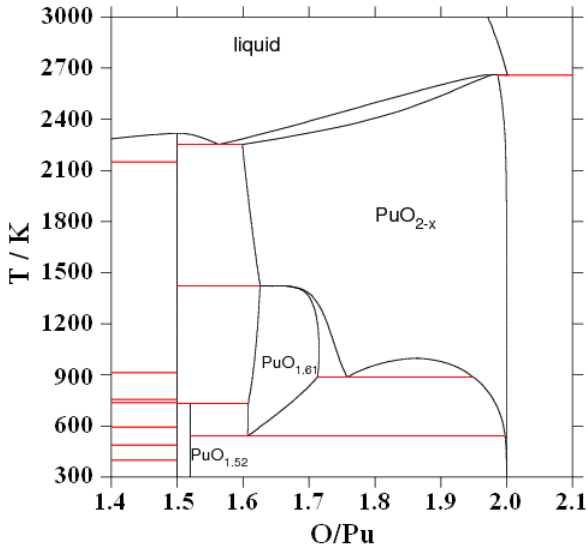

Figure 1. Calculated phase diagram after Guéneau *et al.* [5] slightly adjusted in [6] to improve the description of the small miscibility gap extent in the PuO_{2-x} fluorite phase.

Controversy exists about the partial pressure measurements of plutonium oxides above plutonia at high temperature. The total vapour pressure in the (Pu+O) system has been measured by various authors [7-12] using the Knudsen effusion method combined with collection on targets, the most extensive one performed by Ohse [12] who studied samples of different stoichiometries for three isothermal sections. Most of these authors made the assumption that $PuO_2(g)$ is the major gas species above congruent vaporisation of PuO_{2-x}. In the mass spectrometric studies by Battles *et al.* [13] and Kent [14], the partial pressures of PuO(g) and $PuO_2(g)$ above plutonia have been measured. Both authors found similar data for the total pressure but the results are not in agreement concerning the major species in the vapour phase. Battles *et al.* claimed that PuO(g) is the major constituent whereas Kent found a higher partial pressure for $PuO_2(g)$. Measurements of the vaporisation of PuO_2 in oxygen, air and argon were performed using transpiration method by Pardue and Keller [15]. These data exhibit a large experimental scatter and are not sufficiently accurate for quantitative assessment. Later, Ronchi *et al.* [16] reported for the first time the existence of PuO_3 gaseous species as deduced from mass spectrometric measurements for PuO_2 as well as $(U,Pu)O_2$ samples.

In order to understand the (solid+gas) phase equilibrium in the binary plutonium-oxygen phase diagram, studies were also undertaken for the (Pu_2O_3-PuO_{2-x}) two-phase domain. For this region the total pressure measurements were performed using the same Knudsen effusion technique in reducing conditions by Phipps *et al.* [17] and Ackermann *et al.* [8], or by studying a sample of known composition by Messier *et al.* [11] and Ohse *et al.* [12]. The only mass spectrometric investigation of the (Pu_2O_3-PuO_{2-x}) two- phase domain has been made by Battles *et al.* [13] who observed PuO(g) as a major species in the vapour along with detectable quantities of gaseous PuO_2 and Pu.

This paper describes the results of a new study of the vaporisation behaviour and phase relations in the Pu-O system. A Knudsen cell mass spectrometry facility was used to analyse the total pressure in the (Pu_2O_3-PuO_{2-x}) and PuO_{2-x} phase fields. Partial pressure data were assessed based on ionisation efficiency curves recorded for constant temperature.

4.2 Samples and experimental method

4.2.1 Sample preparation

The plutonium dioxide (sample 1) used for the present study were fragments from a *ca.* 2 mm height disk. The isotopic composition of the plutonium, based on thermal ionisation mass spectrometry analysis, was 93.54 wt% ^{239}Pu and 6.32 wt% ^{240}Pu, the remnant was constituted by the ^{238}Pu, ^{241}Pu and ^{242}Pu isotopes, each less than 0.1 wt%. The pellets have been prepared by sol gel method, followed by calcination, compaction and sintering at 1873 K for several hours in Ar/H_2 atmosphere. After sintering, thermogravimetric analysis (TGA) was performed using a Netzsch Sta 409C/CD apparatus. TGA scans were recorded at a heating rate of 5 K·min^{-1} until 1273 K in air, showing the O/Pu ratio to be 1.834 ± 0.007. The uncertainties of this measurement type were analysed with the GUM Workbench© software [18]. Furthermore the samples obtained after the latter thermal treatment, corresponding to the stoichiometric dioxide, were also used, which we further refer to as sample 2. The X-ray diffraction analysis using Cu-Kα radiation performed on the dioxide sample (sample 2) indicated a single fluorite-type phase. The lattice parameter of the PuO_2

sample was found to be (0.5401 ± 0.0001) nm, consistent with the results from earlier studies [19].

In general, plutonium dioxide can be reduced to hexagonal Pu_2O_3 by reaction with plutonium metal, very dry hydrogen or carbon. Hexagonal plutonium sesquioxide, referred to as β-Pu_2O_3 is a line compound isostructural with the A-type rare earth sesquioxides. In the present study, the data for the (Pu_2O_3-PuO_{2-x}) two-phase domain were obtained from a sample prepared by the reduction of the dioxide by plutonium metal, a method used before by Holley *et al.* [20]. For this purpose, fragments of the plutonium dioxide disks were ground and mixed with chips of metallic plutonium, kept in a quartz tube under argon atmosphere. High resolution gamma spectrometry on the Pu metal revealed 0.2 wt% of ^{241}Am content, relative to the total plutonium content. The metal was added with a stoichiometric excess of approximately 20 wt%. The product thus obtained (sample 3) was transferred and annealed in a closed tantalum Knudsen cell up to about 1800 K for few hours under vacuum. Following this procedure the obtained "black sintered mass" contained excess of plutonium metal which was removed by heating the same cell, opened in this step, up to temperatures of about (2100 to 2200) K. The sublimation of the metal was monitored using the mass spectrometer. After few more hours, when the Pu^+ signal decreased significantly (of two orders of magnitude), the heating was stopped. The container was used as a liner for a Knudsen cell and the vapour pressure measurement was started under vacuum. All the operations and handlings were done in a nitrogen atmosphere glove box.

4.2.2 Mass spectrometric measurements

The experimental facility consists of a Knudsen cell coupled with a quadrupole mass spectrometer designed to study radioactive materials (actinide compounds and irradiated material) at high temperature, and has been built in glove box shielded by 5 cm thick lead bricks. The mass spectrometer is a quadrupole QMG422 from Pfeiffer Vacuum which offers a mass range of (1 to 512) amu. The mass filter is made of molybdenum rods, 8 mm in diameter and 200 mm in length. It is equipped with a cross beam electron bombardment ion source, an axial Faraday cup and a SEM (Secondary Electron Multiplier) located at 90° to the filter axis. The sintered samples (in weights of few tens of mg up to 100 mg) were loaded into the

cells, centred in a high temperature furnace made of a tungsten coil-heating element surrounded by seven cylindrical thermal shields. The whole system is placed in a high vacuum chamber.

The behaviour of the plutonium oxide samples was studied under different conditions: mass spectrometric measurements have been conducted in vacuum using tungsten, iridium or tantalum cells, and in oxidative conditions using a ThO_2 cell, having a small orifice at the bottom for the oxygen gas inlet. Iridium cells were used as an alternative for the standard tungsten cells, the latter material being less suitable, as possible reactions at high temperature with the solid dioxide sample could be expected [8,13]. Plutonium oxide samples as received (sample 1, with O/Pu = 1.834) have been heated in such cells up to 2230 K by 10 $K \cdot min^{-1}$. Tantalum cells have been used for the sample 3, being known to assist in reduction process, due to its affinity for oxygen [7,17].

For the measurements in oxidising conditions, a new Knudsen cell assembly has been implemented. Compatibility tests between plutonium oxide and various cell materials, proposed for the oxidative conditions (e.g. Al_2O_3, ZrO_2, MgO or ThO_2), revealed that ThO_2 is the best high temperature material with non-reactive properties for oxides. A schematic drawing of the Knudsen cell mass spectrometric assembly and the cell used in this study is given in Figures 2(a) and (b), respectively. The ThO_2 liner (h = 12 mm, wall thickness less than 1 mm, oxygen gas inlet with diameter d < 0.5 mm, effusion orifice with diameter between 0.5 and 1 mm) is introduced in a yttria-stabilized zirconia (YSZ, with 5% Y_2O_3) cell support. A comparison with the conventional cell type made of Al_2O_3, used for previous measurements [21] is also given. Since the melting point of alumina is slightly over 2300 K, the conventional cell has a much lower thermal resistance than the YSZ/ThO_2 cell. Pure oxygen gas (mass fraction purity 0.99999) was introduced in the cell and the gas flow was controlled. In the course of the measurements the temperature was increased stepwise by 10 $K \cdot min^{-1}$ up to about 2200 to 2300 K.

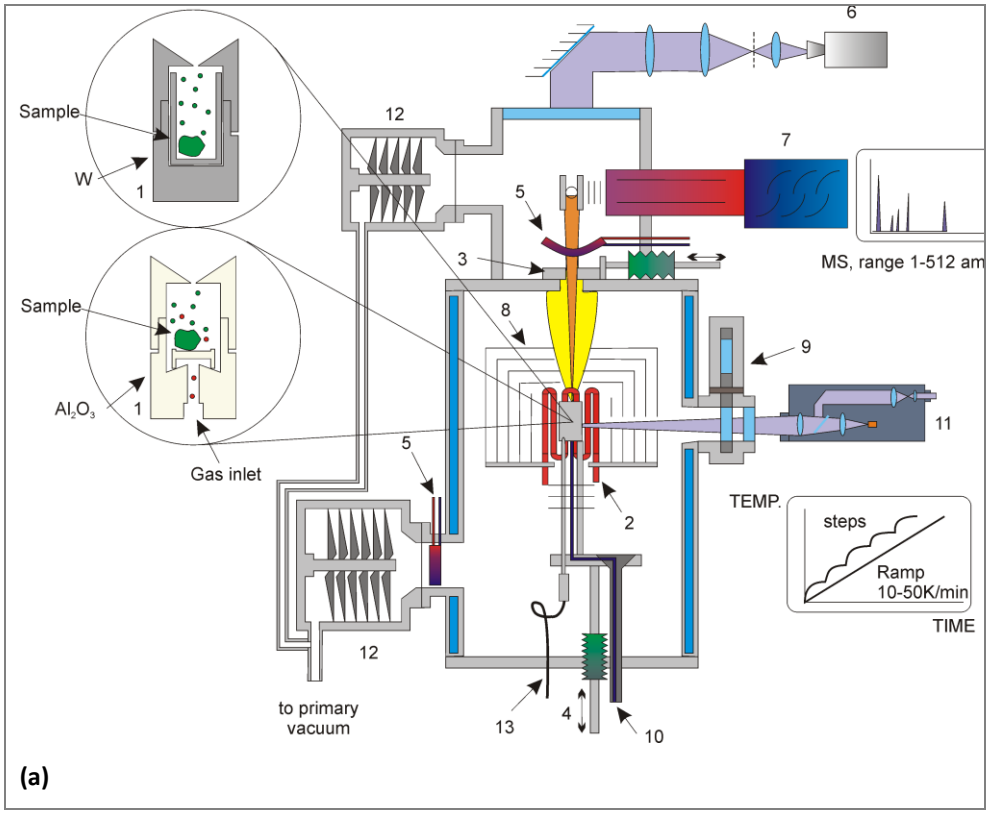
Sample
W
1
Sample
Al_2O_3
1
Gas inlet
12
6
7
5
3
8
9
11
MS, range 1-512 am
TEMP.
steps
Ramp
10-50K/min
TIME
5
2
12
to primary
vacuum
13
4
10
(a)

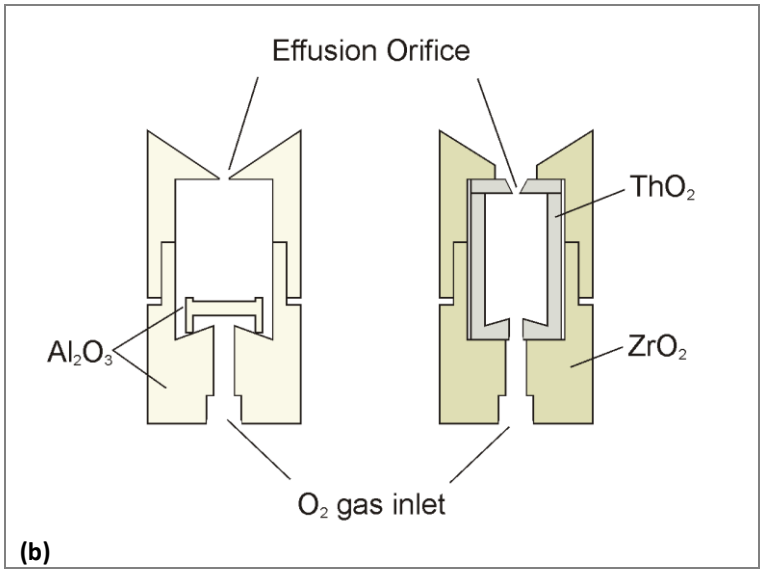
Effusion Orifice
ThO_2
ZrO_2
Al_2O_3
O_2 gas inlet
(b)

Figure 2. **(a)** The Knudsen cell mass spectrometer assembly. (1): the Knudsen cell; (2): tungsten resistant coil; (3): molecular beam chopper for reference noise diagram; (4): cell lift facilities for fast heating/cooling; (5): liquid nitrogen trap to reduce noise; (6): CCD camera to align the cell hole and chopper diaphragm; (7): quadrupole mass spectrometer; (8) thermal shield (three in tungsten and four in tantalum); (9): revolving protection windows; (10): inlet gas capillary; (11): linear pyrometer; (12): turbo molecular pump; (13): removable W/Re thermocouple.
(b) The Knudsen cell assembly with ThO_2 insert and ZrO_2 cell holder (right), compared to the conventional Al_2O_3 cell and sample holder (left).

The temperature recording of the Knudsen cell assembly was calibrated by measurement of the melting points of standard materials (Zn, Cu, Fe, Pt, Al_2O_3), as described in a former publication [22]. Temperature is a very important parameter in mass spectrometry as the vapour pressure function is directly dependant on it according to the basic mass spectrometry relation [23,24]:

$$P_i = I_i^+ \cdot T \,/\, K_i\,, \tag{1}$$

where P_i is the vapour pressure of species i, T is the temperature at which the pressure is calculated, I_i^+ and K_i are the intensity of the molecular beam and the calibration factor, respectively, for a species i. The calibration factor contains an instrumental term, K_g, which is independent of species i, and a term, χ_i, which is dependent of species i and includes the ionisation cross-section, σ_i, the efficiency of the secondary ion multiplier, γ_i, and the isotopic weight of species i, f_i. Therefore the calibration factor K_i is described as:

$$K_i = \mathcal{K}_g \cdot \chi_i\,, \tag{2}$$

where

$$\chi_i = \sigma_i \cdot \gamma_i \cdot f_i\,. \tag{3}$$

For each gaseous species i the three parameters have to be evaluated. The measurements have been carried out using an ionisation energy of 40 eV, value at which the atomic ionisation cross-sections for the studied species were calculated using the program SIGMA [23,25,26]. In early studies the calculated maximum ionisation cross-section was involved [27,28]. The ionisation cross-sections at low energies were then estimated by assuming that the cross-section varies quasi-linearly up to the maximum with the

excess energy above the ionisation energy for species i, E_i, according to the relation:

$$\sigma_i \approx \sigma_m \cdot (E - E_i) / (E_m - E_i), \quad (4)$$

where σ_m is the ionisation cross-section at the maximum of the ionisation efficiency curve, E is the applied ionisation energy, and E_m is the maximum ionisation energy of the species i considered. It has been shown that this approximation lead to significant deviations [23]. For molecular cross sections calculations the additive rule proposed by Otvos and Stevenson [28] was used. For the species considered in this study, an approximation for the secondary electron multiplier is used [29], $\gamma_i = \delta / \mathrm{M}_i^{1/2}$, where δ is a constant independent of species i. The isotopic abundance, f_i, is calculated accurately from the atomic abundance and the composition of the ions species i.

The Knudsen cell mass spectrometer assembly was calibrated by vaporising a known quantity of reference material, silver (a metal with a well-known vapour pressure), together with the sample. Silver is relatively inert in this system and vaporised completely below 1500 K, before the sample evaporation started. From the ion intensities of the silver isotopes (I^+_{Ag}), ^{107}Ag and ^{109}Ag, and the vapour pressure of silver (P_{Ag}) reported by Hultgren *et al.* [30], the global calibration factor for silver (K_{Ag}) was determined experimentally using equation (1):

$$K_{\mathrm{Ag}} = (I_i^+ \cdot T) / P_{\mathrm{Ag}}. \quad (5)$$

Furthermore, the second-law vaporisation enthalpy of Ag ($\Delta_{\mathrm{vap}}H$) was compared and found in agreement with the value derived from the data of Hultgren *et al.* [30] for the same temperature range.

The integrated Hertz-Knudsen equation provides the mass loss, Δm_i, by effusion during a period of time, $\Delta \mathrm{t}$, for a molecule or species i:

$$\Delta m_i = P_i \cdot \mathrm{S} \cdot \mathrm{C} \cdot \Delta \mathrm{t} \cdot \{M_i / (2 \cdot \pi \cdot R \cdot T)\}^{1/2}, \quad (6)$$

where S is the effusion orifice surface, C is the Clausing factor of the orifice, M_i is the molar mass of the effused gaseous species i, and R is the ideal gas constant, R = 8.314472 J·K^{-1}·mol^{-1}. The Clausing factor is obtained by integrating over the whole angular distribution of molecular flows when

taking into account the shape of the effusion orifice [23]. For an ideal orifice, for which the lid is considered infinitely thin, C = 1. For an orifice with a short but finite channel, the coefficient applies for any effused flow. The Clausing factor expression for a cylindrical channel has been reviewed by Santeler [31] and is a relation between the length and the radius of a cylindrical channel.

Relations (5) and (6) give the possibility of calculating the K_{Ag}, which is a value calculated from silver vaporisation or integration of the product $(I^{+}_{\mathrm{Ag}} \cdot T^{1/2})\delta t$ along the experiment and the total mass loss:

$$K_{\mathrm{Ag}} = \{(\mathrm{S} \cdot \mathrm{C} \cdot M^{1/2}_{\mathrm{Ag}}) \big/ (\Delta m_{\mathrm{Ag}} \cdot (2 \cdot \pi \cdot R)^{1/2})\} \cdot \sum (I^{+}_{\mathrm{Ag}} \cdot T^{1/2})\delta t \,. \tag{7}$$

From (2), the instrumental factor equals

$$\mathcal{K}_g = K_i / \chi_i, \tag{8}$$

for species *i*, and

$$\mathcal{K}_g = K_{\mathrm{Ag}} / \chi_{\mathrm{Ag}}\,, \tag{9}$$

for silver.
And then the calibration factor K_i for species *i* becomes

$$K_i = K_{\mathrm{Ag}} \cdot \chi_i / \chi_{\mathrm{Ag}}, \tag{10}$$

Consequently for each temperature, *T,* the pressure is deduced from the relation (1), which together with (10) becomes

$$P_i = \{(I^{+}_i \cdot T) / K_{\mathrm{Ag}}\} \cdot (\chi_{\mathrm{Ag}} / \chi_i), \tag{11}$$

and thus including the calibration factor relation (2) becomes

$$P_i = \{(I^{+}_i \cdot T) / K_{\mathrm{Ag}}\} \cdot (M^{1/2}_i / M^{1/2}_{\mathrm{Ag}}) \cdot (\sigma_{\mathrm{Ag}} / \sigma_i) \cdot (f_{\mathrm{Ag}} / f_i)\,, \tag{12}$$

As a result,

$$P_i = \{(I^{+}_i \cdot T) / K_{\mathrm{Ag}}\} \cdot M^{1/2}_i \cdot J_i\,, \tag{13}$$

where

$$J_i = M^{-1/2}_{\mathrm{Ag}} \cdot (\sigma_{\mathrm{Ag}} / \sigma_i) \cdot (f_{\mathrm{Ag}} / f_i)\,. \tag{14}$$

Relation (13) gives the equation for determination of the pressure of species *i*, taking into account the calibration factor obtained by vaporising a known quantity of silver as a reference material together with the sample.

Ionisation efficiency curves for Pu^+, PuO^+ and PuO_2^+ were primarily recorded to have insight of the dissociative ionisation processes and the composition of the gaseous phase. They were measured at different isotherms for which the mass spectrometer ion signals had an appreciable high signal (> 2 decades over the background) and the gaseous phase is in equilibrium with the condensed phase. During the scan, the energy of ionising electrons was increased stepwise by 0.5 eV while the temperature was kept constant. The resolution of the offset between the applied cathodic voltage and the effective electron energy spectrum has been described in a previous study [32].

The first ionisation potentials of silver and a known gas composition of krypton, helium, argon, neon and xenon have been taken as standards. The energy range covered by the calibration was from (7.5 to 24.5) eV. The results showed a good linear dependence (the regression coefficient is equal to 0.998) for extrapolating the scale up to 40 eV. The electron energy calibration does not apply to the measurements in oxygen flow for which an internal calibration has been done, based on the well known Pu appearance potential value [33].

4.3 Experimental results

4.3.1 Measurements of the PuO_{2-x} phase field in vacuum

The measurements were performed on few fragments of plutonium oxide disks as received (sample 1), in weight of (80 to 90) mg, under vacuum in tungsten and iridium cells. The results of the measurements of samples in tungsten and iridium cell agree well and the total pressures from these measurements in the temperature range from (2000 to 2230) K can be represented respectively by the equations:

$$\ln(P/\mathrm{Pa}) = (27.76\pm0.65) - (64440\pm332) \cdot (T/K)^{-1}, \quad (15)$$

$$\ln(P/\mathrm{Pa}) = (27.61\pm0.60) - (64264\pm380) \cdot (T/K)^{-1}. \quad (16)$$

For the measurements performed in tungsten cells, the mass spectrometer identified tungsten oxides in the vapour phase, whilst for the measurements performed in iridium cells no iridium bearing oxide species were found. For T = 2230 K the spectrometric signals were recorded as a function of the energy of the ionising electrons (Figure 3). The appearance potential of PuO was found to be 6.4 eV. The sensitivity was not high enough to determine accurately the appearance potential of PuO_2. The background for this species was higher than for both monoxide and metal but a value of about 8.5 eV could be estimated. The ion intensity of Pu^+ increases above (13 and 19) eV as a result of dissociation processes of PuO and PuO_2, respectively. The mass spectrometric measurements showed no change in the ion signals while temperature was kept constant.

At this temperature (T = 2230 K) the measurement was stopped and the temperature was quickly decreased. Figure 4 shows the derived partial pressure of PuO_2, PuO and Pu observed and measured at 40 eV as well as the pressures assessed with applied corrections for the dissociation processes, both as a function of the inverse temperature. Based on Figure 4, the vapour consists of 81% PuO_2, and 19% PuO, indicating that the dioxide is the major species in the vapour, almost four times higher than the monoxide.

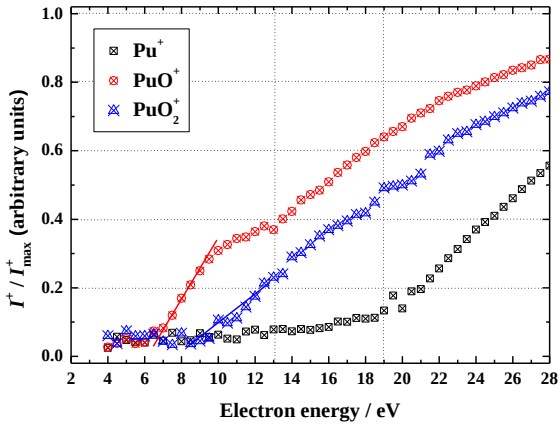

Figure 3. Ionisation efficiency curves for different plutonium bearing ion species created by ionisation of the vapour above PuO_{2-x} at 2230 K as a function of the applied electron energy.

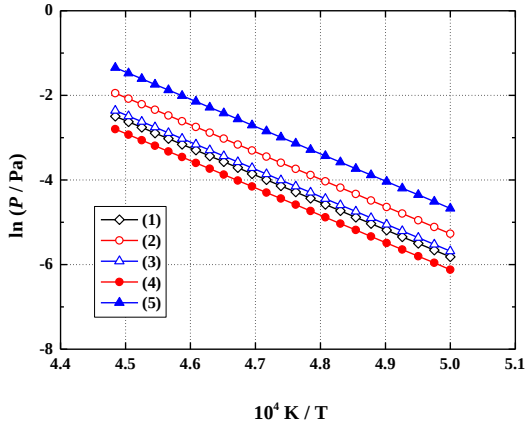

Figure 4. The mass spectrometric partial vapour pressure curves above PuO_{2-x} measured under vacuum in a tungsten Knudsen cell, against the inverse of the temperature: (1), (2), (3): plutonium, plutonium monoxide and plutonium dioxide as observed; (4), (5): plutonium monoxide and dioxide, corrected for the dissociation processes.

Furthermore the fraction of PuO_2^+ observed at 40 eV represents only 38% of the total amount of plutonium dioxide, considering all the fragmentation processes involved with increasing electron energy. Considering the congruent vaporisation of plutonium dioxide at T = 2230 K, the stoichiometry of the condensed phase is in direct relation with the atomic flow ratio between oxygen and plutonium, ϕ_O / ϕ_{Pu} [34], for which:

$$\phi_O = F_O + F_{PuO} + 2 \cdot F_{PuO_2} + 2 \cdot F_{O_2}, \quad (17)$$

$$\phi_{Pu} = F_{Pu} + F_{PuO} + F_{PuO_2}, \quad (18)$$

where F_i is the molecular flow of the species i. In vacuum F_i is a function of the ratio between the partial pressure, P_i and molar mass, M_i, of species i and can be calculated using the Hertz-Knudsen relation [32,34]:

$$F_i = (\alpha_i \cdot P_i) / (2 \cdot \pi \cdot M_i \cdot R \cdot T)^{1/2}, \quad (19)$$

where α_i is the evaporation coefficient of the species i, which at equilibrium is taken equal to unity, $\alpha_i = 1$, and R is the ideal gas constant, R = 8.314472 $J \cdot K^{-1} \cdot mol^{-1}$. Using equation (19), the atomic flow of oxygen from (17) becomes:

$$\phi_O = P_O / (M_O \cdot T)^{1/2} + P_{PuO} / (M_{PuO} \cdot T)^{1/2} + 2 \cdot P_{PuO_2} / (M_{PuO_2} \cdot T)^{1/2} + 2 \cdot P_{O_2} / (M_{O_2} \cdot T)^{1/2}, \quad (20)$$

and the atomic flow of Pu from (18) becomes:

$$\phi_{Pu} = P_{Pu} / (M_{Pu} \cdot T)^{1/2} + P_{PuO} / (M_{PuO} \cdot T)^{1/2} + P_{PuO_2} / (M_{PuO_2} \cdot T)^{1/2}. \quad (21)$$

Since P_O, P_{O_2} and P_{Pu} are marginally low, the O/Pu ratio depends only on the PuO and PuO_2 partial pressures and their molar masses for the given temperature when congruency is attained. Accordingly, the calculated nonstoichiometry of the plutonium oxide, sample 1, equals O/Pu = 1.79 ± 0.02. This result is in agreement to the value found by TGA on the same sample 1, for which the O/Pu ratio is 1.824 ± 0.011. The TGA measurement was performed subsequent to the mass spectrometric measurement, in the same conditions as detailed in section 2.1 (~1300 K, in air).

4.3.2 Measurements of the (Pu_2O_3 - PuO_{2-x}) two-phase field

The compound "in situ" formed by the reaction of PuO_2 and Pu metal (sample 3), as described in the previous section, was measured in the mass spectrometer after the two-steps fabrication. During the entire measurement all the isotopes were scanned. Figure 5 shows the mass spectrometric signals from this measurement in vacuum plotted against the electron energy. The PuO signal represents without doubt the major vapour species followed by the metal and the dioxide.

The total pressure measurements over the (Pu_2O_3-PuO_{2-x}) two-phase domain in the tantalum cell for the temperature range from 2000 to 2250 K are represented by the equation:

$$\ln(P/\text{Pa}) = (30.98 \pm 0.17) - (66138 \pm 370) \cdot (T/\text{K})^{-1}. \quad (22)$$

The derived partial pressure of the three gaseous species observed and measured at 40 eV are shown in Figure 6 as well as the pressures assessed when applying corrections for the dissociation processes, both as a function of the inverse temperature. Plutonium dioxide has the lowest pressure, the pressure of atomic plutonium being slightly higher. The total pressure is determined by the monoxide partial pressure which is

distinctively high. In this case it was not possible to carry out thermogravimetric analysis, the sample was stuck to the bottom of the tantalum crucible, being not possible to be removed in order to be reoxidised.

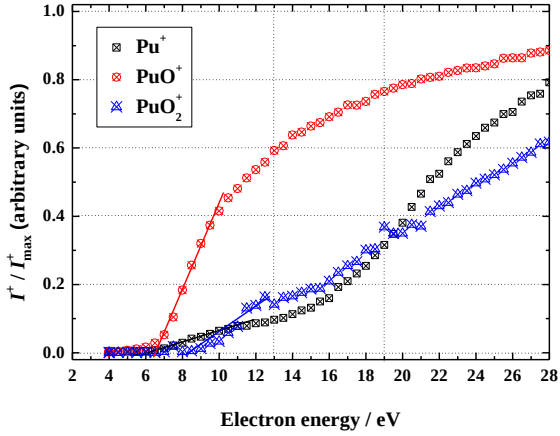

Figure 5. Ionisation efficiency curves for different plutonium bearing ion species created by ionisation of the vapour in the (Pu_2O_3-PuO_{2-x}) two-phase domain at 2200 K as a function of the applied electron energy.

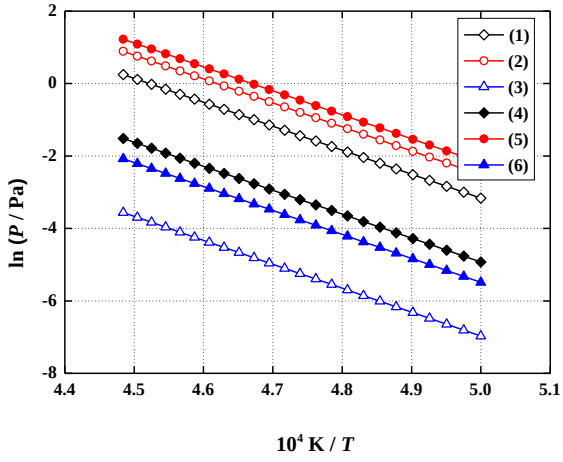

Figure 6. The mass spectrometric partial vapour pressure curves above the (Pu_2O_3-PuO_{2-x}) two-phase domain measured under vacuum in a tungsten Knudsen cell, against the inverse of the temperature: (1), (2), (3): plutonium, plutonium monoxide and plutonium dioxide as observed; (4), (5), (6): plutonium metal, monoxide and dioxide, corrected for the dissociation processes.

4.3.3 Measurements of the PuO_{2-x} phase field in oxygen

The mass spectrometric measurements for PuO_2 (sample 2) were performed in a YSZ/ThO_2 cell, with the aim of examining the vapour pressure of a composition as close as possible to the pure stoichiometric O/Pu = 2.00 phase boundary. The sample placed in the thoria cell was heated in "quasi vacuum", i.e. a high purity oxygen flow was directed into the cell. Since the oxygen pressure applied (ca. 100 Pa) is above the equilibrium pressure for PuO_2 we assume the results refer to a very near stoichiometric composition ($1.98 \leq O/Pu \leq 2.00$). For this measurement the temperature was increased stepwise with 10 $K \cdot min^{-1}$ up to 2270 K. At that temperature the measurement was stopped, the sample was cooled and then reheated in vacuum using the same heating rate. These conditions approach those of measurements in W or Ir cells (in vacuum). At the end of the experiment, the temperature was rapidly decreased and the sample was taken out of the container. TGA was performed in the same conditions as detailed in section 2.1 (~1300 K, in air), indicating the O/Pu ratio to be 1.837 ± 0.014.

The vapour pressure of the sample in oxygen can be represented by the equation:

$$\ln(P/\mathrm{Pa}) = (30.48 \pm 0.09) - (67985 \pm 195) \cdot (T/\mathrm{K})^{-1}, \qquad (23)$$

and the ionisation efficiency curves are given in Figure 7. It must be remarked that for the measurement in oxidizing conditions the total pressure was higher than in vacuum and the ionisation efficiency curves indicated a slightly higher PuO_2^+ signal (i.e. at 13 eV) than the one recorded in vacuum.

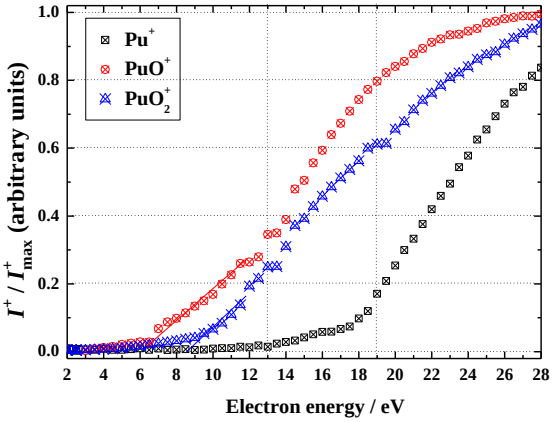

Figure 7. Ionisation efficiency curves for different plutonium bearing ion species created by ionisation of the vapour above PuO_{2-x} in an oxygen flow at 2250 K as a function of the applied electron energy.

4.4 Discussion

4.4.1 Vapour speciation and vapour pressure

The main disagreement for the solid-gas equilibria in the substoichiometric PuO_{2-x} phase domain concerns the speciation in the vapour. Whereas all the effusion studies on the vaporisation of PuO_{2-x} are based on the assumption that PuO_2 is the major contributor to the total vapour pressure, direct mass spectrometric measurements are not in agreement about this. Battles *et al.* [13] stated that PuO(g) was the main vapour species above PuO_{2-x} whilst Kent [14] claimed that was PuO_2(g).

The experiments by Battles *et al.* [13] were carried out using ionising electron energy of 13 eV in order to avoid any dissociative processes. In that study, the ionisation cross section values used for the pressure assessment were valid for ionizing electron energies several times larger than those actually used. The application of these ionisation cross section values at low ionizing energies, i.e. 13 eV, has been already questioned [23]. Furthermore several corrections were made for the different electron multiplier efficiencies for the three molecules under investigation, Pu, PuO and PuO_2. As described in the second section of this paper (2.2) our measurements have been carried out using an ionisation energy of 40 eV

and the molecular cross section were determined by the additive rule from the values for the atomic cross sections. The experimental information provided in the work of Kent [14] is unfortunately quite limited (in his work, Kent [14] reported only the equations for the partial pressure for each phase, the experimental details remaining unpublished).

As shown in Figure 4 our results are in agreement with those by Kent [14], indicating that the dioxide has with no doubt the highest partial pressure. The total vapour pressure data reported in our work are consistent as well with the study Kent [14]. But as shown in Figure 8, also the other studies [7-13], including Battles *et al.* [13], agree well with our results, with the exception of Mulfort and Holley [7].

With respect to the vapour speciation in the (Pu_2O_3-PuO_{2-x}) two-phase domain our observations agree with the mass spectrometric study by Battles *et al.* [13] that PuO(g) is major contributor of the vapour composition. For the total vapour pressure a reasonable agreement between the experimental studies [8,11-13,16] is observed (Figure 9), which is confirmed by our results.

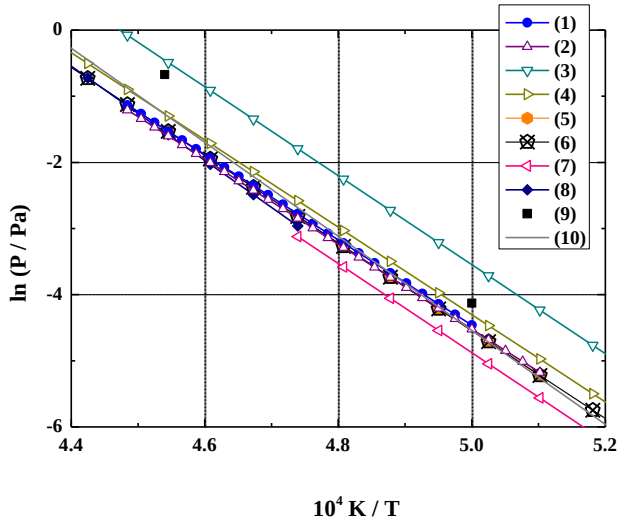

Figure 8. Total vapour pressure results above plutonium dioxide samples. (1): this study, measurements over $PuO_{1.834}$ in a W cell. (2): this study, measurements over $PuO_{1.834}$ in an Ir cell. (3): data by Mulfort and Holley [7]. (4): data by Pascard [10]. (5): data by Kent [14]. (6): data by Battles *et al.* [13]. (7): data by Ackermann *et al.* [8]. (8): data by Messier [11]. (9): data by Ohse [12]. (10): assessed data by Guéneau *et al.* [5].

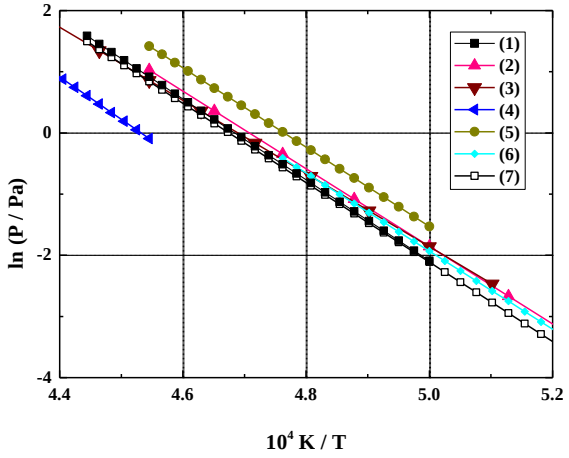

Figure 9. Total vapour pressure results for the (Pu_2O_3-PuO_{2-x}) phase field. (1): this study, measurements over ($Pu+PuO_2$) in a Ta cell. (2): data by Ackermann *et al.* [8]. (3): data by Battles *et al.* [13]. (4): data by Messier [11]. (5): data by Ohse [12]. (6): data by Phipps [17]. (7): data by Guéneau *et al.* [5].

The results of the mass spectrometric measurements (at 40 eV) of plutonium dioxide in oxidising conditions in the ThO_2 cell are shown in Figure 10. A significant difference between vacuum and oxygen conditions is observed, indicating that a shift in composition occurred and the variation of the PuO_2 pressure with temperature is dependent on the composition of the condensed phase. In contrast, the vapour pressure of NpO_2 does not change under similar conditions [22]. The slightly higher PuO_2^+ signal observed in oxygen (Figure 7) compared to the measurements in vacuum (Figure 3) at similar temperature, indicates that the sample clearly has a higher O/Pu ratio.

The vapour pressure resulting from the measurement in vacuum in thoria cell approach the value reported by vaporisation in W or Ir cells (in vacuum) above $PuO_{1.834}$ (shown in section 3.1, Figure 4) and we thus assume that the results refer to a close substoichiometric composition.

The results of Pardue and Keller [15] who carried out vapour pressure measurements by means of transpiration method in oxygen, air and argon flux are difficult to be quantitatively compared to the present study. The data from that study for the temperature range of (1723 to 2048) K are very scattered (Figure 10 - insert graph). Furthermore those performed

under 1 atm of O_2, attributed to stoichiometric dioxide, are about one order of magnitude lower than our results.

The PuO_3^+ vapour species, reported by Ronchi *et al.* [16], was not detected neither in the experiments in oxidative conditions nor in vacuum conditions. Ronchi *et al.* [16] performed mass spectrometric measurements over PuO_2 and $(U,Pu)O_2$ in vacuum and oxidative conditions by introducing CO_2 gas into the Knudsen cell, and suggested that the formation of plutonium trioxide vapour is due to a chemical process involving oxygen absorption of the sample. Although the imposed oxygen pressure was higher in our work, we did not detect PuO_3. However, the signal-to-noise ratio in our experiments was about one order of magnitude lower than in the work of Ronchi *et al.* [16]. The question whether PuO_3(g) must be excluded as an equilibrium vapour species could therefore not be answered with certainty, and requires a dedicated experiment.

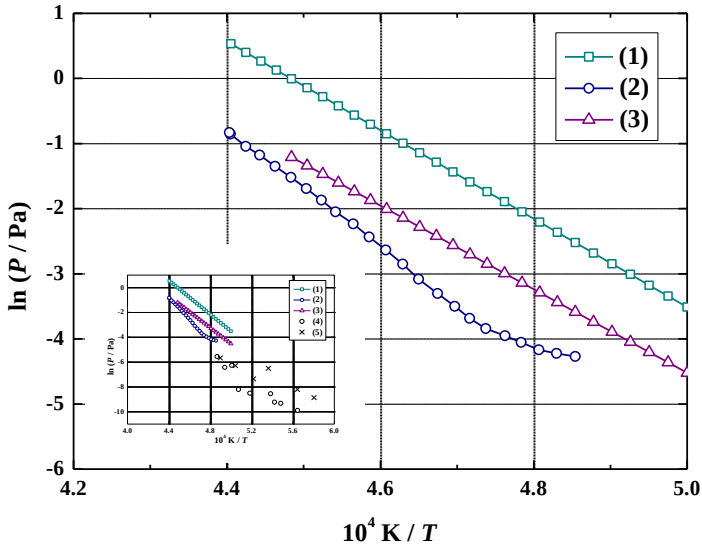

Figure 10. The total vapour pressure results of PuO_2 in ThO_2 cell from this study. (1) oxidative conditions. (2) in vacuum. (3): over $PuO_{1.834}$ in Ir cell. (4) and (5) data by Pardue and Keller [15] by transpiration method from measurements in oxygen and air streams, respectively.

4.4.2 Ionisation and dissociation energies

The ionisation energy (IE) and dissociation energy (DE) values deduced from the ionisation efficiency curve measurements are given in Tables 1 and 2 together with available literature data [33,36-38]. Good agreement is generally found. The ionisation potential of the neutral plutonium atom equal to 6.0262(1) eV was determined by two- and three-step resonance photoionisation observation of the threshold of ionisation and of Rydberg series by Worden *et al.* [33]. A very close value of 6.1 eV has been measured by electron impact high temperature mass spectrometry [32]. In this last work [32] the IEs for PuO and PuO_2 have been reported and adjusted in a later publication [35] by the same authors to 6.2 and 6.6 eV, respectively. These values [35] were in better agreement with the data by Santos *et al.* [36] and Gibson *et al.* [37] who performed Fourier transform ion cyclotron resonance (FTICR) mass spectrometric measurements on atomic and molecular actinide ions and neutrals (Table 1).

Table 1. Ionisation energy (IE) values for plutonium, plutonium monoxide and dioxide: comparison between this work and existing literature data.

Species	IE (this work); eV	IE (literature); eV
Pu	6.0 ± 0.3	6.0262(1) [33]; 6.1 [32]
PuO	6.4 ± 0.3	6.1±0.2 [38]; 6.2 [35]; 6.6 [32]
PuO_2	$8.5^{(*)}$	6.6 [35]; 7.03 ± 0.12 [36,37]; 10.1 [32]

$^{(*)}$ apparent value; it could not be determined accurately due to high background.

The dissociation energy (DE) values for PuO_2 into PuO^+ and Pu^+, and PuO into Pu^+ were measured for the first time by Capone *et al.* [32] by electron ionisation mass spectrometric method. The DE values were derived from the summation of the bond dissociation energy BDE(PuO^+-O), BDE(Pu^+-O), respectively, or the BDE(PuO-O), BDE(Pu-O), respectively, with the IE values for the corresponding involved species. As shown in Table 2 these values are in good agreement with the current results, measured with the same equipment. From the ionisation energy of PuO and the dissociation energy of (Pu^+-O), derived from FTICR mass spectrometric measurements by Gibson *et al.* [38] and Santos *et al.* [36], respectively, the estimated dissociative ionisation energy of PuO into Pu^+ has to be larger than 12.65

eV. This estimated value agrees well with 13.00 eV found in our study. A good agreement with the work of Santos *et al.* [36] is also obtained for the dissociative ionisation energy of PuO_2 into Pu^+ (Table 2).

Table 2. Dissociation energy (DE) values for PuO_2 and PuO: comparison between this work and estimated values from literature, as explained in the text.

Dissociative ionisation process	DE (this work); eV	DE (literature); eV
$PuO_2+e^-\rightarrow PuO^+ +O+2\cdot e^-$	12.5 ± 0.6	12.80 [32]; 12.41 ± 0.23 [36]
$PuO_2+e^-\rightarrow Pu^+ +2\cdot O+2\cdot e^-$	19.0 ± 1	19.20 [32]; ≥ 18.96 [36]
$PuO+e^-\rightarrow Pu^+ +O+2\cdot e^-$	13.0 ± 0.6	13.00 [32]; ≥ 12.65 [36,38]

4.4.3 Vapour pressure as a function of the O/Pu ratio: comparison to the data by Ohse [12]

An extensive study has been performed by Ohse [9,12] (together with Ciani [9]) on the vapour pressure of substoichiometric plutonium oxides. The later extensive work [12] is less known to the public, the data being published in a semi-annual report of the Institute for Transuranium Elements.

Ohse [9,12] investigated the substoichiometric range of plutonium oxide for a wide composition range from O/Pu = 1.45 to 1.97 using an effusion technique in W and Ta cells combined with high-temperature thermal analysis. Figure 11 shows the total pressure-composition diagram for two isotherms at 2000 K and 2200 K, which indicate an univariant behaviour in the two-phase region of O/Pu = 1.50 to 1.61, and a bivariant behaviour in the single phase field from O/Pu = 1.61 to 2.00.

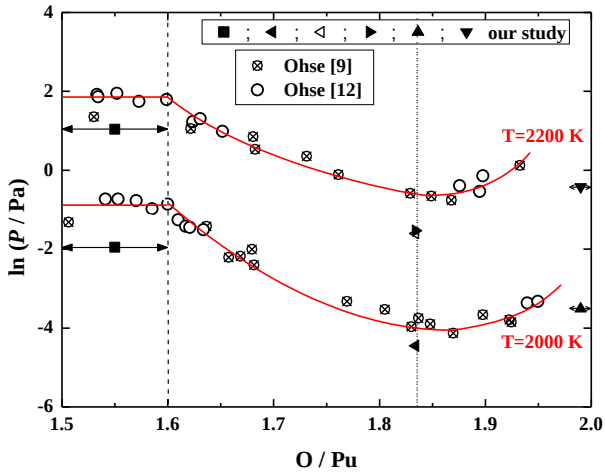

Figure 11. The total vapour pressure data from Ohse [9,12] for T = 2000 K and T = 2200 K (crossed [9] and empty [12] circles) as a function of the stoichiometry. Comparison to our study in the two-phase domain for which O/Pu varies between 1.5 and 1.6, for O/Pu = 1.834 and for the measurements in high purity oxygen flow when O/Pu = 1.98.

The initial rapid change of the starting composition at $PuO_{2.00}$ during annealing has been assumed in all previous studies reported in this paper. Before congruency was attained, a strong preferential loss of oxygen occurred in all cases, for which the kinetics of oxygen loss appeared to be parabolic. This behaviour is therefore emphasised by the oxygen pressure which becomes steep around O/Pu approaching 2.00. A slight increase of the vapour pressure of the plutonium bearing species above the congruent vaporisation was proved by Ohse [9,12] with experimental data. The reported results [9,12] indicated a decrease of the vapour pressure from both phase boundaries at O/Pu = 2.00 and 1.61, respectively, with a minimum around the congruent composition, for which O/Pu = 1.86 at 2000 K and O/Pu = 1.84 at 2200 K. Our pressure results are consistent within one order of magnitude with the absolute data by Ohse [9,12]. For O/Pu close to 2.00, a reasonable agreement is observed with our measurements performed in ThO_2 cell in oxidative conditions (Figure 11).

4.4.4 Comparison to the CALPHAD model for the Pu-O system

The results from this study can be compared to the recent assessment of (plutonium+oxygen) system by Guéneau *et al.* [5,6] which describes the (O+Pu) binary system using the CALPHAD method together with the available thermodynamic data of all the phases, the phase diagram, the oxygen potential and the vapour pressure data versus O/Pu ratio and temperature. The thermodynamic functions of the gaseous species were taken from the database by Glushko *et al.* [39]. The reported results are in good agreement with the thermodynamic analysis by Ackermann *et al.* [8] for the PuO_{2-x} phase.

Figure 12 shows the total vapour pressure as a function of the O/Pu ratio calculated from the Pu-O model [5,6] for T = 2000 K (Figure 12(a)) and T = 2200 K (Figure 12(b)). The assessed total pressure, P_{tot}(Pu), refers to the sum of the plutonium bearing species: Pu, PuO and PuO_2 species, and P_{tot} = P_{tot}(Pu)+ P(O)+ $P(O_2)$, the latter calculation with the aim to emphasize the congruent composition. The values by Ackermann *et al.* [8] and Battles *et al.* [13] are also included (Figures 12(a) and (b)). Our results for the total pressure (with the major contribution from PuO) in the two-phase domain and for congruent vaporisation composition (O/Pu = 1.834) in W and Ir cells agree well with the assessed data from the CALPHAD model [5,6]. However, the other partial pressure values agree within one order of magnitude. Our results for the congruent composition are within close values with the model.

The results of the measurements of plutonia in the YSZ/ThO_2 cell are found to be higher than the calculated total vapour pressure (Figure 12), in agreement with the work of Ohse [9,12], as discussed in the previous section. This indicates that the model developed for the Pu-O system may need adjustment for the O/Pu range close to 2.00.

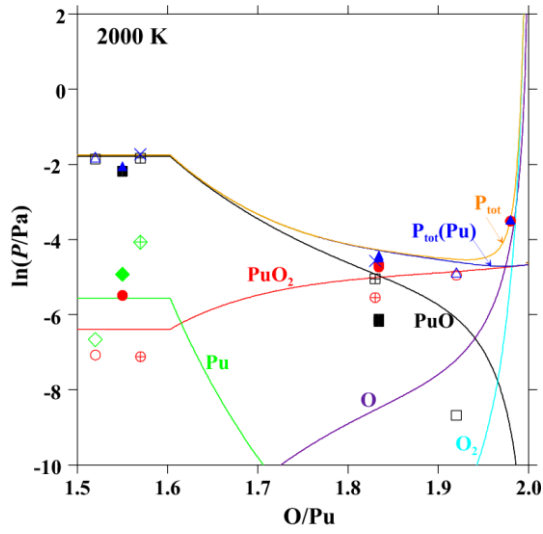

(a)

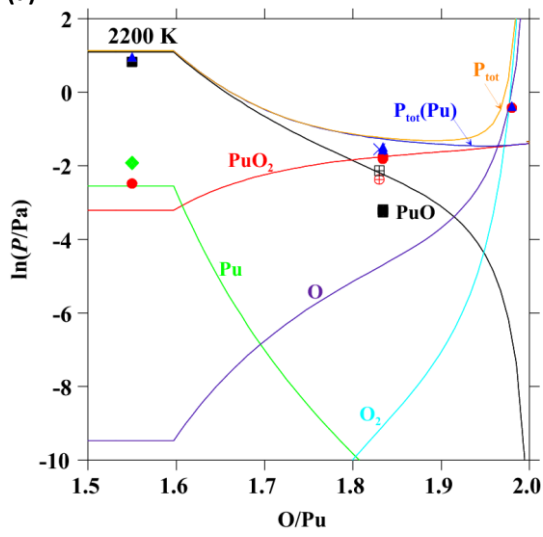

(b)

Figure 12. The total and partial vapour pressure data of Pu (green), PuO (black), and PuO_2 (red) as a function of the O/Pu ratio given by the CALPHAD model [5,6] for the Pu-O system at T = 2000 K **(a)** and T = 2200 K **(b)**. The calculated P_{tot}(Pu) and P_{tot} from the model [5,6] correspond to $P_{tot}(Pu) = P(PuO_2) + P(PuO) + P(Pu)$ and $P_{tot} = P_{tot}(Pu) + P(O) + P(O_2)$. The results from this study are represented by the full symbols. (▲): total pressure, as a sum of $P(PuO_2) + P(PuO) + P(Pu)$; (●): PuO_2 partial pressure; (■): PuO partial pressure; (♦): Pu partial pressure; crossed symbols: data by Battles *et al.* [13] for $P(PuO_2)$, $P(PuO)$ and $P(Pu)$, respectively. Open symbols: data by Ackermann *et al.* [8] for $P(PuO_2)$, $P(PuO)$ and $P(Pu)$, respectively.

4.4.5 The enthalpy of formation of PuO_2(g)

Because we have demonstrated that the measurements of plutonia in the YSZ/ThO_2 cell refer to the reaction:

$$PuO_2(s) = PuO_2(g), \quad (24)$$

the results can be analysed to obtain the enthalpy of sublimation of PuO_2, neglecting the eventual slight deviation from stoichiometry of the solid phase, which seems justified. Using the assessed thermodynamic data for PuO_2(cr) and PuO_2(g) by Konings *et al.* [40], we obtain $\Delta_{sub}H°$(298.15 K) = (627± 7) kJ·mol^{-1} by second law analysis and $\Delta_{sub}H°$(298.15 K) = (616 ± 6) kJ·mol^{-1} by third law analysis, the uncertainties including the estimated uncertainties of the thermal functions of the solid and gaseous phase. The agreement between the two values is good, and the third-law analysis shows almost no temperature dependence. When combined with the enthalpy of formation of PuO_2(cr), the enthalpy of formation of PuO_2(g) can be derived from these values as $\Delta_fH°$(298.15 K) = -(428 ± 7) kJ·mol^{-1} and $\Delta_fH°$(298.15 K) = -(440 ± 7) kJ·mol^{-1}, respectively.

These values are significantly more negative than the values recommended by Glushko *et al.* [39], $\Delta_fH°$(298.15 K) = -(412 ± 20) kJ·mol^{-1}, and Cordfunke *et al.* [41], $\Delta_fH°$(298.15 K) = -(410 ± 20) kJ·mol^{-1}. The values in these assessments have been derived from the work of Ackermann *et al.* [8] for $PuO_{1.92}$, based on the PuO_2 partial pressure and the integral data for PuO_2(cr). If we assume that PuO_2 is the predominant vapour species, and re-analyse the results of Ackermann *et al.* [8] with the same auxiliary data for the solid and gas phases as used in our work, we obtain $\Delta_fH°$(298.15 K) = -425 kJ·mol^{-1} by second-law analysis, in poor agreement with the third-law value, $\Delta_fH°$(298.15 K) = -547 kJ·mol^{-1}.

Figure 13 shows the result of a calculation of the vapour pressure and composition at T = 2000 K using the model from Guéneau *et al.* [5,6] adjusted only for a lower value of the enthalpy of formation of gaseous PuO_2, $\Delta_fH°$(PuO_2(g), 298.15 K) = -428 kJ·mol^{-1}, which is our value derived from the second law analysis.

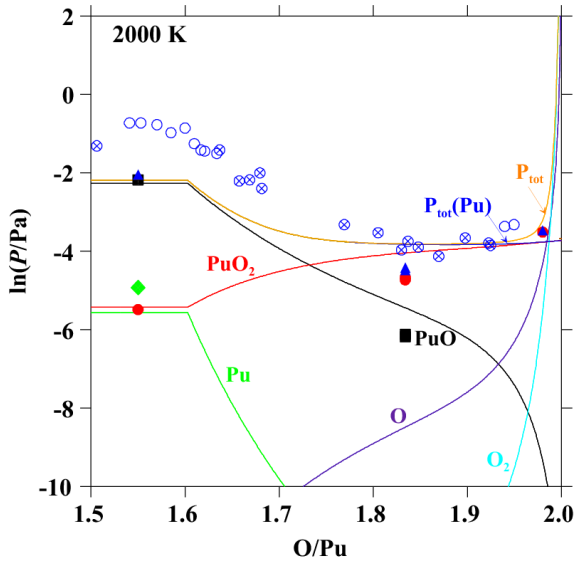

Figure 13. The total and partial vapour pressure data of Pu (green), PuO (black), and PuO_2 (red) as a function of the O/Pu ratio given by the CALPHAD model [5,6] for the Pu-O system at T = 2000 K when $\Delta_f H°(PuO_2(g), 298.15\ K) = -(428 \pm 7)$ kJ·mol^{-1} and $\Delta_f H°(PuO(g), 298.15\ K) = -53.9$ kJ·mol^{-1}. The calculated $P_{tot}(Pu)$ and P_{tot} from the model [5] correspond to $P_{tot}(Pu) = P(PuO_2) + P(PuO) + P(Pu)$ and $P_{tot} = P_{tot}(Pu) + P(O) + P(O_2)$. Crossed circles: data by Ohse and Ciani [9]; open circles: data by Ohse [12]; other symbols: our work as (▲): total pressure, as a sum of $P(PuO_2) + P(PuO) + P(Pu)$; (●): PuO_2 partial pressure; (■): PuO partial pressure; (♦): Pu partial.

The values corresponding to the partial pressures function of the O/Pu ratio at T = 2000 K are reported in Table 3. In the two-phase domain an increase is observed for the assessed PuO_2 pressure. In order to keep the $P(PuO)/P(PuO_2)$ ratio, the enthalpy of formation for PuO(g) was slightly amended to $\Delta_f H°(PuO(g), 298.15\ K) = -53.9$ kJ·mol^{-1}, which is the value that best represents the current results. This value is within the uncertainty of -(61.9 ± 25) kJ·mol^{-1} as recommended by Glushko *et al.* [39] and used in the assessment for the Pu-O model. The total pressure decreases as the stoichiometry becomes closer to O/Pu = 2.00. For O/Pu = 1.834 the total pressure is higher comparing to the value obtained in the previous analysis (Figure 12(a)). Furthermore at O/Pu ≈ 2.00 the assessed total pressure from the model [5,6] is in better agreement with our value obtained from the measurement in oxygen in the YSZ/ThO_2 cell. As only one parameter was changed in the whole model (we lowered the value $\Delta_f H°(PuO_2(g), 298.15\ K)$

according to our findings) the model does not follow the increase in total pressure for the O/Pu approaching 2.00, as found by us as well as by Ohse [12]. Further adjustments of the model are required for a better description of the gaseous phase at compositions close to the stoichiometric dioxide.

Table 3. The partial pressures values (in Pa) as a function of the O/Pu ratio at T = 2000 K, calculated using the model from Guéneau *et al.* [5,6] adjusted only for a lower value of the enthalpy of formation of gaseous PuO_2, $\Delta_f H°(PuO_2(g), 298.15\ K) = -428\ kJ \cdot mol^{-1}$.

O/Pu ratio	P(Pu)	P(PuO)	P(PuO_2)	P(O)	P(O_2)
1.5 - 1.6	$3.83 \cdot 10^{-3}$	$1.04 \cdot 10^{-1}$	$4.39 \cdot 10^{-3}$	$2.15 \cdot 10^{-6}$	$1.02 \cdot 10^{-10}$
1.65	$3.67 \cdot 10^{-4}$	$4.20 \cdot 10^{-2}$	$7.54 \cdot 10^{-3}$	$9.11 \cdot 10^{-6}$	$1.83 \cdot 10^{-9}$
1.70	$5.44 \cdot 10^{-5}$	$1.95 \cdot 10^{-2}$	$1.09 \cdot 10^{-2}$	$2.85 \cdot 10^{-5}$	$1.79 \cdot 10^{-8}$
1.75	$1.21 \cdot 10^{-5}$	$1.04 \cdot 10^{-2}$	$1.39 \cdot 10^{-2}$	$6.80 \cdot 10^{-5}$	$1.02 \cdot 10^{-7}$
1.80	$3.53 \cdot 10^{-6}$	$6.06 \cdot 10^{-3}$	$1.54 \cdot 10^{-2}$	$1.36 \cdot 10^{-4}$	$4.09 \cdot 10^{-7}$
1.85	$1.15 \cdot 10^{-6}$	$3.65 \cdot 10^{-3}$	$1.81 \cdot 10^{-2}$	$2.52 \cdot 10^{-4}$	$1.40 \cdot 10^{-6}$
1.90	$3.11 \cdot 10^{-7}$	$1.98 \cdot 10^{-3}$	$1.97 \cdot 10^{-2}$	$5.06 \cdot 10^{-4}$	$5.64 \cdot 10^{-6}$
1.95	$2.46 \cdot 10^{-8}$	$5.84 \cdot 10^{-4}$	$2.16 \cdot 10^{-2}$	$1.88 \cdot 10^{-3}$	$7.82 \cdot 10^{-5}$
1.96	$1.02 \cdot 10^{-8}$	$3.79 \cdot 10^{-4}$	$2.21 \cdot 10^{-2}$	$2.96 \cdot 10^{-3}$	$1.93 \cdot 10^{-4}$
1.97	$3.09 \cdot 10^{-9}$	$2.11 \cdot 10^{-4}$	$2.25 \cdot 10^{-2}$	$5.43 \cdot 10^{-3}$	$6.50 \cdot 10^{-4}$
1.98	$4.59 \cdot 10^{-10}$	$8.23 \cdot 10^{-5}$	$2.31 \cdot 10^{-2}$	$1.42 \cdot 10^{-2}$	$4.48 \cdot 10^{-3}$
1.99	$2.28 \cdot 10^{-11}$	$1.85 \cdot 10^{-5}$	$2.36 \cdot 10^{-2}$	$6.46 \cdot 10^{-2}$	$9.19 \cdot 10^{-2}$
2.00	$2.42 \cdot 10^{-20}$	$6.09 \cdot 10^{-10}$	$2.40 \cdot 10^{-2}$	$2.00 \cdot 10^{+3}$	$8.84 \cdot 10^{+7}$

4.5 Summary and Conclusions

Knudsen cell mass spectrometric measurements on plutonium oxide have been performed for different experimental conditions. The ionisation efficiency curves were recorded for plutonium bearing oxide ionic species to provide insight into the vapour composition. The partial vapour pressures over Pu-O phase fields have been derived taking into account the dissociation processes occurred up to 40 eV, energy at which the signals were recorded. The PuO_3^+ species was not observed among the equilibrium vapour species for the vaporisation of the studied samples.

Good agreement with available literature data was found in terms of the total pressure. In the (Pu_2O_3-PuO_{2-x}) two-phase region the system we found PuO as the dominant species in the vapour. For the congruent vaporisation composition ($PuO_{1.834}$) our study showed PuO_2 to be the main vapour species. This is consistent with the mass spectrometric study of Kent [14]. The total pressure obtained is in good agreement with the effusion studies [7-12] in which the data were assessed based on the assumption of PuO_2 being the dominant vapour species. The measurement in oxidative conditions, for which the condensed phase composition corresponded to a O/Pu ratio very close to 2.00, showed a significant difference with the results in vacuum, indicating that the variation of the PuO_2 pressure with temperature is dependent of the composition of the condensed phase in the studied range.

A comparison to the CALPHAD model of the (Pu+O) system by Guéneau *et al.* [5,6], which is in good agreement with the thermodynamic analysis by Ackermann *et al.* [8] for the whole PuO_{2-x} composition, revealed a reasonable consistency with our experiments, except for the conditions close to 2.00. For this composition range we agree with the findings of Ohse [9,12], who reported that the total pressure increased for O/Pu between 1.85 and 2.00. Our results showed that these measurements can be interpreted to apply to the $PuO_2(cr) = PuO_2(g)$ equilibrium and do not need to be corrected for the PuO(g) contribution, as suggested by Ackermann *et al.* [8]. Overall, in terms of absolute total pressure, our results are in close agreement to the model, the partial pressure values slightly disagree, however with a consistent major vapour species contribution for each of the phases.

4.6 References

[1] D.R. Olander, Fundamental aspects of nuclear reactor fuel elements, Technical Information Center, Energy Research and Development Administration, Oak Ridge, Tenn. and Springfield, Va., 1976.

[2] T.D. Chikalla, C.E. McNeilly, R.E. Skavdahl, J. Nucl. Mater. 12 (1964) 131.

[3] The Plutonium-Oxygen and Uranium-Plutonium-Oxygen Systems: A Thermochemical Assessment, Technical Report Series No. 79, IAEA, Vienna, 1967.

[4] H.A. Wriedt, Bull. All. Ph. Dia. 11 (1990) 184.

[5] C. Guéneau, C. Chatillon, B. Sundman, J. Nucl. Mater. 378 (2008) 257.

[6] C. Guéneau, N. Dupin, C. Martial, J.C. Dumas, S. Gossé, S. Chatain, B. Sundman, To be submitted to the J. Nucl. Mater. (2011).

[7] R.N.R. Mulford, C.E. Holley, Report LA-DC-8266, USAEC, Los Alamos Scientific Laboratory, 1966.
[8] R.J. Ackermann, R.L. Faircloth, M.H. Rand, J. Phys. Chem. 70 (1966) 3698.
[9] R.W. Ohse, C. Ciani, Thermodynamics of Nuclear Materials, IAEA, Vienna (1967) 545.
[10] R. Pascard, Paper submitted to the Panel on Thermodynamics of Plutonium Oxides: The Plutonium-Oxygen and Uranium-Plutonium-Oxygen Systems: A Thermochemical Assessment, Technical Report Series No. 79, IAEA, Vienna, 1967.
[11] D.R. Messier, J. Am. Ceram. Soc. 51 (1968) 710.
[12] R.W. Ohse, Progress Report No. 5, European Institute for Transuranium Elements, Karlsruhe, Germany, 1968.
[13] J.E. Battles, J.W. Reihus, W.A. Shinn, Report ANL-7575, USAEC, Argonne National Laboratory, 1969.
[14] R.A. Kent, Thermodynamic Analysis of MHW Space Electric Power Generator, Los Alamos Scientific Laboratory Report LA-5202-MS, March 1973.
[15] W.M. Pardue, D.L. Keller, J. Am. Ceram. Soc. 17 (1964) 610.
[16] C. Ronchi, F. Capone, J.-Y. Colle, J.-P. Hiernaut, J. Nucl. Mater. 280 (2000) 111.
[17] T.E. Phipps, G.W. Sears, O.C. Simpson, J. Chem. Phys. 18 (1950) 724.
[18] The 'GUM Workbench Pro' software, Version 2.3.2.33 © ’96-’99 by Metrodata Gmbh Germany, distributed and supported by Danish Technological Institute, Denmark.
[19] D. Taylor, Trans. J. Brit. Ceram. Soc. 83 (1984) 32.
[20] C.E. Holley, R.N.R. Mulford, E.J. Huber, E.L. Head, F.H. Ellinger, C.W. Bjorklund, Proc. Second United Nations Int. Conf. Peaceful Uses Atomic Energy 6 (1958) 215.
[21] J.-P. Hiernaut, J.-Y. Colle, R. Pflieger-Cuvellier, J. Jonnet, J. Somers, C. Ronchi, J. Nucl. Mater. 344 (2005) 246.
[22] P. Gotcu-Freis, J.-Y. Colle, J.-P. Hiernaut, R.J.M. Konings, J. Chem. Thermodyn. 43 (2011) 492.
[23] J. Drowart, C. Chatillon, J. Hastie, D. Bonnell, Pure Appl. Chem. 77 (2005) 683.
[24] M.G. Inghram, J. Drowart, High Temperature Technology, McGraw-Hill, New York, 1959.
[25] J.B. Mann, Recent developments in Mass Spectrometry, in: Proceedings of the Conference on Mass Spectroscopy, Tokyo, K. Ogata, T. Hayakawa (Eds.), University Park Press, Baltimore, MD, 1970.
[26] D.W. Bonnell, J.W. Hastie, Program SIGMA, A Fortran code for computing atomic ionisation cross-sections, NIST, Gaithersburg, MD, unpublished work, 1990-1997.
[27] J.B. Mann, J. Chem. Phys. 46 (1967) 1646.
[28] J.W. Otvos, D.P. Stevenson, J. Amer. Chem. Soc. 78 (1956) 546.
[29] R.T. Grimley, The Characterisation of High Temperature Vapors, J.L. Margrave (Ed.), John Wiley&Sons, Inc. New York, 1967.
[30] R. Hultgren, R.L. Orr, P.D. Anderson, K.K, Kelley, Selected Values of Thermodynamic Properties of Metals and Alloys, John Wiley & Sons, Inc. 1963.
[31] D.J. Santeler, J. Vac. Sci. Technol. A 4 (1986) 338.
[32] F. Capone, J.-Y. Colle, J.-P. Hiernaut, C Ronchi, J. Phys. Chem. A 103 (1999) 10899.

[33] E.F. Worden, L.R. Carlson, S.A. Johnson, J.A. Paisner, R.W. Solarz, J. Opt. Soc. Am. B 10 (1993) 1998.
[34] L. Dumas, C. Chatillon, E. Quesnel, J. Crys. Growth 222 (2001) 215.
[35] F. Capone, J.-Y. Colle, J.-P. Hiernaut, C. Ronchi, J. Phys.Chem. A 109 (2005) 12054.
[36] M. Santos, J. Marcalo, A. Pires de Matos, J.K. Gibson, R.G. Haire, J. Phys. Chem. A 106 (2002) 7190.
[37] J.K. Gibson, M. Santos, J. Marcalo, J. Paulo Leal, A. Pires de Matos, R.G. Haire, J. Phys. Chem. A 110 (2006) 4131.
[38] J.K. Gibson, R.G. Haire, J. Marçalo, M. Santos, A. Pires de Matos, J.P. Leal, J. Nucl. Mater. 344 (2005) 24.
[39] V.P. Glushko, L.V. Gurvich, I.V. Veits, V.A. Medvedev, G.A. Khachkuruzov, V.S. Yungman, G.A. Bergman, Thermodynamic Properties of Individual Substances, V.P. Glushko (Ed.), Vols. 1 – 4, Nauka, Moscow, 1978 - 1982.
[40] R.J.M. Konings, O. Benes, D. Manara, D. Sedmidubsky, L. Gorokhov, V.S. Iorish, The thermodynamic properties of f-elements. Part II. The Lanthanide and Actinide Oxides, J. Phys. Chem. Ref. Data, submitted.
[41] E.H.P. Cordfunke, R.J.M. Konings, P.E. Potter, G. Prins, M.H. Rand, Thermochemical data for reactor materials, fission product, E.H.P. Cordfunke, R.J.M. Konings (Eds), North-Holland, Amsterdam, 1990.

Chapter 5

The vaporisation behaviour of americium dioxide by use of mass spectrometry

Abstract

*The vaporisation behaviour of americium dioxide in vacuum at high temperatures up to 2400 K has been studied. A Knudsen cell coupled with a mass spectrometer was used to perform vapour pressure measurements. The ionisation efficiency curves of Am^+, AmO^+ and AmO_2^+ were simultaneously recorded. Appearance potentials of the key molecular species were determined by varying the energy of the ionising electrons at constant temperature. The partial and total vapour pressures of the oxides have been measured as a function of the temperature. The results on the vapour pressure of pure americium dioxide samples are discussed together with the available literature data on plutonium dioxide containing small amounts of americium. Additional measurements have been performed on a mixed dioxide sample of plutonium containing 6.1 wt% americium.**

*This chapter is reprinted with kind permission of Elsevier: "The vaporisation behaviour of americium dioxide by use of mass spectrometry. P. Gotcu-Freis, J.-Y. Colle, J.-P. Hiernaut, R.J.M. Konings. Journal of Nuclear Materials 409 (2011) 194-198".

5.1 Introduction

Partitioning and transmutation (P&T) of americium from spent fuel is considered an attractive waste management option. Currently ^{241}Am, a product of the beta-decay of ^{241}Pu, accumulates in spent fuel or is included in the vitrified high level waste from reprocessing, and subsequently decays by alpha emission ($t_{1/2}$ = 432.2 years) to the long lived ^{237}Np. With the P&T technology ^{241}Am, as well as the ^{243}Am isotope also present in much smaller concentrations spent fuel, can be separated (partitioned) from the spent fuel and then fissioned (transmuted) to produce short-lived fission products, thus helping to reduce the long-term environmental impact of nuclear waste from nuclear power generation. The development of advanced minor actinide bearing fuels for the next generation nuclear reactors is therefore essential and demands a better knowledge of the properties of the complex fuel materials that contain americium.

Vapour pressure is a very important thermophysical property of nuclear fuel for predicting the possible behaviour under normal operation and accident conditions. An ideal tool for having insight into the vapour composition is mass spectrometry. The most important (and most widely used) method for the study of equilibrium vapours is Knudsen effusion mass spectrometry in which a Knudsen cell is coupled with a mass spectrometer to determine the partial vapour pressure of the different components of the vapour.

The actinide oxides show complex vaporisation behaviour that is reasonably well characterised for the uranium-oxygen system (see e.g. the assessment by Guéneau *et al.* [1]) but hardly for the minor actinides. Very little is known about the vaporisation behaviour of AmO_{2-x} and the stability of the americium oxides in the gaseous phases. Approximate data on vapour pressure of americium oxides exist only from the measurements of plutonium oxides containing very small amounts of americium [2,3] using Knudsen effusion method combined with collection on platinum targets. In the view of extreme dilution Raoult's approximation was used to derive the vapour pressure of AmO_{2-x} in these studies. More recently, Fourier transform ion cyclotron resonance (FT-ICR) mass spectrometric studies of the thermochemistry of americium oxides in the gas-phase [4] were performed. Santos *et al.* [4] determined the ionisation energies for AmO

and AmO_2 by two types of experiments: change-transfer "bracketing" with AmO_2^+ and AmO^+ reactivity with dienes. The ionisation energy value for AmO^+ was adjusted in a later publication by Gibson *et al.* [5] for the actinide oxide series. Theoretical studies for AmO using multiconfigurational relativistic quantum chemical methods by Kovacs *et al.* [6] provided a value for the ionisation energy (IE) that is in close agreement. No direct measurements were carried out to yield the dissociation energies (DEs) for AmO_2 into AmO^+ and Am^+, and AmO into Am^+. The values for the oxygen dissociation energy of neutral and ion americium oxide bearing species considered as bond dissociation energy (BDE) were estimated in the same study by Santos *et al.* [4] by ion cyclotron resonance (ICR) mass spectrometry. The BDE of (Am-O) bond is consistent with the value reported by Haire [7] based on correlation between dissociation energy and electronic configuration, but a lower value was computed by Kovacs *et al.* [6] using quantum chemical methods.

In the present paper we report the first experimental results for the vapour pressure above pure americium dioxide samples using high temperature Knudsen cell mass spectrometry. Additional measurements of the vapour pressure above a mixed oxide sample of plutonium dioxide with a small amount of americium were included and discussed together with existing literature data. Furthermore ionisation efficiency curves for Am^+, AmO^+ and AmO_2^+ were recorded to provide insight into the dissociative ionisation processes and the composition of the gaseous phase, which under Knudsen conditions, is in equilibrium with the condensed phase.

5.2 Samples and experimental method

For the present study samples of americium dioxide, in the form of high purity powder from Oak Ridge National Laboratory, were used. Due to the high radioactivity of the samples, their manipulation was carried out in nitrogen atmosphere glove boxes, equipped with additional lead-glass shielding and lead gloves. For safety reasons, considering the state of the sample (fine powder), the amount used for the further measurements was minimised to about 30 mg. Prior the vapour pressure measurements, the samples were annealed to $AmO_{2.00}$ in air up to about 1200 K for few hours as was previously reported by Sari and Zamorani [8].

In addition, measurements were performed on a mixed oxide sample of plutonium-americium, $Pu_{0.939}Am_{0.061}O_{2-x}$. For its fabrication a combination of the external gelation, also known as gel supported precipitation (GSP), and infiltration routes was used, followed by compaction and sintering under Ar/H_2 atmosphere, at 1873 K [9]. An americium nitrate solution with a concentration of 300 ± 1 g(Am)·dm^{-3} has been used for the infiltration step. After infiltration, the obtained spheres were dried at room temperature overnight and thereafter calcined under an air atmosphere to convert the nitrate into oxide. These two last procedures were repeated to obtain the desired concentration. The final Am content (in wt%) was determined by gravimetric analysis before and after the infiltration step, with an absolute accuracy of about 1%. The O/(Pu+Am) ratio obtained by this treatment is estimated to be between 1.75 and 1.85, typical for these sintering conditions [10]. It should, however, be noted that these values are not representative for the temperatures at which the mass spectrometric measurements in this study have been made.

The mass spectrometric measurements on pure americium oxides have been performed in tungsten and iridium Knudsen cells. The measurement on the mixed oxide sample was made in a tungsten cell with an iridium foil (further referred to as W/Ir cell) placed as a sample holder. Iridium foils and cells were used in order to avoid the direct contact between the solid or vapour dioxide sample and the cell material, whereby reactions at high temperature can occur [2,11]. Due to the low amount of samples used final characterisation of the remaining residue was not possible.

The Knudsen cell mass spectrometer assembly was calibrated by vaporising a known quantity of silver together with the sample. The temperature of the Knudsen cell assembly was calibrated by measurement of the melting points of standard materials (Zn, Cu, Fe, Pt, Al_2O_3). Further details of the experimental technique were presented in another publication [12]. The experimental temperature was increased stepwise by 10 K/min up to 2200 K for the measurements on pure americium oxide and higher (up to 2400 K) for the measurements carried on the mixed oxide sample. For all the samples the vapour pressure data were determined while the temperature was systematically increased.

For the study on the dioxide sample several isothermal measurements were carried on. Ionisation efficiency curves were measured at a

temperature at which the americium bearing oxide ions had a sufficiently high signal. While the temperature was kept constant the energy of ionising electrons was increased stepwise by 0.5 eV. The offset between the applied cathodic voltage and the effective electron energy spectrum was solved as described previously [13].

The first ionisation potentials of silver and a known gas composition of krypton, helium, argon, neon and xenon have been taken as standards. The energy range covered was from 7.5 to 24.5 eV. The results showed a good linear dependence (the regression coefficient is equal to 0.998) for extrapolating the scale up to 40 eV. The errors quoted in this paper are 1σ standard deviation [13].

5.3 Experimental results

5.3.1 Ionisation efficiency curves

The mass spectrometric measurements were carried out using ionisation energy of 40 eV. The ions observed by electron impact technique were AmO_2^+, AmO^+, Am^+. Measurements of the ionisation efficiencies were made for different isotherms, for which the resulting mass spectrometric signals were measured as a function of the energy of the ionising electrons. The appearance and dissociation potentials of the key molecular species were determined. The appearance potential is defined as the minimum energy required to produce a given ion and its accompanying neutral fragments from a given molecule, ion, or radical [14], considering both ionisation and dissociation processes. When only ionisation occurs, the appearance potential is called the ionisation potential or ionisation energy (IE), essentially given by the minimum energy required to remove an electron from the neutral molecules, atoms, or radicals.

The mass spectrometric signals were recorded as a function of the energy of ionising electrons for several isotherms up to 2200 K. In Figure 1 results are shown for T = 2175 K. The measured ionisation energy (IE) of AmO^+ was found equal to 6.5 eV. The low IE value of Am^+ equal to 6.0 eV shows that simple ionisation process occurred. The increase in the AmO^+ mass spectrometric signal above 11 eV (Figure 1) probably results from the fragmentation of the AmO_2 species. A slight increase in the Am^+ signal is

observed above 12.5 eV which results from the fragmentation of AmO (with the corresponding inflection on the AmO^+ curve) and above 17.0 eV, which possibly marks the dissociation of AmO_2^+. The shape of the AmO_2^+ curve above 10 eV is determined by the ionisation and fragmentation processes. As the AmO_2^+ signal was very low (only slightly above the background), the sensitivity was not high enough to accurately determine the value for the appearance potential of AmO_2 but a value of about 7.5 eV could be reasonably estimated.

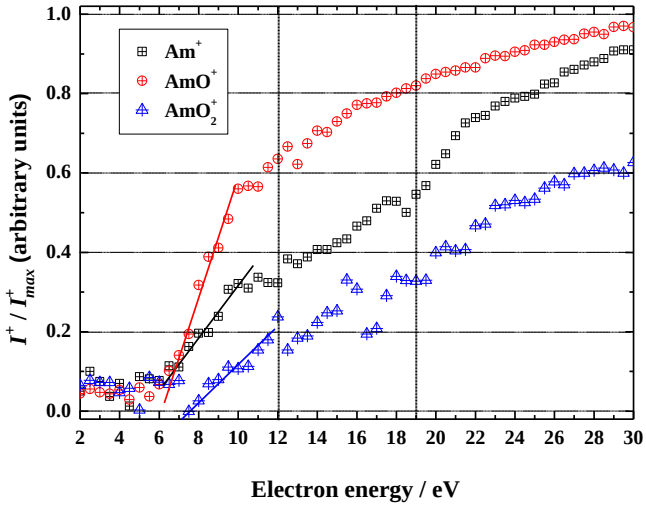

Figure 1. Ionisation and fragmentation efficiency curves of Am^+, AmO^+ and AmO_2^+ from molecules created by ionisation of americium dioxide sample, represented as the ratio I^+ / I^+_{max} measured at 2175 K.

5.3.2 Total vapour pressure

The total pressure evolution was monitored in the temperature range from 2000 to 2200 K. Isothermal measurements above 2100 K registered constant pressure in relative short time. The total pressure measurements in the tungsten cell can be represented by the equation:

$$\ln(P/\text{Pa}) = (27.56\pm0.14) - (66011\pm310) \cdot (T/\text{K})^{-1}, \quad (1)$$

The experiment was repeated with same type of americium dioxide sample in an iridium cell for the same temperature range. The coefficients of equation (1) were found slightly higher:

$$\ln(P/\text{Pa}) = (29.15\pm0.74) - (69655\pm634) \cdot (T/\text{K})^{-1}. \quad (2)$$

The total vapour pressure of americium bearing oxide species measured during the vaporisation of the $Pu_{0.939}Am_{0.061}O_{2-x}$ sample in a W/Ir cell (heated stepwise by 10 $K \cdot min^{-1}$) is given by the following equation for the temperature range 2270 to 2400 K:

$$\ln(P/\text{Pa}) = (30.93\pm0.25) - (72737.6\pm820) \cdot (T/\text{K})^{-1}. \quad (3)$$

5.3.3 Partial vapour pressure over pure americium oxide sample

During isothermal measurements at low temperature when the energy of ionising electrons was scanned, constant mass spectrometric signals were observed. The ionisation efficiency curve obtained from electron impact measurements provided insight into the vapour composition and the fragmentation patterns of AmO_2 and AmO were derived. The signal intensities were corrected for all the dissociation processes below 40 eV and the partial pressure of the oxide species as function of the temperature was obtained.

The results show that about 49% of AmO_2 dissociates into AmO and 33% of AmO_2 into Am metal. Hence the final vapour composition is approximately 18% Am, 35% AmO and 47% AmO_2. Figure 2 shows the measured total vapour pressure data together with the partial pressures observed at 40 eV and the assessed partial pressures for the dissociation processes involved up to 40 eV in the temperature range from 2000 up to 2200 K. Americium dioxide is the major vapour species but is not significantly higher than the monoxide. The metal appears to be about one decade lower than the dioxide.

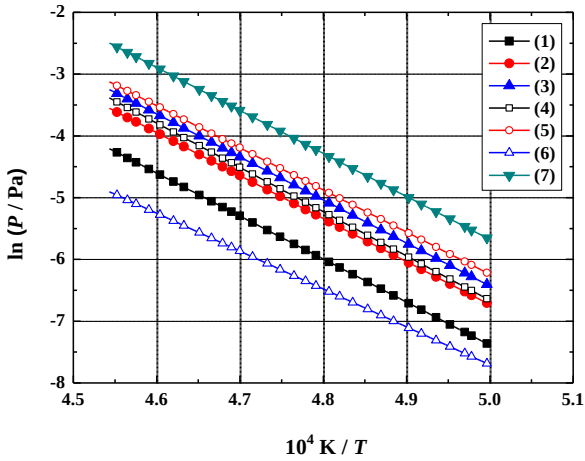

Figure 2. The mass spectrometric partial vapour pressure curves (1-6) above americium dioxide measured in this study under vacuum in an iridium Knudsen cell, against the inverse of the temperature: (1), (2), (3) - of americium, americium monoxide and americium dioxide, respectively, corrected for the dissociation processes; (4), (5), (6) - of americium, americium monoxide and americium dioxide, respectively, observed at 40 eV. (7): total vapour pressure ΣAmO_x^+, with x = 0, 1 and 2, calculated as a sum of partial pressure of americium bearing oxide species.

5.4 Discussion

The comparison between our results and the previous studies can be quantitatively shown only in terms of the total vapour pressure (Figure 3). The literature data for the vapour pressure of americium oxide refer to measurements of plutonium oxides containing very small amounts of americium [2,3]. These measurements were performed in two different cell materials: tungsten and rhenium by Ackermann *et al.* [2] and tungsten by Ohse *et al.* [3], in both cases using the Knudsen effusion method combined with collection on platinum targets. Ackermann *et al.* [2] observed congruent vaporisation for O/Pu = 1.92 ± 0.03 at 2025 K in both cell materials. This value, representing the congruent vaporisation composition in Pu-O system, differ significantly from the other experimental data [3,11,12,15]. Ohse *et al.* [15] reported a lower value for the congruent composition, O/Pu being in the range of 1.89 - 1.84 for temperatures from 1800 K and up to 2200 K. In the view of extreme dilution of the americium in the $(Pu,Am)O_{2-x}$ solid solution Raoult's law was used in both studies to estimate the total vapour pressure above pure americium dioxide.

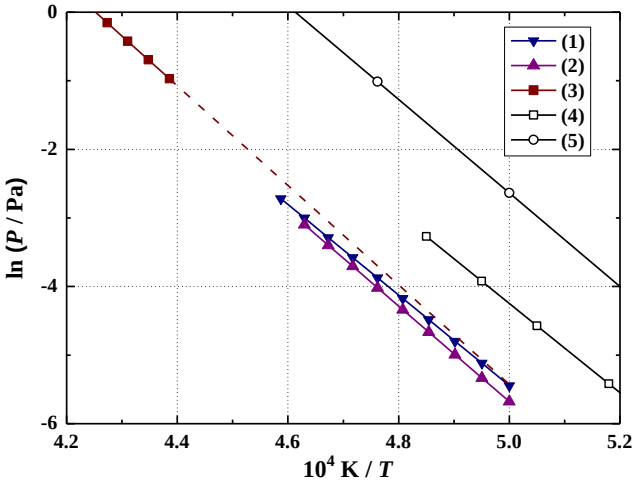

Figure 3. Total vapour pressure of the Am bearing species for different samples. (1) and (2): this study - pure AmO_2 in W and Ir cells, respectively. (3): this study - the vapour pressure measurements of americium oxide bearing species from the vaporisation of $Pu_{0.939}Am_{0.061}O_{2-x}$ sample in W/Ir cell; the dashed line represents the extrapolation to T = 2000 K. (4) and (5) extrapolated from PuO_2 with low americium content using Raoult's law by Ackerman *et al.* [2] and Ohse *et al.* [3], respectively.

In this study we have performed mass spectrometric measurements on pure americium dioxide samples. Figure 3 shows that the results of the present study are slightly lower than those by Ackermann *et al.* [2]. Our data for the vaporisation of the mixed plutonium oxide containing 6.1 wt% Am, for which Raoult's law appears to be justified, extrapolated to T = 2000 K, are in line with the pure dioxide data. The data from Ohse *et al.* [3] are higher by a factor larger than two. In both studies [2,3] the abundance ratio of Am/Pu on the targets was determined by alpha-spectrometry. Since the initial plutonium dioxide sample contained the ^{238}Pu isotope as well, which cannot be discriminated from the ^{241}Am by this technique, Ohse *et al.* [3] derived the ^{238}Pu content from the total alpha activity after Am chemical separation. The measurements were made assuming the O/(Pu+Am) ratio in the solid phase equal to 1.94. An error in evaluation of this ratio or either a wrong estimation of the Am content in the PuO_{2-x} host sample would of course distinctively bring a change in the final absolute americium oxide vapour pressure. Particularly, an underestimation of the Am content would result in an increase in the final americium oxide vapour

pressure. Due to the small amount of the sample used in the current study and its solid state (fine powder) it was not possible to measure the final O/Am composition. However the slopes of the ln (*P*) against 1/*T* curve (representing the enthalpy of vaporisation, $\Delta_{vap}H$) of our measurements are consistent with both literature references [2,3].

The vaporisation of americium dioxide shows a different behaviour compared to other actinide dioxides, i.e. neptunium and even plutonium dioxides at similar temperatures [10,12]. The vapour composition above americium oxide consists of all the three species, AmO, AmO_2 as well as Am, whereas in the case of vaporisation of plutonium and neptunium oxide, the dioxide is the major species in the vapour followed by the monoxide and no metallic vapour has ever been observed at this temperature. Clearly, a substantial change occurs in the composition of the initial americium dioxide for temperatures higher than 2000 K, which is not surprising considering the high oxygen potential of AmO_{2-x}. According to the CALPHAD model developed for the Am-O system [16], the calculated oxygen potential for temperatures between 2000 and 2200 K is higher than 200 $kJ \cdot mol^{-1}$ at O/Am close to 2.00, and drops steeply to about -100 $kJ \cdot mol^{-1}$ when the O/Am ratio reaches approximately 1.60. For comparison, the calculated oxygen potential of PuO_{2-x} is between -400 and -300 $kJ \cdot mol^{-1}$ for O/Pu ratios between 1.84 and 1.92 [19]. Therefore at the high temperature of our measurement the pure AmO_2 is much more reduced than PuO_2. Since there is not a large difference between the vapour pressures for pure AmO_{2-x} and $Pu_{0.939}Am_{0.061}O_{2-x}$ samples, for which we infer different O/metal ratios and thus oxygen potentials, it can be concluded that the total pressure in Am-O system does not vary strongly in the range 1.60 < O/Am < 1.83.

The values found for the IE of Am^+ and AmO^+ are in good agreement with existing literature [4-7,17,18] (Table 1). The IE(Am) was found 6.0±0.3 eV, consistent with the findings by Trautmann [17] and Koehler et al. [18], both with similar result 5.9738(2) eV. Santos *et al.* [4] determined the IEs for AmO and AmO_2 by two types of experiments: change-transfer "bracketing" with AmO_2^+ and AmO^+ reactivity with dienes. A value equal to 5.9 ± 0.2 eV for AmO^+ was reported [4], which was adjusted in a later publication by Gibson *et al.* [5] for IE(AmO) to 6.2 ± 0.2 eV. Multiconfigurational relativistic quantum chemical methods of AmO by Kovacs *et al.* [6] yielded 6.3 eV for the IE(AmO), which is also very close to our experimental value.

Furthermore for a better overview, the current and literature results are given in Figure 4.

Table 1. Ionisation energy (IE) values for americium, americium monoxide and dioxide: comparison between this work and existing literature data.

Species	**IE** (this study)/eV	**IE** (literature)/eV
Am	6.0 ± 0.3	5.9738(2) [17,18]
AmO	6.5 ± 0.3	5.9 ± 0.2 [4]; 6.2 ± 0.2 [5]; 6.3 [6]
AmO_2	$7.5^{(*)}$	7.23 ± 0.15 [4]

$^{(*)}$ apparent value; it could not be determined accurately due to high background.

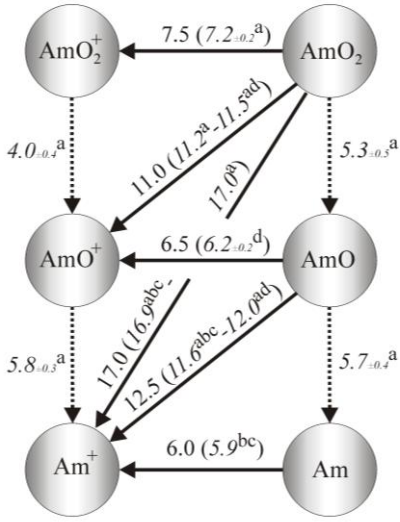

Figure 4. Measured ionisation and dissociation energies of neutral and positively charged americium oxides. The values set in italics are taken from literature: a - values from [4]; b, c - values from [17,18]; d - value from [5]. The values for the dissociative ionisation processes set on diagonals, in brackets, are assessed from the BDE(AmO^+-O), BDE(Am^+-O), respectively, and the BDE(AmO-O), BDE(Am-O), respectively, with the IE values for the corresponding involved species.

There are no direct measurements of dissociation energy (DE) values for AmO_2 into AmO^+ and Am^+, and AmO into Am^+. However these DE values can be derived from the summation of the BDE (AmO^+-O), BDE(Am^+-O),

respectively, or the BDE(AmO-O), BDE(Am-O), respectively, with the IE values for the corresponding involved species (Figure 4). From the ionisation energy of AmO and the dissociation energy of (Am^+-O), derived from ICR mass spectrometric measurements, Santos *et al.* [4] estimated the dissociation energy of (Am-O) of 5.73 ± 0.37 eV. A similar value, 5.7 eV, was found by Haire [7], based on correlation between dissociation energy and electronic configuration, much higher than the computed value of 4.6 eV reported by Kovacs *et al.* [6]. For this reason we used the values from Santos *et al.* [4] in our comparison. In Figure 4 the assessed values for the dissociative ionisation energy are given on diagonals in brackets and a very good agreement with the results from this study was found (Table 2).

Table 2. Dissociation energy (DE) values for AmO_2 and AmO: comparison between this work and the estimated values from literature.

Dissociative ionisation process	**DE** (this study) eV	**DE** (literature) eV
$AmO_2+e^-\rightarrow AmO^+ +O+2\cdot e^-$	11.0 ± 0.6	11.27 ± 0.43 estimated from [4] 11.56 ± 0.53 estimated from [4,5]
$AmO_2+e^-\rightarrow Am^+ +2\cdot O+2\cdot e^-$	17.0 ± 0.9	17.07 ± 0.53 estimated from [4] 16.90 ± 0.64 estimated from [4,17,18]
$AmO+e^-\rightarrow Am^+ +O+2\cdot e^-$	12.5 ± 0.6	12.00 ± 0.37 estimated from [4,5] 11.60 ± 0.40 estimated from [4,17,18]

5.5 Summary and Conclusions

Knudsen cell mass spectrometric measurements on pure americium dioxide and plutonium oxide sample containing a small amount of americium have been performed. The electron impact was recorded through measurement of the ionisation efficiency curves for Am^+, AmO^+ and AmO_2^+. The appearance and dissociative ionisation potential values were found in good agreement with the available literature data. For the first time the partial vapour pressure of the observed americium oxide bearing species have been derived. The data were assessed taking into account the dissociation processes occurring up to 40 eV, the energy at which the signals were recorded. For temperatures below 2200 K the initial

sample of americium dioxide was reduced significantly since some amount of metallic vapour, originated from the condensed phase, was observed. The oxygen potential has a significant contribution to the high temperature chemistry of Am-O system since it drastically varies with the O/metal ratio, from O/Am ≤ 2.0 up to ≈ 1.6.

The results for the total vapour pressure showed lower values than the existing literature reports estimated from the discordant measurements of plutonium oxides containing very small amounts of americium [2,3]. In these reports [2,3] the americium content was extrapolated by alpha-spectrometry techniques from the plutonium oxide host sample and some corrections were applied for the disintegration rates corresponding to ^{238}Pu contribution. Our results on pure americium dioxide samples are slightly lower than the values from Ackermann *et al.* [2] and distinctively lower than reported by Ohse *et al.* [3]. The data for the plutonium oxide samples with 6.1 wt% americium content were interpreted using Raoult's law and showed a close behaviour to the pure americium dioxide.

5.6 References

[1] C. Guéneau, M. Baichi, D. Labroche, C. Chatillon, B. Sundman, J. Nucl. Mater. 304 (2002) 161.
[2] R.J. Ackermann, R.L. Faircloth, M.H. Rand, J. Phys. Chem. 70 (1966) 3698.
[3] R.W. Ohse, Progress Report no. 5, European Institute for Transuranium Elements, Karlsruhe, Germany (1968) p. 26.
[4] M. Santos, J. Marcalo, J.P. Leal, A. Pires de Matos, J.K. Gibson, R.G. Haire, Int. J. Mass Spectrom. 228 (2003) 457.
[5] J.K. Gibson, R.G. Haire, J. Marcalo, M. Santos, A. Pires de Matos, J.P. Leal, J. Nucl. Mat. 344 (2005) 24.
[6] A. Kovacs, R.J.M. Konings, J. Raab, L. Gagliardi, Physical Chemistry Chemical Physics 10 (2008) 1114.
[7] R.G. Haire, J. Alloy. Comp. 213-214 (1995) 185.
[8] C. Sari, E. Zamorani, J. Nucl. Mater. 37 (1970) 324.
[9] A. Fernández, R.J.M. Konings, J. Somers, D. Haas, J. Mat. Sci. Lett. 22 (2003) 119.
[10] P. Gotcu-Freis, J.-Y. Colle, J.-P. Hiernaut, R.J.M. Konings, J. Chem. Thermodyn. 43 (2011) 492.
[11] J.E. Battles, J.W. Reihus, W.A. Shinn, USAEC, Argonne Nat. Lab., Rep. ANL 7575 1969.
[12] P. Gotcu-Freis, J.-Y. Colle, J.-P. Hiernaut, F. Naisse, C. Guéneau, R.J.M. Konings, J. Chem. Thermodyn. 43 (2011) 1164..
[13] F. Capone, J.-Y. Colle, J.-P. Hiernaut, C. Ronchi, J. Phys. Chem. A 103 (1999) 10899.

[14] R.W. Kiser, Introduction to Mass Spectroscopy and its Applications, Prentice-Hall Inc., New York, 1965.
[15] R. W. Ohse, C. Ciani, *Thermodynamics of Nuclear Materials*, IAEA, Vienna (1967) 545.
[16] P. Gotcu-Freis, J.-Y. Colle, C. Guéneau, N. Dupin, B. Sundman, R.J.M. Konings, J. Nucl. Mater. (2011) Article In Press, Accepted Manuscript.
[17] N. Trautmann, J. Alloys Compd. 213/214 (1994) 28.
[18] S. Köhler, R. Deiβenberger, K. Eberhardt, N. Erdmann, G. Herrmann, G. Huber, J.V. Kratz, M. Nunnemann, G. Passler, P.M. Rao, J. Riegel, N. Trautmann, K. Wendt, Spectrochemica Acta Part B 52 (1997) 717.
[19] C. Guéneau, C. Chatillon, B. Sundman, J. Nucl. Mater. 378 (2008) 257.

Chapter 6

A thermodynamic study of the Pu-Am-O system

Abstract

*Vapour pressure measurements were performed on a $(Pu_{0.756}Am_{0.244})O_{2-x}$ sample using Knudsen cell mass spectrometry. The total and partial vapour pressures of the gaseous species have been measured in the temperature range from 2000 to 2300 K. The evolution of the plutonium and americium bearing species was also determined as a function of time, in order to evaluate the congruent vapour composition. At constant temperature, the energy of ionising electrons was stepwise increased and the ionisation efficiency curves were recorded. The results were combined with the assessment of the Pu-Am-O system using the CALPHAD method. To obtain the model of this ternary system, the data on the Pu-Am and Am-O binaries have been evaluated and the optimised phase diagrams are presented. A consistent thermodynamic description of the ternary was obtained which allows the calculation of the ternary phase diagram, the oxygen potential for $(Pu,Am)O_{2\pm x}$ and the equilibrium partial vapour pressures.**

*This chapter is reprinted with kind permission of Elsevier: "A thermodynamic study of the Pu-Am-O system. P. Gotcu-Freis, J.-Y. Colle, C. Guéneau, N. Dupin, B. Sundman, R.J.M. Konings. The Journal of Nuclear Materials, doi: 10.1016/j.jnucmat.2011.05.014 ". Article In Press, Accepted Manuscript.

6.1 Introduction

The irradiation of the fuel in a nuclear reactor generates minor actinides (MAs: Np, Am, Cm), which are long-lived nuclides. Americium is of particular interest as its production increases with fuel burnup and cooling time, and has among the minor actinides the highest contribution to the long term radiotoxic inventory of the nuclear waste. In order to reduce this radiotoxic inventory, partition and transmutation has been proposed: minor actinides are separated (partitioned) from the spent fuel and then fissioned (transmuted) in order to produce short-lived fission products. Transmutation of minor actinides is foreseen in fast neutron systems: fast nuclear reactors (FNR) or Accelerator-Driven Systems (ADS). This can be done by incorporating small amounts of MAs (up to 5%) in uranium plutonium mixed oxide fuels, or larger amounts in MA-bearing blankets (e.g. $(U,Am)O_{2-x}$) or dedicated transmutation fuels or targets (e.g. $(Pu,Am)O_{2-x}$ in MgO or Mo matrices). For the latter option, the study of the Pu-Am-O system is of high importance.

The investigation of this ternary system was started lately in several laboratories to obtain precise data on the thermophysical properties of potential fuel and target compositions. In fact, the existing data on the ternary Pu-Am-O system are limited. The phase relations of PuO_{2-x} containing 9% Am were studied by means of X-ray diffraction analysis, ceramography and differential thermal analysis, with different O/M (M=Pu+Am) ranging from 1.90 to 2.00 [1]. In addition, the oxygen potential measurements [2] on the same samples were performed using thermogravimetric analysis with H_2O/H_2 gas equilibrium and dilute O_2 gas at 1123, 1273 and 1423 K. Recently, oxygen potential measurements were reported for $Pu_{0.5}Am_{0.5}O_{2-x}$ at T = 1333 K using the electromotive force method [3]. Data on the vapour pressure, another important fuel design property, of the mixed Pu/Am oxides are lacking. Data only exist for plutonium oxides containing very small amounts of americium produced by decay of ^{241}Pu [4,5] and were derived from the measurements by the Knudsen effusion method combined with collection on platinum targets.

The objective of the present study is to provide experimental data on the variation of the total pressure of plutonium and americium bearing species over $(Pu,Am)O_2$ solid solutions. For that purpose a sample with an initial

Am content of 24.4% was studied in the temperature range from 2000 up to 2300 K. The gaseous species were analysed as function of time and temperature by means of Knudsen effusion mass spectrometry. The current results have been combined with the CALculation of PHAse Diagrams (CALPHAD) assessment of the Pu-Am-O system. This approach describes the ternary system based on the description of each of the binary constituting system, together with the available data: the phase diagram, the heat increments, the heat of formation of the compounds, the oxygen potential and the vapour pressure data versus O/M (M = Pu+Am) ratio and temperature. The CALPHAD method offers a reliable and versatile method to assess phase diagrams and thermodynamic properties, based on the Gibbs energy modelling of each phase, using suitable models containing a relatively small number of variable coefficients. This work constitutes part of the international project FUELBASE [6,7] on the modelling of nuclear fuels, dedicated to the description of the thermodynamic properties and phase equilibria of the multi-component U, Pu, Am, Np, (C, N, Si, Ti, Zr, Mo) O system, required for the prediction of candidate fuel behaviour in fast reactor systems.

6.2 Mass spectrometric measurements for $Pu_{0.756}Am_{0.244}O_{2-x}$

The plutonium-americium mixed dioxides sample used for the mass spectrometric study was a fragment from a *ca.* 2 mm height disk with an Am/M content of 24.4%. The amount of neptunium accumulated in the sample by alpha-decay of ^{241}Am was calculated, from the initial chemical analysis reports, as 0.94 wt% at the time of these measurements. The isotopic composition of the plutonium, based on thermal ionisation mass spectrometry analysis, was found to be 91.5 wt% ^{239}Pu and 8.304 wt% ^{240}Pu, the remainder was constituted by the ^{238}Pu, ^{241}Pu and ^{242}Pu isotopes, each less than 0.15 wt%. The measurement uncertainties are the total combined uncertainties with a coverage factor of 2.

The material was fabricated from PuO_2 beads, produced by external gelation (also known as gel supported precipitation - GSP), followed by an infiltration step to incorporate the americium [8]. For the infiltration step, an americium nitrate solution with an americium concentration of (300 ± 1) $g \cdot dm^{-3}$ was used. After infiltration, the obtained particles were dried at room temperature overnight, and thereafter calcined under an air

atmosphere to convert the nitrate into oxide. These two last steps were repeated to obtain the desired Am concentration. Finally the powder was compacted and sintered in an Ar/H_2 atmosphere, at 1873 K. The final Am content (in wt%) was determined by gravimetric and gamma-spectrometric analysis before and after the infiltration step, with an absolute accuracy of about 1%. The O/M ratio is estimated to be between 1.75 and 1.85, typical for these sintering conditions. Before the mass spectrometric measurements, the sample was heated for a few hours in air at 1173 K as was previously reported by Sari and Zamorani [9], in order to ensure the stoichiometry of the sample corresponding to O/M = 2.00.

The experimental facility, consisting of a Knudsen cell coupled with a quadrupole mass spectrometer, has been presented in detail in another publication [10]. The sample (in weight of 70 mg) was heated in a tungsten Knudsen cell which had an iridium foil placed at the bottom (from now on referred to W/Ir cells). Iridium foils were used to avoid the direct contact between the solid sample and the cell material, which is less suitable for measurements with oxides at high temperature [10]. The mass spectrometric measurements were carried out using an ionisation energy of 40 eV. Isothermal measurements showed a variation of the signal intensities of the vapour species as a function of time. The sample was heated for a significant period at T = 2300 K, until the intensities of the vapour species were constant over the time. The energy of the ionising electrons was then stepwise increased by 0.5 eV up to 40 eV. Figure 1 presents the plutonium (a) and americium (b) bearing ion species, created by ionisation of the vapour above $Pu_{0.756}Am_{0.244}O_{2-x}$ at 2300 K as a function of the applied electron energy. Americium appears at low electron energy (around 6 eV), and thus is present as atomic species in the vapour. Atomic plutonium appears at higher electron energy, and is the product of the dissociation of the monoxide (above 13 eV) and dioxide (above 19 eV). The monoxide and dioxide ion species were present as parent ions in both vapour phase systems.

The results on the measurements performed in the W/Ir cells are obtained in the temperature range from 2000 to 2300K and can be represented by the following equations, corresponding to the total vapour pressure of the plutonium and americium species, respectively, in the vapour above the mixed oxide sample:

$$\ln(P(Pu_{tot})/Pa) = (26.30\pm0.50) - (62453\pm1023) \cdot (T/K)^{-1}, \quad (1)$$

$$\ln(P(Am_{tot})/Pa) = (29.01\pm0.40) - (70052\pm857) \cdot (T/K)^{-1}. \quad (2)$$

Using the fragmentation patterns obtained in previous studies on pure plutonium dioxide [10] and on americium dioxide [11] samples, the signal intensities were corrected for dissociation processes occurring at 40 eV, and the contribution of each species in the vapour was evaluated. Thus for congruency at T = 2300 K the vapour consists of 73% PuO_2 and 27% PuO with respect to the total plutonium oxide pressure, $P(Pu_{tot})$, and 46% AmO, 41% AmO_2 and 13% Am, with respect to the total americium oxide pressure, $P(Am_{tot})$.

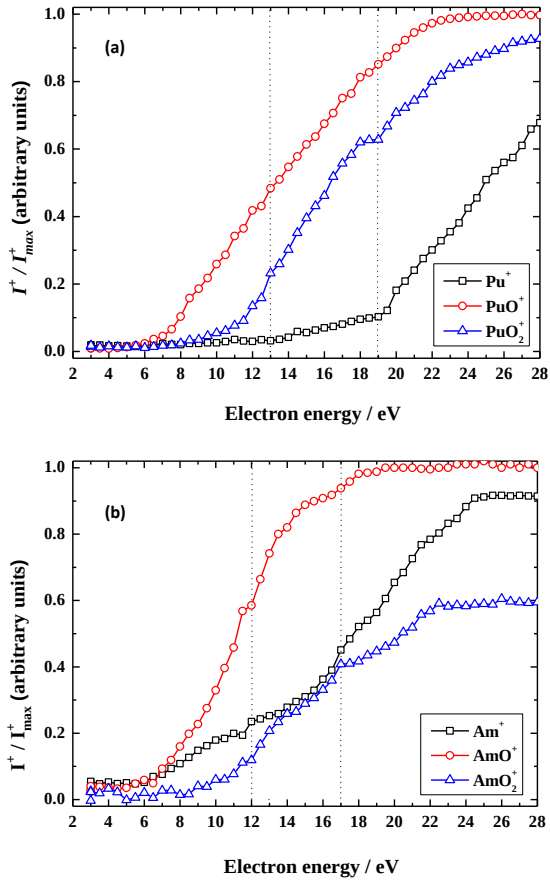

Figure 1. Ionisation efficiency curves for plutonium **(a)** and americium **(b)** bearing ion species created by ionisation of the vapour above $Pu_{0.756}Am_{0.244}O_{2-x}$ at 2300 K as a function of applied electron energy.

After completion of the mass spectrometric measurements, thermogravimetric analysis (TGA) was performed on the remnant of the $Pu_{0.756}Am_{0.244}O_{2-x}$ sample in air at 1173 K for 8 hours. All the sample manipulations were performed in a dry nitrogen glove box. The results indicated the final O/M of the remnant as 1.715 ± 0.04. Additional gamma spectrometric measurements indicated the final content of americium in the sample corresponding to the ratio Am/M=24 ± 5 %.

6.3 Thermodynamic modelling

In order to develop the model for the Pu-Am-O system, the three binary systems Pu-Am, Pu-O and Am-O had to be assessed. The model for the Pu-O system was recently reported by Guéneau *et al.* [7] using the CALPHAD method in which the Gibbs energy of each phase is assessed. A slight change of the model was made in [12] to improve the description of the small miscibility gap extent in the PuO_{2-x} fluorite phase and take into account the new melting point measured for PuO_2 [13]. The calculated phase diagram is presented in Figure 2 and the description of the phases of this system will not be further discussed hereunder.

Thermodynamic models for the AmO_{2-x} phase have already been proposed by Thiriet and Konings [14] who applied the approach by Lindemer and Besmann [15-18], modelling this phase as a regular solution, and lately by Besmann [19], describing it by the compound energy formalism [20]. However, the modelling of the thermodynamic behaviour of AmO_{2-x} still could not include all the experimental results and a full assessment of the Am-O system which describes the complete phase diagram has not been developed. Since no complete model for the Am-O system exists, an assessment was performed in the context of this work. To set up a complete thermodynamic description of the ternary Pu-Am-O system, an additional binary Pu-Am system, needed to be assessed and it is therefore reported as well in the present work.

The available experimental data and the models used to describe the different phases are discussed first in this section. Finally the assessed parameters and different calculations compared to experimental data are presented.

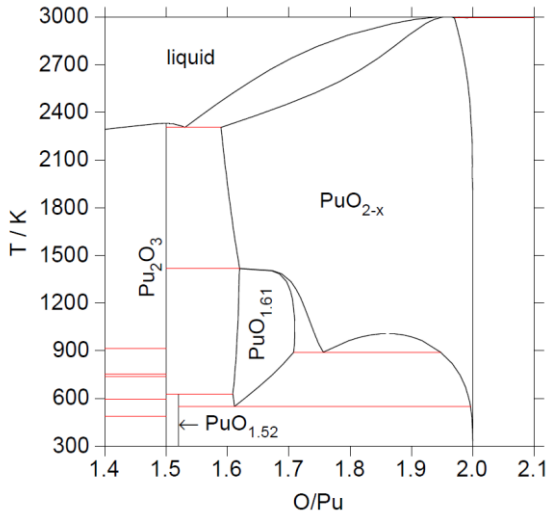

Figure 2. Calculated phase diagram after Guéneau *et al*. [12], slightly adjusted from [7] to improve the description of the small miscibility gap extent in the PuO_{2-x} fluorite phase and take into account the new melting point measured for PuO_2 [13].

6.3.1 Experimental data

6.3.1.1 Am-Pu system

The phase diagram of the binary Am-Pu system was determined by Ellinger *et al.* [21] for the complete composition range for temperatures below 1173 K by means of micrograph analysis and X-ray diffraction. The used Am contained impurities up to 0.52 wt%, with lanthanum being the main contaminant. Since Am is volatile, the control over the composition was checked by radio analysis. Samples containing nominally up to 50 at% Am were obtained using an induction melting. The Pu rich alloys were prepared by arc-furnace. The extended range of stability of the *fcc* (*δ*-Pu, *β*-Am) solid solution phase was determined by X-ray analysis. A peritectic reaction of liquid at the Pu rich side was estimated at (665 ± 15) °C, and the existence of the liquid was observed in the quenched samples. There was no mention of the *bcc*-form of Am (*γ*-Am). The melting point of Am was given as (994 ± 7) °C, which is significantly lower than the nowadays accepted value of 1449 K [22].

The assessed phase diagram proposed in Massalki's compilation [23] is incomplete. It corresponds to Ellinger's [21] phase diagram adding the *γ*-Am form but without proposing any connection of the *β*-Am/*γ*-Am to the rest of the phase diagram. Many phase boundaries are uncertain being presented as dashed lines.

The application of Brewers model as made by Ogawa [24] predicts the *bcc* (*ε*-Pu, *γ*-Am) and *fcc* (*δ*-Pu, *β*-Am) continuous solid solutions in the whole range of composition. Okamoto [25] proposed an updated assessed phase diagram where the equilibria between the liquid, *bcc* and *fcc* phases are taken from Ogawa [24] calculations and those between the *fcc*, *α*-Am, *α*-Pu, *β*-Pu and *γ*-Pu from Ellinger *et al.* [21].

During the Thermodynamics of Nuclear Fuels Actinet meeting in Saclay-2006, Turchi [26] discussed this system. Two experimental phase diagrams were presented, the one assessed by Massalski *et al.* [23] based on Ellinger's report [21] and another one with a continuous *bcc* field from Shushakov *et al.* [27] based on experimental data. Also, two calculated phase diagrams were shown reproducing both topologies. The experimental data by Shushakov *et al.* [27] are much higher in temperature than the Ellinger [21] solidus on the Pu side and lower than accepted transitions for pure Am. This could be linked with the significant presence of impurities in the samples. They also disagree on the extend of the (*α* - Am + *fcc*) field.

6.3.1.2 Am-O system

Versions of the Am-O phase diagram have been earlier proposed [9,28-30] and the available data have been collected into several large reviews [31,32].

The binary americium oxides are limited to the sesquioxide Am_2O_3, the non stoichiometric dioxide AmO_{2-x} and the intermediate compound $AmO_{1.62}$. Studies on americium oxides include the determination of the enthalpies of formation for solid Am_2O_3 [33] and AmO_2 [34], the measurement of the melting temperature of Am_2O_3 [35], and AmO_2 [36], both corrected for ITS-90 [37], to 2481 ± 15 K, and 2386 K, respectively. There is no experimental data in the Am-Am_2O_3 field of the phase diagram.

In the work by Chikalla and Eyring [38] (X-ray diffraction on quenched and annealed samples between 1.5 < (O/Am) < 2.0) three structure types have been identified for americium sesquioxide: the cubic, hexagonal and monoclinic. Since the rare earth monoclinic B-type phase was found only in the quenched samples, apparently it exists only at elevated temperatures, between 733 K and 1273 K. It has been suggested that the existence of B-type sesquioxide was probably the result of an insufficient equilibrium time as it is difficult to reach equilibrium in rare earth oxide transformations [39]. In this later study [39] the monoclinic B-form is attributed to a metastable phase stabilised by minor impurities, particularly Sm and other lanthanide elements. Considering the ionic radius of Am^{3+}, the B-type structure is probably the stable room temperature modification, as Pu_2O_3 and Cm_2O_3 have A-type B-type structures, respectively [37]. This would be consistent with the work of Wallmann [40] who reported the transformation to the rare-earth A-type La_2O_3 structure between 1073 and 1173 K.

The study of Sari and Zamorani [9], based on DTA and ceramographic procedures, revealed additional particularities for the Am-O system. In particular, they report a two-phase miscibility gap between a slightly substoichiometric dioxide AmO_{2-x} ($0.17\text{-}0.05 \leq x \leq 0.32\text{-}0.38$) in the temperature range 1130-1300K, and a high temperature *bcc* C'-type AmO_{2-x} phase ($0.32 \leq x \leq 0.39$), isostructural with the Am_2O_3 C-type occurring at room temperature. A comparison of the Am-O system with similar systems such as Pu-O, Pr-O, Tb-O, and Ce-O, indicated a higher temperature for the miscibility gap. The phase diagram data proposed by Thiriet and Konings [14] were chosen for the modelling in this study. Due to the lack of the experimental data, the *bcc* C-type phase will be considered as a stoichiometric compound, $AmO_{1.61}$, and only the hexagonal form (A) of Am_2O_3 is introduced into the assessment.

In addition to the structural data and the phase relations, several studies of the oxygen pressure-temperature-composition equilibria have been performed [28,29,41]. The experimental methods, temperature range and sample stoichiometry are summarised in Table 1.

The experimental data are not easy to compare since they were performed at different O/Am ratios and temperatures. For the comparison of these

data, for each study, all the experimental values were fitted and calculated for fixed O/Am ratios.

Table 1. The oxygen potential data on AmO_{2-x}: available reference data, experimental method description, temperature and stoichiometry range.

Reference data	Experimental method	Temperature range (K)	O/Am range
[28]	- electromotive force method; galvanic cell: Pt / MgO-AmO_{2-x}/ Y_2O_3-ThO_2 / FeO/Fe / Pt	930 - 1425	1.50 - 2.00
[29]	- electromotive force method; galvanic cell: Pt / AmO_{2-x} /Zr(Ca)O_{2-x} / air, Pt	1333	1.50 - 1.99
[41]	- thermogravimetric isopiestic technique	1139 - 1445	1.80 - 2.00

A comparison of two of the data sets [28,41] is given in Figure 3. The results are presented for $\mu(O_2)$, in kJ·mol^{-1}, as function of temperature, for fixed O/Am ratios ranging from 1.94, corresponding to the lowest temperature for which the oxygen potential was measured in [41], up to 1.98. It must be remarked, however, that for any temperature for which the O/Am ratio is constant, there is no region with equal oxygen potential values.

For a proper comparison of the three sets of data, the results of the oxygen potential from [28,41] had to be extrapolated to 1333 K, i.e. the temperature of measurements performed by Otobe *et al.* [29]. As shown in Figure 4, the discrepancies of these three sets are very large, varying up to 50 kJ·mol^{-1} for O/Am between 1.94 and 1.98, and about 200 kJ·mol^{-1} for O/Am = 1.67. For samples with O/Am ratios less than 1.67, corresponding to the largest gradient of $\mu(O_2)$ (Figure 4), it has been emphasised [9] that the involved low reaction rates might introduce difficulties and lead to errors in the investigations.

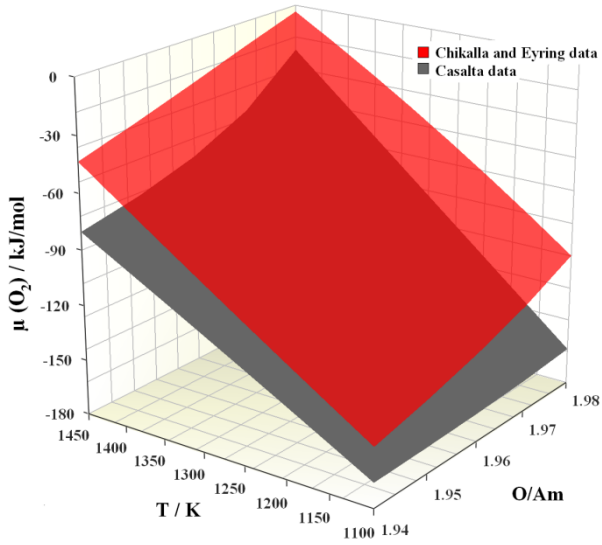

Figure 3. Comparison between the data by Casalta [28] with the results by Chikalla and Eyring [41], for the oxygen potential results as $\mu(O_2)$ versus *T* / K in AmO_{2-x} field at fixed O/Am ratio.

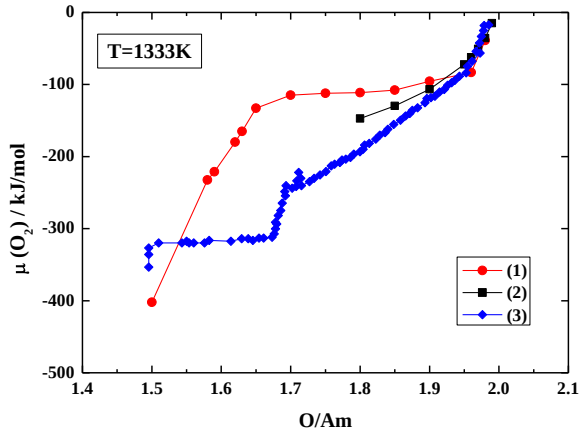

Figure 4. Oxygen potential from [28,29,41], plotted as a function of O/Am ratio for *T* = 1333 K. (1) -●- Casalta [28], (2) -■- Chikalla and Eyring [41], (3)-◆- Otobe *et al.* [29].

The results on the oxygen potential measurements were then compared, in Figures 5(a) and 5(b), with those of Sari and Zamorani [9], with respect to the miscibility gap data. Although the data of Chikalla and Eyring [41] do

not describe the miscibility gap, the three lowest isotherms overlap with the experimental points of the miscibility gap (Figure 5(a)). The absence of the miscibility gap in their results could be due to the extrapolation of the low pressure data on a given isotherm from the higher pressure data, in order to reduce the measurement time. At very low oxygen pressure, equilibrium was attained extremely slowly: eight days were required to obtain a single data point. Thus, this procedure did not permit the derivation of the kinetic data, which are particularly important at low temperatures and pressures.

Casalta's data [28] show constant oxygen potential for O/Am between 1.65 and 1.90. However, the two upper isotherms are outside the miscibility gap found by Sari and Zamorani [9] (Figure 5(b)). The measurements cover the range between $AmO_{1.5}$ and AmO_2, but indicate differences at the $AmO_{1.5}$ side with respect to the hexagonal Am_2O_3. A similar galvanic cell composed of an Y_2O_3/ThO_2 electrolyte and a FeO/Fe reference electrode was described by Markin and Rand [42]. These authors obtained good agreement for Ni/NiO electrode as long as Fe,FeO/electrolyte interface was cleaned between each set of measurements. When this precaution was not fulfilled, discrepancies up to 20 $kJ \cdot mol^{-1}$ were found. Thus it could be an explanation for the higher results found by Casalta [28] in the region of the miscibility gap as well.

Casalta [28] studied the variation of the oxygen potential with temperature, in both AmO_2 and AmO_2-MgO pellets with 0, 20, 30, 50 and 100% americium dioxide. It has been pointed out that the weight loss in the AmO_2-MgO pellets during the sintering process was assumed to be only due to the reduction of the americium dioxide. The sintering was performed for maximum 6 hours, from 1450 K up to about 1770 K. This is in disagreement with later studies [43] which claimed the instability of actinides diluted in MgO composites above 1400 K. It was not clearly stated how the stoichiometry of the AmO_2 pellets was determined for the 1.96; 1.85; 1.65. Finally, the possible slow reaction rates at low oxygen pressure, eventually enhanced by the dilution in MgO, were not considered. For these reasons it is likely that the results of Casalta [28] should be used with caution.

The results of Otobe *et al.* [29] at a constant temperature (T = 1333 K) are slightly above the miscibility gap described by Sari [9]. They are consistent

with those of Chikalla and Eyring [41] for stoichiometries close to 2.00. The agreement with Casalta [28] is poor. On the basis of their results, Otobe *et al.* [29] proposed the presence of the intermediate phases of Am_7O_{12} and Am_9O_{16} in the Am-O system.

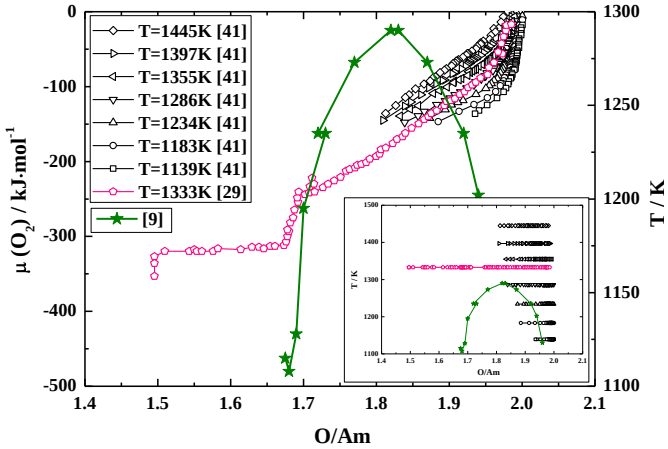

(a)

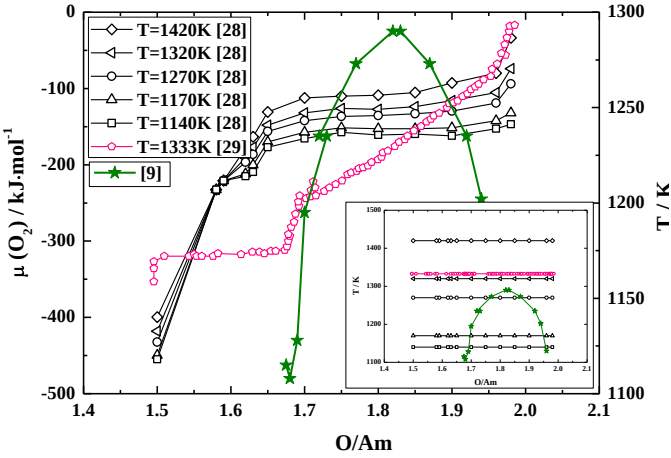

(b)

Figure 5. **(a)** Oxygen potential function of O/Am for Chikalla and Eyring [41] and Otobe *et al.* [29], and **(b)** Casalta [28] and Otobe *et al.* [29]. For comparison between these measurements and Sari's [9] results for the region of demixing of the AmO_{2-x} phase; the temperature is shown as secondary axis with respect to the O/Am ratio. The insets show the temperature versus O/Am representation of Sari [9] and Otobe *et al.* [29] with Chikalla and Eyring [41] in Figure 5(a), and Casalta [28] in Figure 5(b), respectively.

An attempt was made in the present study to fit the oxygen potential data by Otobe *et al.* [29] with the current model, but it was observed that the very low values for the oxygen potentials cannot be reconciled with the phase diagram data. When the low values of the oxygen potential in the region 1.5 < O/Am < 1.7 as found by Otobe *et al.* [29] were imposed in the optimisation, the miscibility gap found by Sari [9] could not be described. Furthermore the calculated americium oxide vapour pressure data above AmO_2 samples were found inconsistent with our experiments [11] in that case. Therefore the phase boundary data for the sesquioxide were given higher weight than the measurements of oxygen potentials close to O/Am = 1.5.

To obtain a thermodynamic model consistent with the existence of the miscibility gap in the *fcc*-phase studied by Sari [9], only the oxygen potential data from Chikalla [41] for compositions and temperatures outside the miscibility gap (data with O/Am ratio lower than ~1.9) were selected for the present assessment.

6.3.1.3 Pu-Am-O system

The available ternary phase diagram data are limited to the experimental investigations on the phase relation of PuO_{2-x} with addition of 9% americium by mean of XRD analysis, ceramography and DTA by Miwa *et al.* [1]. Two oxygen potential measurements are known for the ternary system: on sample with same 9% Am content by thermogravimetric analysis with H_2O/H_2 gas equilibrium and dilute O_2 gas at 1123, 1273 and 1423 K by Osaka *et al.* [2] and on sample with 50% Am by electromotive force method at 1333 K by Otobe *et al.* [3] using the same experimental system as for the AmO_{2-x} study [29]. It was concluded that the effect of Am addition to PuO_{2-x} on the phase relation was to increase the miscibility gap temperature [1]. The aspects of the oxygen potential could be interpreted based on several interactions between Pu and Am and sequentially their valence state changes [2]. $Am_{0.5}Pu_{0.5}O_{2-x}$ should be composed of a single fluorite-type phase over $0.02 < x \leq 0.22$ and the mixed phases of fluorite type and $(Am,Pu)_9O_{16}$ at x = 0.23 [3]. The discrepancies of this study with the other available data in the binary Am-O system make its reliability questionable.

6.3.2 Models

In the CALPHAD approach, semi-empirical models for the stable phases are used to describe their Gibbs energies as a function of composition and temperature. In these models, adjustable parameters are optimised to obtain an algebraic expression for the Gibbs energies as a function of both composition and temperature. The procedure was performed using the PARROT module of the Thermo-Calc software [44,45]. Essentially this module is used to minimise the error sum between the experimental information and the values calculated using the description of the Gibbs free energies of each of the phases of the system.

6.3.2.1. Pure element and stoichiometric phases

The Gibbs energy functions of all the phases considered in this system are referred to the stable element reference (SER) state, the stable state for the element at 298 K and 10^5 Pa [22,46,47]. The Gibbs energies for the pure elements as well as for the phases considered stoichiometric are expressed only as a function of temperature and pressure. The standard Gibbs energy functions of the elements are described by an equation of the type:

$$G_i^{\circ}(T) - H_i^{SER} = a + b \cdot T + c \cdot T \cdot \ln(T) + \sum_n d_n \cdot T^n. \quad (3)$$

The left-hand-side of the equation is defined as the Gibbs energy, $G_i^{\circ}(T)$, and the enthalpy of the element *i*, H_i^{SER}, relative to the SER, *a*, *b*, *c* and d_n are coefficients, and *n* represents a set of integers, typically taking the values 2, 3, and -1 [22,46,47]. The description of the different phases of the pure elements was taken from the SGTE database [22].

A similar expression was used for stoichiometric compounds:

$$G_{A_\alpha B_\beta}^{\circ}(T) - \alpha \cdot H_A^{SER} - \beta \cdot H_B^{SER} = a + b \cdot T + c \cdot T \cdot \ln(T) + \sum_n d_n \cdot T^n. \quad (4)$$

This equation was used in particular for the description of the Am_2O_3 compound, the terms *c* and d_n being extracted from the SGTE-SSUB [48,49], while *a* and *b* were optimised in the present work. α and β are the

number of mole of, respectively, A and B in the compound under consideration. However, for compounds with no available experimental heat capacity data, the Kopp-Neumann approximation was used to assess only the enthalpy and entropy of formation from the elements. Equation (5) was used for the description of the $AmO_{1.62}$ compound:

$$G^{o}_{A_\alpha B_\beta}(T) - \alpha \cdot G^{o}_{A}(T) - \beta \cdot G^{o}_{B}(T) = a + b \cdot T \,. \qquad (5)$$

6.3.2.2 Gas

The gas phase is described by an ideal mixture of (Am, AmO, AmO_2, O, O_2, O_3, Pu, PuO, PuO_2) gaseous species. The Gibbs energy is expressed by:

$$G^{gas} = \sum_i y_i \cdot G_i^{gas}(T) + R \cdot T \cdot \sum_i y_i \cdot \ln y_i + R \cdot T \cdot \ln(P / P_0) \,, \qquad (6)$$

where y_i is the molar fraction of the species *i* in the gas phase, $G_i^{gas}(T)$ represents the standard Gibbs energy of the gaseous species *i*, P_0 is the standard pressure. The functions for the gaseous species of (Am, Pu, O, O_2 and O_3) were taken from the SGTE substance database [48,49], for PuO, AmO and AmO_2 from a recent reassessment by Konings *et al.* [37]. PuO_2 was modified in order to follow the recommendations from Gotcu-Freis *et al.* [10] taking the enthalpy of formation $\Delta_f H°(PuO_2(g), 298.15\ K)$ = -428 kJ·mol^{-1} rather than -412 kJ·mol^{-1}, as proposed by Glushko *et al.* [49].

6.3.2.3 Liquid

The following ionic two-sublattice model was used to describe the liquid phase:

$$(Am^{3+}, Pu^{3+})_P (O^{2-}, \ Va, \ O, PuO_2)_Q \,. \qquad (7)$$

In this model, the first sublattice contains a mixture of cations, Am^{3+} and Pu^{3+}. The chosen cation charges correspond to the lower oxidation degree for which a stable compound is observed for the element under consideration. The second sublattice contains O^{2-} anions, charged vacancies, Va, neutral associates (PuO_2) and atoms (O). *P* and *Q* are equal to the average charge of the opposite sublattice, i.e. in the general case:

$$Q = \sum_C v_C \cdot y_C \text{ and } P = \sum_A v_A \cdot y_A + Q \cdot y_{Va}, \quad (8)$$

where v_i is the number of charges of species *i*, y_i corresponds to its site fraction, *C* stands for any cation and *A* for any anion. *B* will later be used to stand for any neutral species on the second sublattice. In our particular case, all the cations have a charge of +3 and there is only one anion, O^{2-}. The site fractions in the model can thus be simplified as follows:

$$Q = 3 \text{ and } P = 2 \cdot y_{O^{2-}} + 3 \cdot y_{Va}. \quad (9)$$

The induced charge of the vacancies corresponds to $Q = 3$. *P* varies via the site fractions of the species with the composition in the second sublattice in order to keep the liquid phase electrically neutral. For the metallic composition, the model can be simplified in $(Am^{3+}, Pu^{3+})_3(Va)_3$, while near the sesquioxide it will mostly correspond to $(Am^{3+}, Pu^{3+})_2(O^{2-})_3$. Near pure O, the cation sublattice vanishes and the liquid is only constituted by neutral O in the second sublattice.

In the present work, the Gibbs energy of the liquid phase is given by the following expression:

$$\begin{aligned} G^{liq} = {} & y_{O^{2-}} \cdot \sum_C y_C \cdot {}^\circ G^{liq}_{C:O^{2-}} + Q \cdot y_{Va} \cdot \sum_C {}^\circ G^{liq}_C + Q \cdot \sum_B y_B \cdot {}^\circ G^{liq}_B \\ & + R \cdot T \cdot \left[P \cdot \sum_C y_C \cdot \ln y_C + Q \cdot (y_{O^{2-}} \cdot \ln y_{O^{2-}} + y_{Va} \cdot \ln y_{Va} + \sum_B y_B \cdot \ln y_B) \right] \\ & + y_{Am^{3+}} \cdot y_{O^{2-}} \cdot y_O \left[{}^0L^{liq}_{Am^{3+}:O^{2-},O} + (y_{O^{2-}} - y_O) \cdot {}^1L^{liq}_{Am^{3+}:O^{2-},O} \right] \\ & + y_{Pu^{3+}} \cdot y_{O^{2-}} \cdot y_{Va} \left[{}^0L^{liq}_{Pu^{3+}:O^{2-},Va} + (y_{O^{2-}} - y_{Va}) \cdot {}^1L^{liq}_{Pu^{3+}:O^{2-},Va} \right] \\ & + y_{Pu^{3+}} \cdot y_{O^{2-}} \cdot y_{PuO_2} \cdot {}^0L^{liq}_{Pu^{3+}:O^{2-},PuO_2}. \end{aligned} \quad (10)$$

${}^\circ G^{liq}_{C:O^{2-}}$, ${}^\circ G^{liq}_C$ and ${}^\circ G^{liq}_B$ are the reference terms corresponding to the Gibbs energy of respectively C_2O_3, metallic *C*, and neutral *B*, all considered pure in the liquid state. No interactions parameter is added between the metallic elements assuming an ideal mixing in the metallic liquid. The parameters describing the Pu-O system were already reported in [7,12]. Those determined during the Am-O study are ${}^\circ G^{liq}_{Am^{3+}:O^{2-}}$, corresponding to

the Gibbs energy of the liquid sesquioxide, and ${}^{0}L^{liq}_{Am^{3+}:O^{2-},O}$ and ${}^{1}L^{liq}_{Am^{3+}:O^{2-},O}$, describing the non ideal behaviour of the liquid between the sesquioxides and O.

6.3.2.4 (Pu,Am)O_{2-x}

Like cerium, uranium and plutonium dioxides, AmO_2 adopts a fluorite structure. As for the assessment of U-O [6] and Pu-O [7,12] systems, the compound energy formalism [20] was used to describe this phase. The following three-sublattice model was applied to describe the americium dioxide *fcc* phase:

$$(Am^{3+}, Am^{4+}, Pu^{3+}, Pu^{4+})(O^{2-}, Va)_2(O^{2-}, Va), \qquad (11)$$

similar to the description used for the PuO_{2-x} *fcc*-phase. This was done to describe the Pu-Am-O system and also higher order systems, in particular those involving U for which the phase shows hypersotoichiometry.

The two first sublattices correspond to the crystallographic sites in the fluorite structure, occupied for the ideal structure by americium Am^{4+} and plutonium Pu^{4+} ions in the first one and oxygen anions in the second one. Oxygen vacancies (Va) are added in the oxygen site to describe the sub-stoichiometry of the phase. They come together with a lower degree of oxidation of the elements in the first sublattice (Am^{3+} and Pu^{3+}). The third sublattice describes O in octahedral positions observed in hyperstoichiometric compounds, like in UO_2. This model describes compositions ranging from $MO_{1.5}$ to $MO_{2.5}$ even if in the systems, under consideration here, the phase is not stable for O contents higher than for MO_2. The detailed algorithm for choosing this sublattice model was discussed by Guéneau *et al.* [7,12].

The Gibbs energy associated to the model is:

$$
\begin{aligned}
G^{\mathrm{MO_2}} = & \sum_i \sum_j \sum_k G^{\mathrm{MO_2}}_{i:j:k} \\
& + R\cdot T \sum_i y_i \cdot \ln y_i + 2\cdot R\cdot T \sum_j y_j \cdot \ln y_j + R\cdot T \sum_k y_k \cdot \ln y_k \\
& + \sum_{i_1} \sum_{i_2} \sum_j \sum_k y_{i_2} \cdot y_{i_1} \cdot y_j \cdot y_k \cdot [{}^0L^{\mathrm{MO_2}}_{i_1,i_2:j:k} + (y_{i_1} - y_{i_2}) \cdot {}^1L^{\mathrm{MO_2}}_{i_1,i_2:j:k}] \\
& + \sum_{i_1} \sum_{i_2} \sum_{i_3} y_{i_1} \cdot y_{i_2} \cdot y_{i_3} \cdot L^{\mathrm{MO_2}}_{i_1,i_2,i_3:*:*},
\end{aligned}
\tag{12}
$$

where y_i represents the fraction of the species *i* in the sublattice, $G^{\mathrm{MO_2}}_{i:j:k}$ are the Gibbs energies of the different compounds formed by considering the species *i* in the first sublattice, *j* and *k* in the second and the third sublattices, respectively. ${}^nL^{\mathrm{MO_2}}_{i_1,i_2:j:k}$ are the interaction parameters of the two cations in the first sublattice when the other sublattices are fully occupied by a single species. When these interactions are considered independent of the occupations of those two last sublattices, parameters are used, i.e. ${}^nL^{\mathrm{MO_2}}_{i_1,i_2:*:*}$. The terms $L^{\mathrm{MO_2}}_{i_1,i_2,i_3:*:*}$ correspond to ternary interactions between three cations of the first sublattice.

As described for the Pu-O system [7], only two functions were assessed within the Gibbs energies of formation of the end-members defined by the models, the others being linked to them. The assessed functions correspond to the Gibbs energy of the stoichiometric AmO_2 compound, $GAMO2$, and to the neutral $AmO_{1.5}$, $GAMO15$, corresponding to the configuration: $(\mathrm{Am^{3+}})(\mathrm{O^{2-}_{0.75}}, \mathrm{Va}_{0.25})_2(\mathrm{Va})$. The parameters corresponding to the end members of the model in the binary system Am-O were linked by the following relations:

$$G^{\mathrm{MO_2}}_{\mathrm{Am^{4+}:O^{2-}:Va}} = GAMO2 \tag{13}$$

$$G^{\mathrm{MO_2}}_{\mathrm{Am^{4+}:Va:Va}} = GAMO2 - O2GAS \tag{14}$$

$$G^{\mathrm{MO_2}}_{\mathrm{Am^{3+}:O^{2-}:Va}} = GAMO15 + \frac{1}{4}\cdot O2GAS + 1.12467\cdot R\cdot T \tag{15}$$

$$G^{\mathrm{MO_2}}_{\mathrm{Am^{3+}:Va:Va}} = GAMO15 - \frac{3}{4}\cdot O2GAS + 1.12467\cdot R\cdot T \tag{16}$$

$$G^{MO_2}_{Am^{4+}:O^{2-}:O^{2-}} = GAMO2 + \frac{1}{2}\cdot O2GAS + 200000 \quad (17)$$

$$G^{MO_2}_{Am^{4+}:Va:O^{2-}} = GAMO2 - \frac{1}{2}\cdot O2GAS + 200000 \quad (18)$$

$$G^{MO_2}_{Am^{3+}:Va:O^{2-}} = GAMO15 - \frac{1}{4}\cdot O2GAS + 1.12467\cdot R\cdot T + 200000 \quad (19)$$

$$G^{MO_2}_{Am^{3+}:O^{2-}:O^{2-}} = GAMO15 + \frac{3}{4}\cdot O2GAS + 1.12467\cdot R\cdot T + 200000 \quad (20)$$

$^0L^{MO_2}_{Am^{3+},Am^{4+}:*:*}$ and $^1L^{MO_2}_{Am^{3+},Am^{4+}:*:*}$ were assessed in order to describe the miscibility gap in this phase, reported by Sari [9].

The enthalpy increments for AmO_2 and Am_2O_3 were taken from the SGTE Substance database [48,49] and the enthalpy and entropy terms were optimised during the assessment of the phase diagram. In order to better describe the few experimental data available in the ternary Pu-Am-O system, the ternary interaction parameters: $L^{MO_2}_{Am^{3+},Pu^{3+}:*:*}$, $L^{MO_2}_{Am^{4+},Pu^{4+}:*:*}$, $L^{MO_2}_{Am^{3+},Pu^{4+}:*:*}$, $L^{MO_2}_{Am^{3+},Pu^{3+},Pu^{4+}:*:*}$ and $L^{MO_2}_{Am^{3+},Am^{4+},Pu^{3+}:*:*}$ were assessed.

6.3.2.5 $(Pu,Am)_2O_3$

In the present work, only the hexagonal form of Am_2O_3 was considered. It was treated as a stoichiometric compound in the binary Am-O. The temperature dependence of its Gibbs energy was assessed using an expression similar to equation (4). Thus, the Gibbs energy of the resulting phase in the ternary system is expressed as:

$$G^{M_2O_3} = \sum_i y_i \cdot G^{M_2O_3}_{i:O} + 2\cdot R\cdot T\cdot \sum_i y_i \cdot \ln y_i + x_{Am}\cdot x_{Pu}\cdot {}^0L^{M_2O_3}_{Am,Pu:O}. \quad (21)$$

An interaction parameter, $^0L^{M_2O_3}_{Am,Pu:O}$ was assessed in order to describe the continuous solid solution between Pu_2O_3 and Am_2O_3.

6.3.2.6 Metallic solid solutions

The *fcc* and *bcc* phases are stable for Am and Pu and present an extended reciprocal solution. They were described as regular solution following the expression:

$$G_m^{\varphi} = \sum_i x_i \cdot G_i^{\varphi}(T) + R \cdot T \cdot \sum_i x_i \cdot \ln x_i + x_{\mathrm{Am}} \cdot x_{\mathrm{Pu}} \cdot L_{\mathrm{Am,Pu}}^{\varphi}, \qquad (22)$$

where x_i corresponds to the atomic fraction of *i*, $G_i^{\varphi}(T)$ the Gibbs energy of the pure species *i* in the phase φ, and $L_{\mathrm{Am,Pu}}^{\varphi}$ the interaction parameter between Am and Pu in this phase. Constant interaction parameters were assessed. It seems that Pu shows some solubility in the α-Am phase. A lattice stability for Pu in this structure has been introduced to apply equation (22) for this phase as well. The interaction parameter was kept equal to zero.

6.3.3 Results

6.3.3.1 Am-Pu system

The calculated phase diagram of the Pu-Am system is compared with the experimental data in Figure 6. With only three assessed parameters (Table 2), the topology of the Am-Pu phase diagram is well reproduced. The agreement with the Ellinger's [21] *bcc* limit of the (*bcc*+*fcc*) field is correct. The calculated solidus is higher than found by Ellinger *et al.* [21]. The calculated liquidus data are in good agreement with the experimental data from Shushakov *et al.* [27]. New experiments on this system are required to improve the present thermodynamic description.

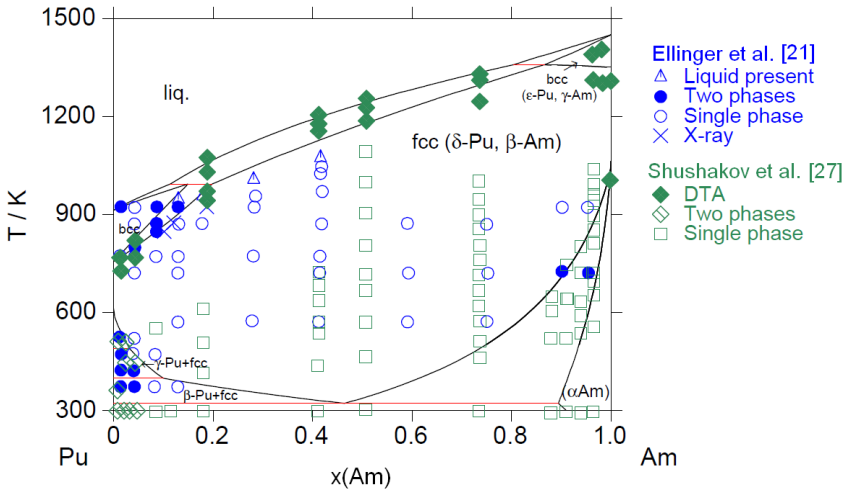

Figure 6. Calculated phase diagram of the Am-Pu system. Comparison with the experimental data from Ellinger *et al.* [21] and from Shushakov *et al.* [27].

Table 2. Thermodynamic parameters assessed during the present work, relative to the stable element reference (SER) state conditions (T=298.15 K, P = 10^5 Pa); the values are expressed in J, K, mol, Pa.

Phase	Gibbs energy (J·mol^{-1})	Reference
Gas	$G_{O}^{gas} - H_{O}^{SER} = OGAS$	[48,49]
(Am, AmO, AmO_2, O, O_2, O_3, Pu, PuO, PuO_2)	$G_{O_2}^{gas} - 2 \cdot H_{O}^{SER} = O2GAS$	[48,49]
	$G_{O_3}^{gas} - 3 \cdot H_{O}^{SER} = O3GAS$	[48,49]
	$G_{Pu}^{gas} - H_{Pu}^{SER} = PUGAS$	[48,49]
	$G_{PuO}^{gas} - H_{Pu}^{SER} - H_{O}^{SER} = PUOGAS$	[37]
	$G_{PuO_2}^{gas} - H_{Pu}^{SER} - 2 \cdot H_{O}^{SER} = PUO2GAS$	This work + [10,37]
	$G_{Am}^{gas} - H_{Am}^{SER} = AMGAS$	[48,49]
	$G_{AmO}^{gas} - H_{Am}^{SER} - H_{O}^{SER} = AMOGAS$	[37]
	$G_{AmO_2}^{gas} - H_{Am}^{SER} - 2 \cdot H_{O}^{SER} = AMO2GAS$	[37]
Liquid	$G_{Am^{3+}:O^{2-}}^{liq} = G_{Am:O}^{M_2O_3} + 74000 - 29.827 \cdot T$	This work
$(Am^{3+}, Pu^{3+})_P(O^{2-}, Va, O, PuO_2)_Q$	${}^{0}L_{Am^{3+}:O^{2-},O}^{liq} = +107215$	This work
	${}^{1}L_{Am^{3+}:O^{2-},O}^{liq} = -400000$	This work

	$G^{liq}_{Pu^{3+}:O^{2-}} = G^{M_2O_3}_{Pu:O} + 113000 - 47.921967 \cdot T$	[7,48]
	$G^{liq}_{PuO_2} = G^{MO_2}_{Pu:O} + 67000 - 22.2 \cdot T$	[12]
	${}^0L^{liq}_{Pu^{3+}:O^{2-},\,PuO_2} = +60000$	[12]
	${}^1L^{liq}_{Pu^{3+}:O^{2-},\,PuO_2} = -20000$	[12]
	${}^0L^{liq}_{Pu^{3+}:O^{2-},\,Va} = +77451.8 + 23.4798 \cdot T$	[12]
	${}^1L^{liq}_{Pu^{3+}:O^{2-},\,Va} = -20231.601$	[12]
$(Am,Pu)O_{2-x}$	$G^{MO_2}_{Am^{4+}:O^{2-}:Va} - H^{SER}_{Am} - 2 \cdot H^{SER}_{O} = GAMO2$	This work
$(Am^{3+}, Am^{4+}, Pu^{3+}, Pu^{4+})(O^{2-}, Va)_2(O^{2-}, Va)$	$G^{MO_2}_{Am^{4+}:Va:Va} - H^{SER}_{Am} = GAMO2 - O2GAS$	This work
	$G^{MO_2}_{Am^{4+}:O^{2-}:O^{2-}} - H^{SER}_{Am} - 3 \cdot H^{SER}_{O} = GAMO2 + \frac{1}{2} \cdot O2GAS + 200000$	This work
	$G^{MO_2}_{Am^{4+}:Va:O^{2-}} - H^{SER}_{Am} - H^{SER}_{O} = GAMO2 - \frac{1}{2} \cdot O2GAS + 200000$	This work
	$G^{MO_2}_{Am^{3+}:Va:Va} - H^{SER}_{Am} = GAMO15 - \frac{3}{4} \cdot O2GAS + 1.12467 \cdot R \cdot T$	This work
	$G^{MO_2}_{Am^{3+}:Va:O^{2-}} - H^{SER}_{Am} - H^{SER}_{O} = GAMO15 - \frac{1}{4} \cdot O2GAS + 1.12467 \cdot R \cdot T + 200000$	This work

$G^{MO_2}_{Am^{3+}:O^{2-}:O^{2-}} - H^{SER}_{Am} - 3\cdot H^{SER}_{O} = GAMO15 + \frac{3}{4}\cdot O2GAS + 1.12467\cdot R\cdot T + 200000$	This work
$G^{MO_2}_{Am^{3+}:O^{2-}:Va} - H^{SER}_{Am} - 2\cdot H^{SER}_{O} = GAMO15 + \frac{1}{4}\cdot O2GAS + 1.12467\cdot R\cdot T$	This work
${}^{0}L^{MO_2}_{Am^{3+},Am^{4+}:*:*} = +32683 - 7.561\cdot T$	This work
${}^{1}L^{MO_2}_{Am^{3+},Am^{4+}:*:*} = -35096 + 19.45\cdot T$	This work
$G^{MO_2}_{Pu^{4+}:O^{2-}:Va} - H^{SER}_{Pu} - 2\cdot H^{SER}_{O} = GPUO2$	[12]
$G^{MO_2}_{Pu^{4+}:Va:Va} - H^{SER}_{Pu} = GPUO2 - O2GAS$	[12]
$G^{MO_2}_{Pu^{4+}:O^{2-}:O^{2-}} - H^{SER}_{Pu} - 3\cdot H^{SER}_{O} = GPUO2 + \frac{1}{2}\cdot O2GAS + 80\cdot T$	[12]
$G^{MO_2}_{Pu^{4+}:Va:O^{2-}} - H^{SER}_{Pu} - H^{SER}_{O} = GPUO2 - \frac{1}{2}\cdot O2GAS + 80\cdot T$	[12]
$G^{MO_2}_{Pu^{3+}:Va:Va} - H^{SER}_{Pu} = GPUO15 - \frac{3}{4}\cdot O2GAS + 1.12467\cdot R\cdot T$	[12]
$G^{MO_2}_{Pu^{3+}:O^{2-}:O^{2-}} - H^{SER}_{Pu} - 3\cdot H^{SER}_{O} = GPUO15 + \frac{3}{4}\cdot O2GAS + 1.12467\cdot R\cdot T + 80\cdot T$	[12]
$G^{MO_2}_{Pu^{3+}:Va:O^{2-}} - H^{SER}_{Pu} - H^{SER}_{O} = GPUO15 - \frac{1}{4}\cdot O2GAS + 1.12467\cdot R\cdot T + 80\cdot T$	[12]

	$G^{MO_2}_{Pu^{3+}:O^{2-}:Va} - H^{SER}_{Pu} - 2\cdot H^{SER}_{O} = GPUO15 + \frac{1}{4}\cdot O2GAS + 1.12467\cdot R\cdot T$	[12]
	${}^{0}L^{MO_2}_{Pu^{3+},Pu^{4+}:Va:Va} = {}^{0}L^{MO_2}_{Pu^{3+},Pu^{4+}:O^{2-}:Va} = +9781.916 + 3.062\cdot T$	[12]
	${}^{1}L^{MO_2}_{Pu^{3+},Pu^{4+}:Va:Va} = {}^{1}L^{MO_2}_{Pu^{3+},Pu^{4+}:O^{2-}:Va} = -17507.472 + 5.4657\cdot T$	[12]
	${}^{0}L^{MO_2}_{Am^{3+},Pu^{3+}:*:*} = -76000$	This work
	${}^{0}L^{MO_2}_{Am^{3+},Pu^{4+}:*:*} = +69555 - 35\cdot T$	This work
	${}^{0}L^{MO_2}_{Am^{4+},Pu^{4+}:*:*} = -10550$	This work
	$L^{MO_2}_{Am^{3+},Am^{4+},Pu^{3+}:*:*} = -300000$	This work
	$L^{MO_2}_{Am^{3+},Pu^{3+},Pu^{4+}:*:*} = -120000$	This work
$PuO_{1.52}$	$G_{PuO_{1.52}} - H^{SER}_{Pu} - 1.52\cdot H^{SER}_{O} = -861515.83 + 345.42685\cdot T - 62.351\cdot T\cdot \ln T - 0.007085\cdot T^2 - 1.6625\cdot 10^{-11}\cdot T^3 + 396830\cdot T^{-1};\ 298.25 < T < 3000\ K$	[7,12]
$PuO_{1.61}$ $(Pu^{3+},Pu^{4+})_2(O^{2-})_3(O^{2-},Va)_1$	$G^{PuO_{1.61}}_{Pu^{3+}:O^{2-}:O^{2-}} - 4\cdot H^{SER}_{O} - 2\cdot H^{SER}_{Pu} = 2\cdot GPUO15 + \frac{1}{2}\cdot O2GAS - 8220 + 6.35403\cdot T$	[12]
	$G^{PuO_{1.61}}_{Pu^{4+}:O^{2-}:O^{2-}} - 4\cdot H^{SER}_{O} - 2\cdot H^{SER}_{Pu} = 2\cdot GPUO2 + 18772 - 6\cdot T$	[12]
	$G^{PuO_{1.61}}_{Pu^{3+}:O^{2-}:Va} - 3\cdot H^{SER}_{O} - 2\cdot H^{SER}_{Pu} = 2\cdot GPUO15 - 8220 + 6.35403\cdot T$	[12]

	$G^{PuO_{1.61}}_{Pu^{4+}:O^{2-}:Va} - 3\cdot H^{SER}_{O} - 2\cdot H^{SER}_{Pu} = 2\cdot GPUO2 - \frac{1}{2}\cdot O2GAS + 18772 - 6\cdot T$	[12]
	$L^{PuO_{1.61}}_{Pu^{3+},Pu^{4+}:O^{2-}:O^{2-}} = L^{PuO_{1.61}}_{Pu^{3+},Pu^{4+}:O^{2-}:Va} = -725.5 + 15.8\cdot T$	[12]
$AmO_{1.62}$	$G_{AmO_{1.62}} - G^{\alpha-Am}_{Am} - 1.62\cdot\frac{1}{2}G^{gas}_{O_2} = -858727 + 137.566\cdot T$	This work
$(Am,Pu)_2O_3$	$G^{M_2O_3}_{Am:O} - 2\cdot H^{SER}_{Am} - 3\cdot H^{SER}_{O} = GAM2O3$	This work
	$G^{M_2O_3}_{Pu:O} - 2\cdot H^{SER}_{Pu} - 3\cdot H^{SER}_{O} = GPU2O3$	[12]
	$L^{M_2O_3}_{Am,Pu:O} = -140000$	This work
α-Am	$G^{\alpha-Am}_{Pu} - G^{\alpha-Pu}_{Pu} = +6000$	This work
bcc-phase	$L^{bcc}_{Am,Pu} = +3000$	This work
fcc-phase	$L^{fcc}_{Am,Pu} = +2000$	This work
Functions	$PUOGAS = -61250.7813 - 67.7537247\cdot T - 25.39529\cdot T\cdot\ln T - 0.027128\cdot T^2 + 6.04248333\cdot10^{-6}\cdot T^3$ $- 5.39170833\cdot10^{-10}\cdot T^4 - 18606.35\cdot T^{-1};\ 298.15 < T < 1200\ K$ $= -92998.0639 + 291.250332\cdot T - 78.23663\cdot T\cdot\ln T + 0.01368435\cdot T^2 - 1.12984333\cdot10^{-6}\cdot T^3$ $+ 3.67271667\cdot10^{-11}\cdot T^4 + 3522860\cdot T^{-1};\ 1200 < T < 4000\ K$	[37]

$$PUO2GAS = -449949.625 + 191.117834 \cdot T - 70.29021 \cdot T \cdot \ln T + 0.006730005 \cdot T^2 - 1.51097967 \cdot 10^{-6} \cdot T^3 + 1.16953917 \cdot 10^{-10} \cdot T^4 + 240537.3 \cdot T^{-1};\ 298.15 < \mathrm{T} < 1500\ \mathrm{K}$$
$$= -434186.792 + 47.3497491 \cdot T - 49.85911 \cdot T \cdot \ln T - 0.00573298 \cdot T^2 + 2.45380167 \cdot 10^{-7} \cdot T^3 + 7.12978917 \cdot 10^{-13} \cdot T^4 - 2060372.5 \cdot T^{-1};\ 1500 < \mathrm{T} < 4000\ \mathrm{K}$$

This work + [10,37]

$$AMOGAS = -26358.1836 - 26.15462 \cdot T - 34.31966 \cdot T \cdot \ln T - 0.00306537 \cdot T^2 + 1.06767 \cdot 10^{-6} \cdot T^3 - 3.33713 \cdot 10^{-10} \cdot T^4 + 134461 \cdot T^{-1};\ 298.15 < \mathrm{T} < 1500\ \mathrm{K}$$
$$= +92514.4991 - 903.368 \cdot T + 85.66885 \cdot T \cdot \ln T - 0.055787 \cdot T^2 + 5.04307 \cdot 10^{-6} \cdot T^3 - 2.35713 \cdot 10^{-10} \cdot T^4 - 21759000 \cdot T^{-1};\ 1500 < \mathrm{T} < 6000\ \mathrm{K}$$

[37]

$$AMO2GAS = -404759.107 + 22.6904318 \cdot T - 44.093 \cdot T \cdot \ln T - 0.0235493315 \cdot T^2 + 9.08436867 \cdot 10^{-6} \cdot T^3 - 2.77264967 \cdot 10^{-9} \cdot T^4 + 3.72651745 \cdot 10^{-13} \cdot T^5 + 139939.435 \cdot T^{-1};\ 298.15 < \mathrm{T} < 1500\ \mathrm{K}$$
$$= -288226.382 - 885.37267 \cdot T + 81.738932 \cdot T \cdot \ln T - 0.085528055 \cdot T^2 + 1.34818538 \cdot 10^{-5} \cdot T^3 - 1.583708 \cdot 10^{-9} \cdot T^4 + 8.9391995 \cdot 10^{-14} \cdot T^5 - 20935730.5 \cdot T^{-1};\ 1500 < \mathrm{T} < 6000\ \mathrm{K}$$

[37]

$$GPU2O3 = -1658471.43 - 295.555729 \cdot T + 38.63916 \cdot T \cdot \ln T - 0.275 \cdot T^2 + 7.79827167 \cdot 10^{-5} \cdot T^3 - 1479357.6 \cdot T^{-1};\ 298.15 < T < 400\ \mathrm{K}$$
$$= -1702523.72 + 677.000904 \cdot T - 122.9535 \cdot T \cdot \ln T - 0.014273645 \cdot T^2 - 3.27260333 \cdot 10^{-11} \cdot T^3 + 750595 \cdot T^{-1};\ 400 < T < 2358\ \mathrm{K}$$
$$= -1804198.06 + 1284.90727 \cdot T - 200 \cdot T \cdot \ln T + 4.1974775 \cdot 10^{-16} \cdot T^2 - 1.3924665 \cdot 10^{-20} \cdot T^3 + 2.01649 \cdot 10^{-6} \cdot T^{-1};\ 2358 < T < 5000\ \mathrm{K}$$

[12]

$$GPUO15 = +3817.7 + \frac{1}{2} \cdot GPU2O3$$ [12]

$$GPUO2 = -1099562.84 + 505.428856 \cdot T - 83.31922 \cdot T \cdot \ln T - 0.00584178 \cdot T^2 - 2.2924116 \cdot 10^{-11} \cdot T^3 + 913506 \cdot T^{-1};\ 298.15 < \mathrm{T} < 3018\ \mathrm{K}$$
$$= -1184422.43 + 898.267142 \cdot T - 131 \cdot T \cdot \ln T + 7.77918 \cdot 10^{-17} \cdot T^2 - 2.17490333 \cdot 10^{-21} \cdot T^3 + 3.521756 \cdot 10^{-7} \cdot T^{-1};\ 3018 < \mathrm{T} < 6000\ \mathrm{K}$$ [12]

$$GAM2O3 = -1731679.36 + 647.345 \cdot T - 115.13 \cdot T \cdot \ln T - 0.011488 \cdot T^2 + 543550 \cdot T^{-1}$$ This work

$$GAMO15 = +2337 + \frac{1}{2} \cdot GAM2O3$$ This work

$$GAMO2 = -954578.79 + 301.966814 \cdot T - 50.08302 \cdot T \cdot \ln T - 0.0591819 \cdot T^2 + 1.80921 \cdot 10^{-5} \cdot T^3 + 544968.5 \cdot T^{-1};\ 298.15 < \mathrm{T} < 500\ \mathrm{K}$$
$$= -963476.666 + 508.678378 \cdot T - 84.73628 \cdot T \cdot \ln T - 5.37432 \cdot 10^{-4} \cdot T^2 - 1.3585645 \cdot 10^{-7} \cdot T^3 + 963812 \cdot T^{-1};\ 500 < T < 2000K$$ This work

6.3.3.2 Am-O system

The optimised parameters are given in Table 2. The phase diagram is presented in Figure 7(a). A magnification of it (Figure 7(b)) shows that the main features of the phase diagram are well reproduced, namely the miscibility gap in AmO_{2-x} and the stability temperature for the $AmO_{1.62}$ compound. Additionally, the experimental points from Chikalla and Eyring [38] and Sari [9] were included in the comparison, and the description agrees, generally well, with the tentative phase diagram by Thiriet and Konings [14]. It is, however, to be remarked that the calculations indicate an incongruent melting of americium dioxide. This is due to the presence of the gas phase in our model. In fact, when heated, americium dioxide is known to lose oxygen above ~1200 K. Thus at the measured melting temperature of 2386 K, according to Mc Henry [36], the americium dioxide cannot be stoichiometric. According to our description, which remains uncertain due to the scarcity of experimental data, the dioxide is allowed to decompose into a liquid and a gas phase (Figure 7(b)).

The calculated oxygen potential versus the O/Am ratio are calculated at 1140, 1180, 1280, 1333, 1355, 1400 and 1445 K and compared to the experimental data [41] in Figure 8(a). The data from O/Am = 1.9-2.0 are reproduced well by the calculations (Figure 8(b)). For lower O/Am ratios, the calculations deviate from Chikalla's data due to the presence of the miscibility gap in the *fcc*-phase and of a two-phase region (AmO_2+$AmO_{1.62}$) at 1140 and 1180 K. In these regions, the calculated oxygen potentials are about 30 $kJ \cdot mol^{-1}$ higher than in reference [28].

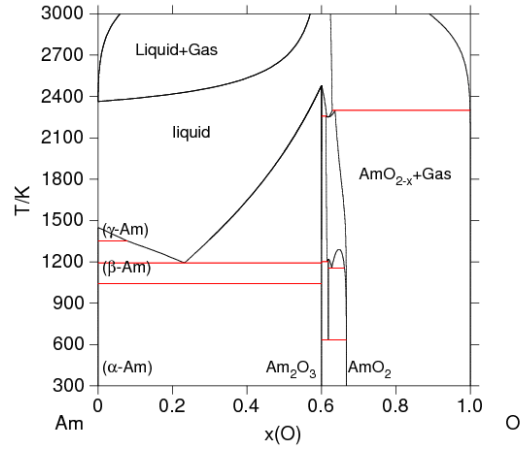

(a)

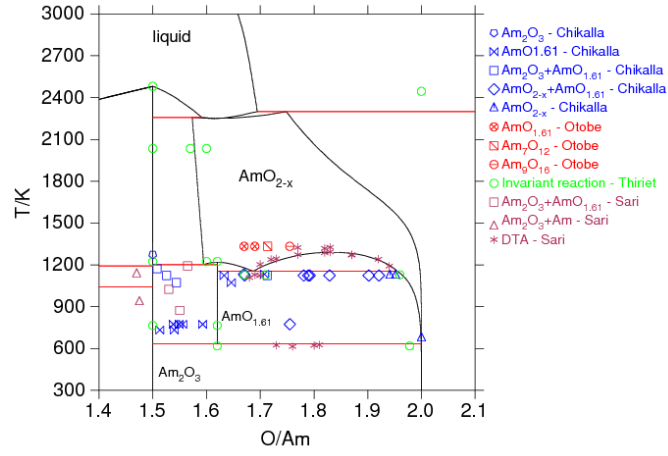

(b)

Figure 7. **(a)** Calculated phase diagram of the Am-O system; **(b)** magnification in the stoichiometry range from 1.4 to 2.1. The experimental data were taken from [9,14,28,29,38,41]

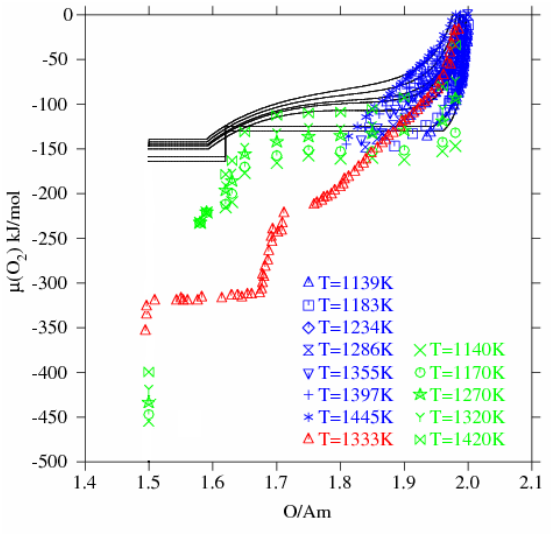

(a)

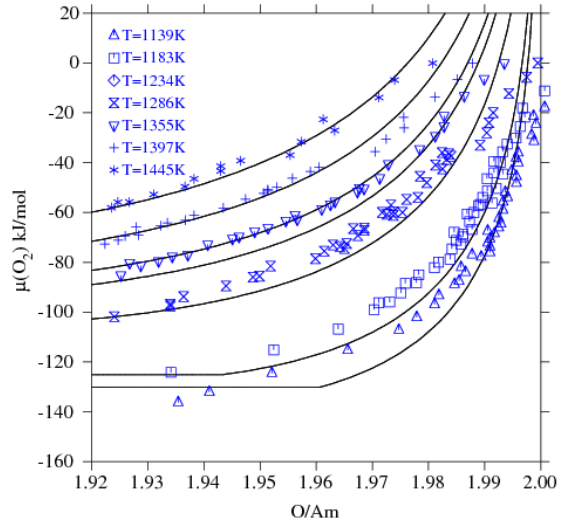

(b)

Figure 8. **(a)** Calculated oxygen potential as a function of the O/Am ratio between 1.4 and 2.1, at 1140, 1180, 1280, 1333, 1355, 1400 and 1445 K. Comparison with the available literature data [28,29,41]. **(b)** Magnification for O/Am between 1.92 and 2.00. The plateau at 1140 and 1180 K corresponds to the two-phase region (AmO_{2-x}+$AmO_{1.62}$).

Furthermore, the enthalpy increments for Am_2O_3 and AmO_2 versus temperature are calculated and compared to the recent measurements by Nishi *et al.* [50] in Figures 9(a) and (b), respectively. The results from Nishi [50] and our calculations compare very favourably. The calculated and reported standard enthalpies and entropies for Am_2O_3 and AmO_2 are given in Table 3 and the agreement is very good.

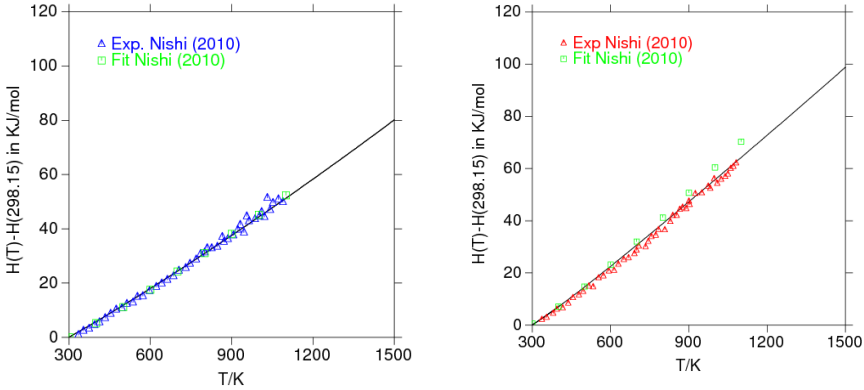

Figure 9. Calculated enthalpy increment as a function of temperature for Am_2O_3 **(a),** and AmO_2 **(b)**, and comparison with experimental data by Nishi *et al.* [50].

Table 3. Standard enthalpies and entropies for Am_2O_3 and AmO_2; calculated data and comparison with the literature.

Phase	$\Delta_f H°$(298.15 K), in kJ·mol^{-1}	$S°$(298.15 K), in J·mol^{-1}·K^{-1}	Reference
Am_2O_3	-1692.7	136.71	Present work
	-(1690.4 ± 8.0)	160 ± 15	[31]
	-(1690.4 ± 8.0)	133.6 ± 5.0	[37]
AmO_2	-931. 7	70.06	Present work
	-(932.3 ± 3.0)	67 ± 10	[31]
	-(932.2 ± 3.0)	75.5 ± 5.0	[37]

Calculations of the vapour pressure data in the Am-O system were performed for comparison with the recent experimental results measured by mass spectrometry [11]. The final O/Am ratio of the sample could not

be measured, due to the small amount material used and its dispersed state (fine powder). In the calculations, the azeotropic condition was obtained by imposing the constraint that the relative oxygen content (O/Am) in the gas and in the solid are equal. In such situation, no minimum in the total pressure was found in isothermal conditions which indicates that no congruent composition exists in the AmO_{2-x} phase. Furthermore, the experimental high partial pressures of Am(g) could not be reproduced by our calculations in the single phase AmO_{2-x} or in the two-phase region (AmO_{2-x}+$AmO_{1.62}$). Finally, a reasonable agreement ($P_{calc}/P_{exp} \approx 10$) between the calculated partial pressures for Am(g), AmO(g), AmO_2(g) and the recent experimental data measured by mass spectrometry in [11] is found for the congruency calculation above the sesquioxide phase Am_2O_3 (Figure 10). The present calculations indicate that the oxygen content of the sample (initially AmO_2) could have been considerably depleted to reach Am_2O_3 at 2200 K during the measurement. This behaviour is in agreement with the calculated phase diagram in Figure 7. In fact, at atmospheric pressure and T = 2200 K, the AmO_2 compound loses oxygen until O/Am equal to ~1.8 is reached. Hence, a lower value is expected under vacuum.

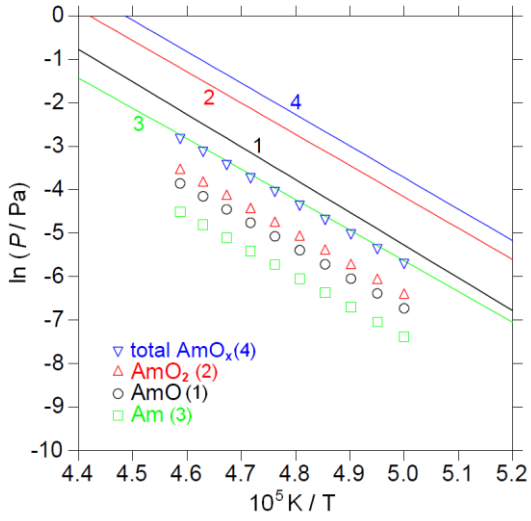

Figure 10. Calculated vapour pressure against the temperature in azeotropic condition above Am_2O_3, in comparison with the experimental data on americium dioxide samples [11]. (1), (2), (3) refer to the calculated pressure of AmO, AmO_2, Am, respectively. (4) refer to the calculated total pressure for the americium bearing species.

6.3.3.3 Pu-Am-O system

For the ternary model, ternary interaction parameters (Table 2) were introduced and adjusted for the (Am,Pu)O_{2-x} solid solution. This was done in order to better represent the oxygen potential data measured by Osaka *et al.* [2] on $Pu_{0.91}Am_{0.09}O_{2-x}$ samples at 1123, 1273 and 1473 K using thermogravimetric analysis with H_2O/H_2 gas equilibrium and dilute O_2 gas, and by Otobe *et al.* [3] on $Pu_{0.5}Am_{0.5}O_{2-x}$ samples at 1333 K using the electromotive force method as well as the miscibility gap identified by Miwa *et al.* [1] at 1273 K for 9% Am content in PuO_{2-x}.

The parameter $L^{MO_2}_{Am^{4+},Pu^{4+}:*:*}$ improved the region close to O/M = 2.00 with respect to Otobe's results [3]. The calculated and experimental data are compared in Figure 11.

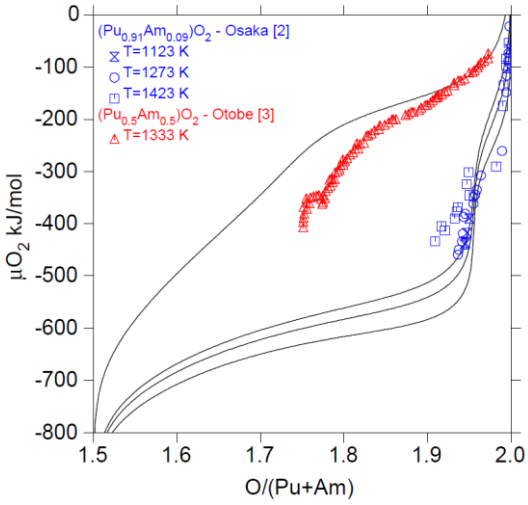

Figure 11. The calculated oxygen potential as a function of O/Am ratio for fixed temperature, compared to the literature data from [2,3].

A very good agreement is obtained for $Pu_{0.5}Am_{0.5}O_{2-x}$ for O/M ratios higher than 1.90. For lower oxygen content the calculated potentials are significantly higher than Otobe's results [3] like in the binary Am-O system. For $Pu_{0.91}Am_{0.09}O_{2-x}$, the calculations reproduce well the experimental data for oxygen stoichiometry close to 2.00. The potentials are underestimated for O/M ratios lower than 1.95. These curves are highly determined by the

description in the binary Pu-O for which many experimental data are available.

A representation of the ternary phase diagram is shown in Figure 12 for T = 1273 K. The parameter $L^{MO_2}_{Am^{3+},Pu^{3+}:*:*}$ was introduced in order to obtain a better fit to the pressure of the americium bearing species (Figure 13(a)). The parameter $L^{MO_2}_{Am^{3+},Pu^{4+}:*:*}$ allowed calculating the miscibility gap close to PuO_2 in agreement with the measurements by Miwa *et al.* [1]. The two other ternary parameters $L^{MO_2}_{Am^{3+},Pu^{3+},Pu^{4+}:*:*}$ and $L^{MO_2}_{Am^{3+},Am^{4+},Pu^{3+}:*:*}$ were introduced in order to obtain a continuity of the miscibility gap from the area studied by Miwa *et al.* [1] to the binary Am-O. One more interaction parameter (Table 2) was assessed for the $(Am,Pu)_2O_3$ solid solution in order to obtain the continuous solid solution between Pu_2O_3 and Am_2O_3 compounds. Furthermore, for a better description of the phase diagram, supplementary experimental data are needed in the ternary Pu-Am-O system. The actual extend of the miscibility gap towards low oxygen content deserves to be characterised as well as its continuity towards the Am-O binary system. The extension and possible continuity of $PuO_{1.61}$ and $AmO_{1.62}$ should also be studied.

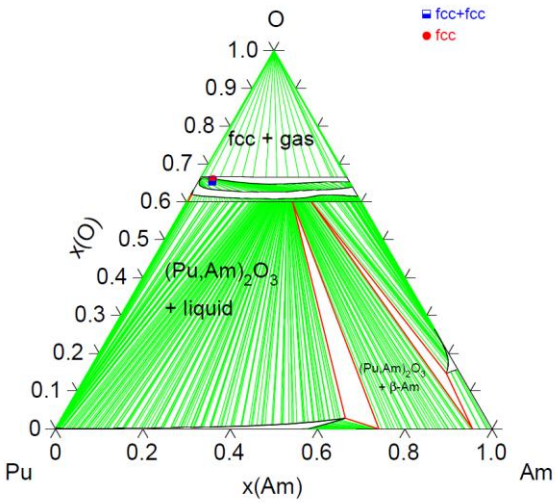

(a)

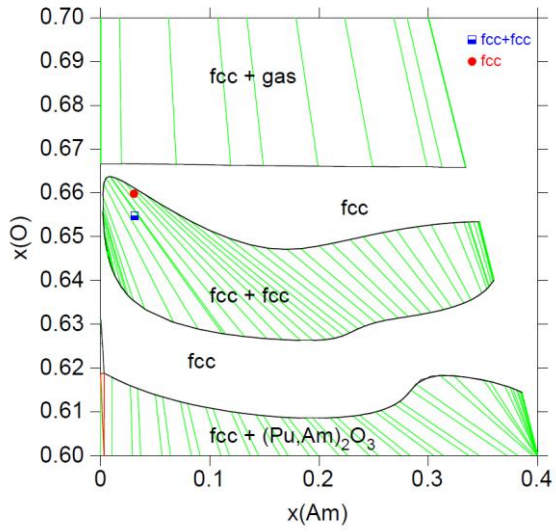

(b)

Figure 12. The isothermal section for the Pu-Am-O system calculated for 1273 K compared to Miwa *et al.* [1] results: **(a)** in the whole composition range; **(b)** for oxygen content between 60 and 70 at.%. The green lines (in the online version) in both Figures correspond to tie-lines.

6.4 Comparison of the mass spectrometric measurements with the ternary model

The vapour pressure data were calculated using the present model by considering a pseudo congruency condition. The relative oxygen content (O/M) in the solid and gas phases were fixed as equal. The comparison with the experimental data on the vaporisation of the $Pu_{0.756}Am_{0.244}O_2$ sample from the present study is shown in Figure 13(a). The assessed results for the total vapour pressure of americium oxide, $P(Am_{tot})$, and plutonium oxide, $P(Pu_{tot})$, are very close to the experimental data. The calculated partial pressures for PuO(g) and AmO_2(g) are higher than the experimental values, while AmO(g) and Am(g) pressures are lower. The pressure of plutonium dioxide, the major vapour species, is the pressure in close agreement with the calculated values. Generally, there is a slight deviation of the calculated pressure values with respect to the measurements.

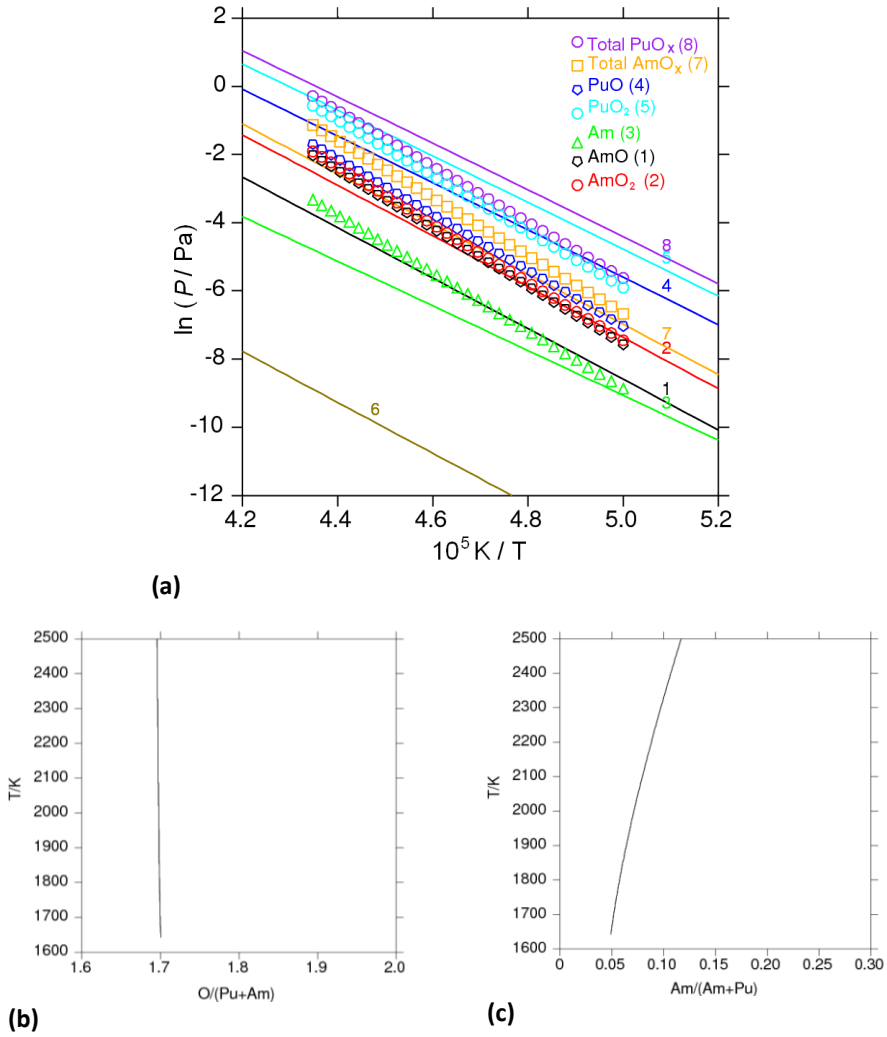

Figure 13. **(a)** Calculated vapour pressure against the temperature for the azeotropic condition in (Pu,Am)O_{2-x} oxide, in comparison with the experimental data on $Pu_{0.756}Am_{0.244}O_{2-x}$ sample from this study. (1), (2), (3) refer to the calculated pressure of AmO, AmO_2, Am, respectively. (4), (5), (6), refer to the calculated pressure of PuO, PuO_2, Pu, respectively. (7) and (8) are the calculated total pressure for the americium and plutonium, respectively, bearing species; **(b)** O/(Am+Pu) ratio in the gas and in the solid phases versus temperature; **(c)** Am/(Am+Pu) ratio in the gas phase versus temperature. The Am/(Am+Pu) ratio of the solid phase is constant, equal to 0.244.

The O/M in the congruent solid and gas phases is calculated as a function of the temperature in Figure 13(b). A good agreement is found with the

experimental final value of the O/M ratio of the sample, found in the TGA post measurement, i.e. 1.72 ± 0.04. The calculations indicated O/M = 1.70 for the sample quenched at 2300 K. The variation of the Am content in the vapour phase is calculated in Figure 13(c). The Am/M content in the gas slightly varies with temperature between 0.07 and 0.10 for T = 2000 - 2300 K.

6.5 Summary and Conclusions

Knudsen cell mass spectrometric measurements on a $Pu_{0.756}Am_{0.244}O_{2-x}$ mixed oxide sample have been performed. The vapour species were analysed as a function of time and congruent vapour pressure data were obtained. The ionisation efficiency curves were recorded for both plutonium and americium bearing oxide ionic species to provide insight into the vapour composition. The partial vapour pressures have been derived between 2000 and 2300 K, taking into account the dissociation processes occurring up to 40 eV, the electron energy at which the intensity signals of the species were recorded. The results indicated PuO_2 as a major component in the vapour, followed by the monoxide. With respect to the total americium oxide pressure, americium dioxide was found close to the monoxide. Am(g) has the lowest pressure over the mixed oxide sample.

Using the CALPHAD method an assessment of the ternary Pu-Am-O system has been performed. For this purpose the data for the Pu-Am and Am-O binary systems had to be evaluated. For both systems the related models were described and the resulted phase diagrams were reported.

The applied model for the Am-O system was similar to the Pu-O model provided by Guéneau *et al.* [7,12]. A comparison of the Am-O experimental data on oxygen pressure-temperature-composition equilibria was made stepwise. Due to the large discrepancy at a low O/Am ratios, a selection of these data was made. Although an attempt was performed to fit the recent oxygen potential data measured by Otobe *et al.* [29], the results were not reasonable with the existing phase diagram data and the vapour pressure measurements performed over AmO_2 samples previously [11]. Therefore a higher weighting was given therefore to the phase boundary functions of the sesquioxide. In order to obtain a thermodynamic model consistent with the existence of the miscibility gap reported by Sari [9], only the oxygen

potential data from Chikalla and Eyring [41] with a composition and temperature range outside the miscibility gap (data with O/Am ratio lower than ~1.9) were selected for the assessment.

The description of the ternary system was constituted from both binaries discussed in this study, and additionally Pu-O from [7], slightly adjusted in [12] to improve the description of the small miscibility gap extent in the fluorite phase and to take into account the recent measured melting point for PuO_2 by De Bruycker *et al.* [13]. Ternary parameters were introduced in order to slightly adjust the fit of the oxygen potential measurements performed by Osaka *et al.* [2] and Otobe *et al.* [3] on PuO_2 samples with 9% and 50% Am content and the miscibility gap in the MO_2 phase reported by Miwa *et al.* [1] for 9% Am content in PuO_{2-x}. Generally the calculations on the vaporisation of the $Pu_{0.756}Am_{0.244}O_{2-x}$ sample showed good agreement with respect to the total pressure of plutonium and americium bearing species. The results of the assessment showed that the Am/M ratio in the gaseous phase slightly varies with temperature and very good agreement was found between the O/M ratio obtained by the post mass spectrometric measurements gravimetric analysis and the calculated values in azeotropic conditions.

The limited available thermochemical data in the Am-O and Am-Pu binaries, which are highly inconsistent, emphasize the need of further studies. Furthermore, additional data to complement the few restricted studies on the Pu-Am-O ternary system are essential. It can be concluded that the current model provides the first practical tool for a comprehensive understanding and prediction of the high temperature behaviour of transmutation fuels and targets.

6.6 References

[1] S. Miwa, M. Osaka, H. Yoshimochi, K. Tanaka, K. Kurosaki, M. Uno, S. Yamanaka, J. Alloys Compd. 444-445 (2007) 610.
[2] M. Osaka, K. Kurosaki, S. Yamanaka, J. Nucl. Mater. 357 (2006) 69.
[3] H. Otobe, M. Akabori, Y. Arai, J. Nucl. Mater. 389 (2009) 68.
[4] R.J. Ackermann, R.L. Faircloth, M.H. Rand, J. Phys. Chem. 70 (1966) 3698.
[5] R.W. Ohse, Progress Report no. 5, European Institute for Transuranium Elements, Karlsruhe, Germany (1968) p. 26.
[6] C. Guéneau, M. Baichi, D. Labroche, C. Chatillon, B. Sundman, J. Nucl. Mater. 304 (2002) 161.

[7] C. Guéneau, C. Chatillon, B. Sundman, J. Nucl. Mater. 378 (2008) 257.
[8] A. Fernández, R.J.M. Konings, J. Somers, D. Haas, J. Mat. Sci. Lett. 22 (2003) 119.
[9] C. Sari, E. Zamorani, J. Nucl. Mater. 37 (1970) 324.
[10] P. Gotcu-Freis, J.-Y. Colle, J.-P. Hiernaut, F. Naisse, C. Guéneau, R.J.M. Konings, J. Chem. Thermodyn., 43 (2011) 1164.
[11] P. Gotcu-Freis, J.-Y. Colle, J.-P. Hiernaut, R.J.M. Konings, J. Nucl. Mater. 409 (2011) 194.
[12] C. Guéneau, N. Dupin, C. Martial, J.C. Dumas, S. Gossé, S. Chatain, B. Sundman, To be submitted to the J. Nucl. Mater.
[13] F. De Bruycker, K. Boboridis, D. Manara, P. Poeml, M. Rini, R.J.M. Konings, Materials Today 13-11 (2010) 52.
[14] C. Thiriet, R.J.M. Konings, J. Nucl. Mater. 320 (2003) 292-298.
[15] T.M. Besmann, T.B Lindemer, J. Nucl. Mater. 130 (1985) 489.
[16] T.B. Lindemer, T.M. Besmann, J. Nucl. Mater. 130 (1985) 473.
[17] T.M. Besmann, J. Brynestad, J. Am. Ceram. Soc. 69 (1986) 867.
[18] T.B. Lindemer, CALPHAD 10 (1986) 129.
[19] T.M. Besmann, J. Nucl. Mater. 402 (2010) 25.
[20] M. Hillert, J. Alloys Compds. 320 (2001) 161.
[21] F.H. Ellinger, K.A. Johnson, V.O. Struebing, J. NucL. Mater. 20 (1966) 83-86.
[22] A. Dinsdale, Calphad 15 (4) (1991) 317.
[23] T.B. Massalski, P.R. Subramanian, H. Okamoto, L. Kacprzak, Binary Alloy Phase Diagrams, 2nd ed., ASM International, 1990.
[24] T. Ogawa, J. Alloys Compd. 194 (1993) 1.
[25] H. Okamoto, J. Phase Equil. 20 (1999) 451.
[26] P. Turchi, Thermodynamics of Nuclear Fuels, Actinet, CEA/DPC Saclay, 27/11-12/01/2006.
[27] V.D. Shushakov, N.S. Kosulin, N.T. Chebotarev, Voprosy Atom. Nauki Tekh., Ser. Materialoved. Novye Mater. 3 (1990) 14.
[28] S. Casalta, PhD Thesis: Etude des proprietes du systeme Am-O en vue de la transmutation de l'americium 241 en reacteur a netrons rapides, University Aix-Marseille I, Marseille 1996.
[29] H. Otobe, M. Akabori, K. Minato, J. Am. Ceram. Soc. 91 (2008) 1981.
[30] H. Okamoto, J. Phas. Equil. Diff. 27 (2006) 197.
[31] R.J. Silva, G. Bidoglio, M.H. Rand, P.B. Robouch, H. Wanner, I. Puigdomenech, Chemical Thermodynamics of Americium, OECD, Nuclear Energy Agency, Elsevier 2004.
[32] W.H. Runde, W.W. Schulz, in: J.J. Katz, L.R. Morss, N.M. Edelstein, J. Fuger, (Eds.), The Chemistry of the Actinide and Transactinide Elements, Springer Netherlands, Dordrecht, 2006.
[33] L.R. Morss, D.C. Sonnenbeerger, J. Nucl. Mater. 130 (1985) 266.
[34] L.R. Morss, J. Fuger, J. Inorg. Nucl. Chem. 43 (1981) 2059.
[35] T.D. Chikalla, C.E. McNeilly, J.L. Bates, J.J. Rasmussen, Proc. Int. Colloq. on High Temperature Phase Transformations, CNRS Publ. 1973, p. 351.
[36] R.E. McHenry, Trans. Am. Nucl. Soc. 8 (1965) 75.

[37] R.J.M. Konings, O. Benes, D. Manara, D. Sedmidubsky, L. Gorokhov, V.S. Iorish, The thermodynamic properties of f-elements. Part II. The Lanthanide and Actinide Oxides, J. Phys. Chem. Ref. Data, submitted.
[38] T.D.Chikalla, L. Eyring, J. Inorg. Nucl. Chem. 30 (1967) 133.
[39] C. Keller, U. Berndt, Transplutonium Elements, W. Müller, R. Lindner (Eds.), 1976, p. 85.
[40] J.C. Wallmann, J. Inorg. Nucl. Chem. 26 (1964) 2053.
[41] T.D. Chikalla, L. Eyring, J. Inorg. Nucl. Chem. 29 (1967) 2281.
[42] T.L. Markin, M.H. Rand, Thermodynamics, vol. 1, IAEA, Vienna 1966, p. 145.
[43] S. Miwa, I. Sato, K. Tanaka, T. Hirosawa, M. Osaka, J. Nucl. Mater. 400 (2010) 32.
[44] B. Jansson, Report TRITA-MAC-0234, Royal Institute Technology, S10044 Stockholm 70, Sweden, April 1984.
[45] B. Sudman, B. Jansson, J.O. Andersson, Calphad 9 (1985) 153.
[46] N. Saunders, A.P. Miodownik, Calphad. A comprehensive guide, Pergamon Materials Series 1998.
[47] H.L. Lukas, S.G. Fries, B. Sundman, Computational Thermodynamics, The Calphad Method, Cambridge Univ. Press (2007).
[48] I. Ansara, B. Sundman, Scientific Group Thermodata Europe, Computer Handling and Determination of Data, P.S. Glaser (Ed.), North Holland, Amsterdam 1986, p. 154.
[49] V.P. Glushko, L.V. Gurvich, G.A. Bergman, I.V. Veyts, V.A. Medvedev, G.A. Khachkuruzov, V.S. Yungman, Thermodynamic Properties of Individual Substances (Termodinamicheskie Svoistva Individual'nykh Veshchestv), Nauka, Moskow 1982.
[50] T. Nishi, A. Itoh, K. Ichise, Y. Arai, J. Nucl. Mater. (2011) doi: 10.1016/j.jnucmat.2011.01.019.

Chapter 7

Vaporisation of candidate nuclear fuels and targets for transmutation of minor actinides

Abstract

*The thermal stability and high temperature behaviour of candidate fuels and targets for transmutation of minor actinides has been investigated. Zirconia-based solid solution, MgO-based CERCER and molybdenum-based CERMET fuels containing Am and/or Pu in various concentrations were heated up to 2700 K in a Knudsen cell coupled with a quadrupole mass spectrometer, to measure their vapour pressure and vapour composition. The results reveal that the vaporisation of the actinides from the samples is not only determined by the thermodynamics of the system but is also related to the dynamic evolution of multi-component mixtures with complex composition or microstructure.**

*This chapter is reprinted with kind permission of Elsevier: "Vaporisation of candidate nuclear fuels and targets for transmutation of minor actinides. P. Gotcu-Freis, J.-P. Hiernaut, J.-Y. Colle, C. Nästrén, A. Fernandez Carretero, R.J.M. Konings. Journal of Nuclear Materials 411 (2011) 119-125".

7.1 Introduction

Partitioning and Transmutation (P&T) is considered an attractive option for the management of nuclear waste. Compared to current approaches (direct geological disposal of spent fuel or vitrified waste from reprocessing) the partitioning of the transuranium elements from the spent fuel leads to a substantial reduction of the radiotoxic inventory of the waste, provided that the separated elements are transmuted (destroyed) in nuclear reactors or dedicated transmutation systems.

Separated plutonium is currently recycled in mixed oxide (MOX) fuels in light water reactors (LWR) in countries where reprocessing of spent fuel is practised. The total amount of plutonium in a MOX reactor core, in practice loaded with one third MOX elements, is not significantly reduced due to breeding of plutonium in the uranium matrix. In addition, the number of plutonium recycling steps in a LWR is limited due to the isotope vector degradation. In fast reactors (FR) the plutonium consumption is higher and multiple recycling steps can be realised. However, as a consequence of plutonium recycling either in LWRs or FRs the quantities of minor actinides (Np, Am, Cm) significantly increase [1].

Transmutation of minor actinides such as americium can be achieved by fission in fast neutron systems, either in fuels, minor actinide bearing blankets or in uranium-free targets. These targets are designed to achieve an optimum transmutation yield [1] by incorporating the minor actinides in a material which is inert under neutron irradiation, the so-called transmutation matrix. During the last decade numerous evaluations and investigations were performed which showed that the fuel and target materials must satisfy some properties such as high melting point, good thermal conductivity, good compatibility with the cladding, low solubility in the coolant and good mechanical properties [2]. In addition, the resistance and response to radiation damage is a very critical parameter.

Several fuel and target concepts are being considered in this paper. In the first place, simple binary and ternary oxide solid solution materials have been studied. Because all the relevant actinides are soluble in the lattice of zirconia or yttria-stabilised zirconia (YSZ), the actinide phase can be mixed with YSZ to give solid solution materials such as $(Pu,Am,Zr)O_{2-x}$ or $(Pu,Am,Zr,Y)O_{2-x}$. The major drawback of these YSZ based materials is their

low thermal conductivity, which is further penalised by the fact that the radiation damage is homogeneously distributed in the solid solution [3]. This can be overcome by composite designs, in which the actinide phase is mixed with a matrix with a high thermal conductivity to form a two-phase mixture. The concepts considered in this work are ceramic-ceramic (CERCER) materials such as $(Pu,Am)O_{2-x}$ dispersed in MgO, as well as ceramic-metal (CERMET) materials such as $(Pu,Am)O_{2-x}$ dispersed in Mo. An additional advantage of the composite design is that the radiation damage is primarily localised in the dispersed phase, in case the inclusions are greater than 100 µm in size [4].

These inert matrix concepts are being explored extensively nowadays with experimental studies involving the development of fabrication procedures [5-7], irradiation tests [5,8-10], fission product behaviour [11] and property measurements [12,13]. The latter are traditionally focussed on thermal conductivity and melting point, which together give the margin between operating and melting temperature. In addition, however, the vaporisation behaviour should be considered for these materials to assess the behaviour of the fuels and targets during temperature excursions in the reactor. Therefore, the present paper reports a study of the vaporisation of a series of candidate nuclear fuels and targets for the transmutation of minor actinides, with focus on the actinides bearing vapour species and species originating from the matrix compounds generated during annealing at high temperatures of up to 2700 K.

7.2 Experimental

7.2.1 Mass spectrometry

The investigated samples were vaporised in vacuum in a Knudsen cell coupled with a quadrupole mass spectrometer (QMG422 from Pfeiffer Vacuum, mass range of 1 to 512 amu), which has been built in a lead-shielded glove box to allow studies on radioactive samples. The samples, in weight of 10 to 25 mg, were heated in a tungsten cell. The system was heated to a maximum temperature of 2700 K. The whole Knudsen cell mass spectrometer assembly was calibrated with silver as described in another paper [14]. All measurements were performed in vacuum using an electron impact energy of 40 eV. Since mainly the total vapour pressure

data are presented, no corrections for the dissociation processes involved are made.

7.2.2 Samples

The samples described here have all been prepared as part of fuel irradiation campaigns in the Phénix fast neutron reactor in France and in the High Flux Reactor in Petten. These experiments are ongoing with successful irradiation completed, being part of the R&D programme. The different samples studied in the present paper are listed in Table 1, with the respective composition of the actinide phase, the fraction of the matrix phase and sintering conditions applied during fabrication process. Samples 1, 6, 7, 10, and sample 11 contained initially a small fraction of 5 wt % and 6 wt %, respectively, of neptunium resulting from the alpha-decay of ^{241}Am.

For the fabrication of (Pu,Am)O_{2-x}, (An,Zr,Y)O_{2-x} and (An,Zr)O_{2-x} pellets, where An represents Am or Pu, a combination of the external gelation, also known as gel supported precipitation (GSP), and infiltration routes were used to generate the precursor powder, followed by compaction and sintering in a suitable optimised atmosphere (Ar/H_2, Ar, air) at 1600 ^{o}C [6]. The final Am content was determined by gravimetric analysis before and after the infiltration step.

To obtain the composite materials, the actinide bearing component was mixed with the required amount of MgO or Mo powder that acts as the fuel matrix. The mixtures were compacted into pellets and then sintered. The sintering atmosphere was Ar/H_2 for the majority of the samples, for samples 10 and 11 the atmosphere was changed at 1000 °C to pure Ar. After the sintering, gravimetric methods generally showed a change in weight of the sample due to reduction of the actinides, resulting in a reduced O/An ratio [15]. Experience has shown that for a thermal treatment in Ar/H_2 at 1600 ^{o}C the O/An ratio is about 1.83 for plutonium oxide [14] and around 1.6 for americium oxide [5]. It is thus clear that the O/An ratio of the actinide phase in all samples is lower than 2.00. However, the initial O/An ratio is of limited relevance to our experiments as the measurements were made in vacuum at temperature hundredths of degrees higher than the sintering temperature, at which the oxygen

equilibrium pressure and hence the O/An ratio will undergo strong chances (see next section).

Table 1. Sample types and sample composition studied in this work, where M=Pu+Am+Zr+Y. The last column indicates the sintering conditions of the samples. Samples 1, 6, 7, 10, and sample 11 contained initially a small fraction of 5 wt% and 6 wt%, respectively, of neptunium resulting from the alpha-decay of ^{241}Am. Sintering conditions according to: (a): 1600°C, 8h, Ar/H_2; (b): 1600°C, 8h, Ar; (c): 1600°C, 4h, Ar/H_2.

Sample n°	Type of sample	Fraction of the metal				Fraction of matrix phase (in vol%)		Sintering conditions
		Pu/M	Am/M	Zr/M	Y/M	MgO	Mo	
s.1	$(Pu,Am)O_{2-x}$	0.797	0.198	-	-	-	-	(a)
s.2	$(Am,Zr,Y)O_{2-x}$		0.057	0.784	0.159	-	-	(b)
s.3	$(Am,Zr,Y)O_{2-x}$		0.066	0.800	0.134	-	-	(a)
s.4	$(Pu,Am,Zr)O_{2-x}$	0.285	0.049	0.666	-	-	-	(a)
s.5	$(Pu,Am,Zr)O_{2-x}$	0.248	0.173	0.579	-	-	-	(a)
s.6	$(Pu,Am)O_{2-x}$ in MgO	0.797	0.198	-	-	70	-	(a)
s.7	$(Pu,Am)O_{2-x}$ in MgO	0.797	0.198	-	-	90	-	(a)
s.8	$(Pu,Am)O_{2-x}$ in MgO	0.500	0.500	-	-	70	-	(c)
s.9	$(Am,Zr,Y)O_{2-x}$ in MgO	-	0.195	0.670	0.135	54	-	(a)
s.10	$(Pu,Am)O_{2-x}$ in Mo	0.792	0.203	-	-	-	85	(a)
s.11	$(Pu,Am,Zr)O_{2-x}$ in Mo	0.220	0.240	0.534	-	-	66	(a)

7.3 Results

7.3.1 $(Pu,Am)O_{2-x}$ solid solution

$(Pu_{0.8}Am_{0.2})O_{2-x}$, sample 1 in Table 1, was studied because it is the included phase of several composite samples. The total plutonium and americium pressures (ΣAnO_y with y = 0, 1, 2) measured for this sample are shown in Figures 1 and 2. It can be seen that the pressures are close to those of the pure oxides, PuO_{2-x} and AmO_{2-x}, as previously performed by us in similar conditions [14,16], although the oxygen-to-metal (O/M) ratio in this solid solution differed somewhat from that in the pure oxides. The slopes of the ln(*P*/Pa) against 1/*T* curves (representing the enthalpy of vaporisation, $\Delta_{vap}H$) are almost parallel to those of the pure oxides. The differences correspond approximately to those expected from the mole fractions (*x*) in the sample assuming ideal behaviour, which would be reflected by a proportional vertical displacement of the vapour pressure curve compared to the pure AmO_{2-x} or PuO_{2-x} equal to ln(*x*). Thus, our results indicate a regular vaporisation behaviour of this material.

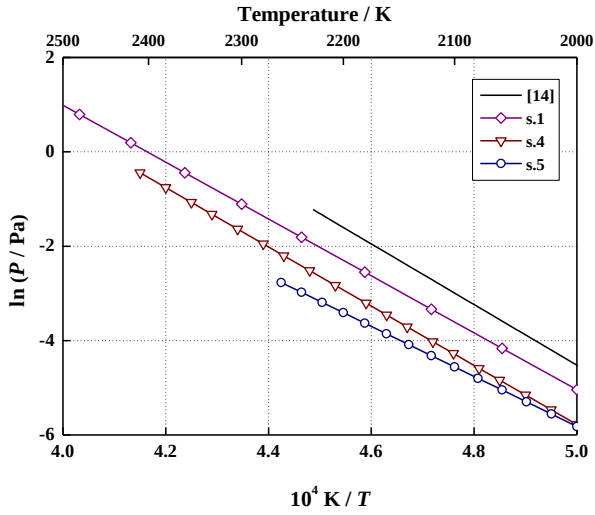

Figure 1. Total vapour pressure of plutonium bearing oxide species (represented as ΣPuO_y with y = 0, 1, 2) from different zirconia-based solid solution samples (see also Table 1) and compared with the vapour pressure of the PuO_{2-x} reference sample [14].

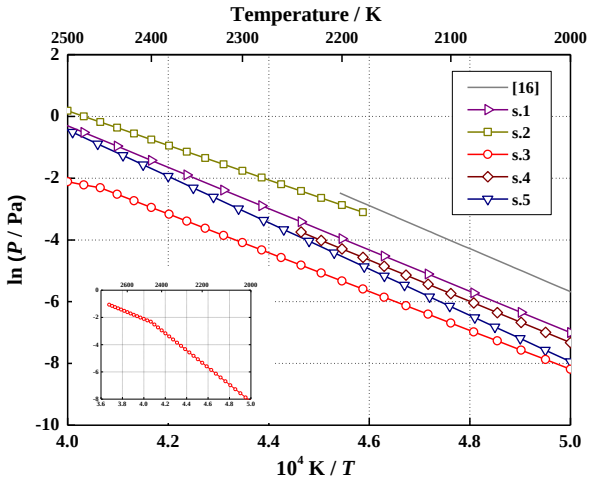

Figure 2. Total vapour pressure of americium bearing oxide species (represented as ΣAmO_y with y = 0, 1, 2) from different zirconia-based solid solution samples (see also Table 1) and compared with the vapour pressure of the AmO_{2-x} reference sample [16]. The insertion presents the total ΣAmO_y vaporisation from sample 3 up to 2700 K.

7.3.2 Zirconia - based solid solutions

Four samples of stabilised zirconia solid solutions were studied (samples 2-5). They contained either Pu or Am, or both. The stabilisation of the cubic phase was achieved by actinides (Pu and/or Am). In case of a low An content (samples 2, 3 in Table 1) by yttrium oxide.

The vaporisation of the zirconia matrix was detectable above about 2350 K, which is about 250 K higher than for the plutonium and americium oxide species. This implies strongly incongruent vaporisation conditions.

The total pressures of the plutonium and americium gaseous species measured above the zirconia-based samples are shown in Figures 1 and 2. The measured pressures above the zirconia solid solutions are lower than those of the actinide oxides alone, PuO_{2-x} and AmO_{2-x}, with the exception of the americium pressure of sample 2, which is almost identical to the pressure of AmO_{2-x}. The slopes of the ln(P) against 1/T curves of the total pressures (ΣAnO_y with y = 0, 1, 2) are in most cases almost parallel to the slopes measured for pure AmO_{2-x} and pure PuO_{2-x}, though generally not

over the whole temperature range of the measurements, e.g. sample 3 (Figure 2).

The total plutonium pressure in samples 4 and 5 (Figure 1), which had similar Pu content (Pu/(Pu+Am+Zr) ≈ 0.25), is very close but somewhat higher than expected for the case of ideal solution behaviour, which would be reflected by a proportional vertical displacement of the vapour pressure curve compared to the pure PuO_{2-x} curves from [14], by –ln(0.25). The corresponding total americium pressures show a similar behaviour. There are two factors that must be taken into account. First, these solutions may not behave ideal, which is known for the PuO_2-ZrO_2 system [17]. Second, the O/M ratio in the samples was not identical to the pure actinide oxides, and moreover changes in a different way due to incongruent vaporisation. Whereas for pure plutonium dioxide the composition of the solid phase changes during the measurements to O/M ≈ 1.8 due to significant oxygen vaporisation, the oxygen will be more strongly bonded in the zirconia solid solutions. As a result, the current measurements refer to a higher O/M in the solid sample. Our measurements for the Pu-O system have shown that the total Pu oxide pressure increases for O/Pu between 1.83 and 2.00 for constant temperature [14]. The pure americium dioxide will be even more reduced, but its vaporisation behaviour for compositions close to O/Am ≈ 2.0 has not been determined [16].

The differences of three orders of magnitude between the ΣAmO_y (with y = 0, 1, 2) vapour pressures of $(Am,Zr,Y)O_{2-x}$ samples 2 and 3 (Figure 2), which have very close compositions, might be explained by the fact that the latter was sintered in Ar/H_2 whereas the former was sintered in Ar. The fact that the total americium pressure of sample 2 is close to that of pure AmO_{2-x} suggests that incomplete reaction has taken place under these conditions, and that some pure AmO_{2-x} remained in the sample. The insertion in Figure 2 presents the total ΣAmO_y vaporisation from sample 3 up to 2700 K, with a change in slope above 2500 K due to the influence of the Am diffusion in the sample.

7.3.3 Magnesia - based composite

This group of samples contained composites made of actinide particles of $(Pu,Am)O_{2-x}$ or $(Am,Zr,Y)O_{2-x}$ dispersed in a matrix of MgO (samples 6 to 9,

see Table 1). The measured vaporisation data are shown in Figures 3-5 for the matrix and the actinides.

MgO is stable under oxidising conditions up to high temperatures. However, in vacuum the equilibrium partial pressure of gaseous Mg increases dramatically, and at temperatures above 2000 K MgO pellets were found to be structurally and geometrically instable [3]. The current experiments confirm that at T > 1400 K the decomposition of MgO is the main reaction for these samples:

$$MgO \leftrightarrow Mg + 1/2\ O_2. \quad (1)$$

The free oxygen reacts with the actinide phase in the sample or eventually with the Knudsen cell material and further displaces the equilibrium in equation (1) to the right. In practise the effect can be represented by the reaction:

$$y\ MgO + (PuAm)O_{2-x} \leftrightarrow (PuAm)O_{2-x+y} + y\ Mg. \quad (2)$$

In Figure 3 the Mg vapour pressure measured above these samples is plotted together with the Mg pressure calculated with the FactSage 5.5© software [18], for equilibrium composition and phases in conditions in a closed system (constant volume) at atmospheric pressure. The calculations were performed for pure MgO, and for a 50/50 mixture of MgO with W or PuO_{2-x}, using evaluated thermodynamic data [19,20]. The Mg signal measured for these samples was higher than that above pure MgO and falls within the domain of MgO mixed with PuO_{2-x}, indicated by the boundary compositions MgO + Pu_2O_3 and MgO + PuO_2 (Figure 3).

Above 2000 K the actinides were also detected in the vapour phase. Figures 4 and 5 show the measured total vapour pressure of the different actinide species (ΣAn bearing oxide species), which can be compared with reference samples of PuO_{2-x} and AmO_{2-x} as well as the pure inclusion phases. For sample 6, with the $(Pu_{0.80}Am_{0.20})O_{2-x}$ included phase, the vapour pressure of Pu is almost identical to that of the sample 1 (Figure 4). Sample 7, the same included material but more diluted in MgO, initially shows a very similar behaviour, but a change in the curve occurs around 2200 K.

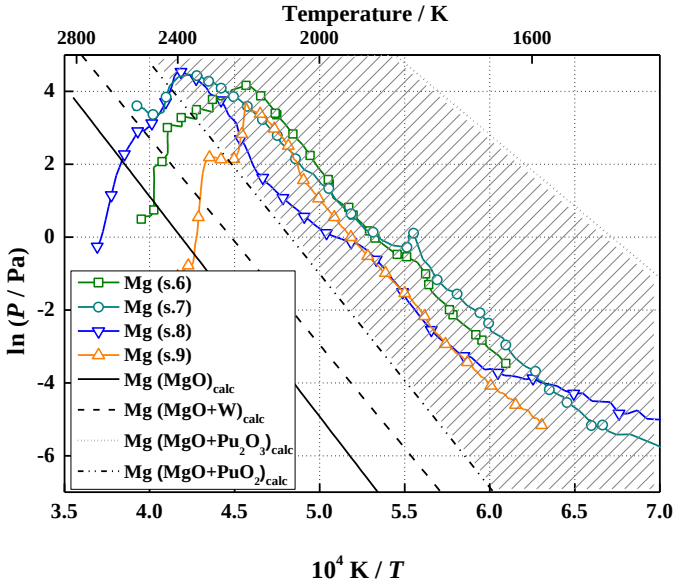

Figure 3. Total vapour pressure of Mg above samples 6 to 9 (see Table 1) and mean curve, compared with the total pressure calculated above pure MgO, mixture (50/50) of MgO with W and with Pu_2O_3 and PuO_2 obtained from thermodynamic assessments [18-20].

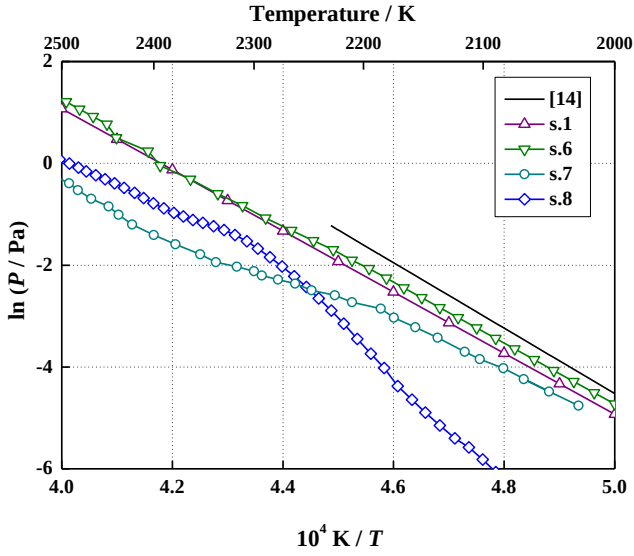

Figure 4. Total vapour pressure of plutonium oxide bearing species (represented as ΣPuO_y with y = 0, 1, 2) plotted in an Arrhenius type graph: ln (*P*/Pa) vs. 10^4 K/*T*. The vapour

pressure results of samples 6-8 (see Table 1) are compared with the data of PuO_{2-x} sample from reference [14].

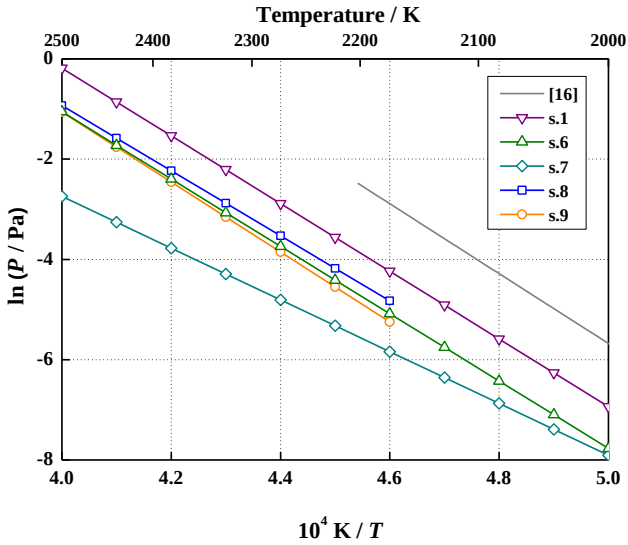

Figure 5. Total vapour pressure of americium oxide bearing species (represented as ΣAmO_y with y = 0, 1, 2) plotted in an Arrhenius type graph: ln (*P*/Pa) vs. 10^4 K/*T*. The vapour pressure results of samples 6-9 (see Table 1) are compared with the data of AmO_{2-x} sample from reference [16].

In contrast, sample 8, in which the composition of the included phase is changed to $(Pu_{0.50}Am_{0.50})O_{2-x}$, initially has a lower vapour pressure with a distinct different slope, but approaches "normal" values above 2275 K. The americium pressure of the sample 6 (Figure 5) is somewhat lower than that of the included phase and that of sample 7 is significantly lower. This suggests a relation with the dilution in the matrix. The americium pressure of samples 8 and 9 is close to that of 6. Moreover, as shown in Figure 6, the change in O/M of the included phase in samples 6 and 7 is very different from the pure $Pu_{0.8}Am_{0.2}O_{2-x}$ as endued by a very different $P(AmO)/P(AmO_2)$ ratio.

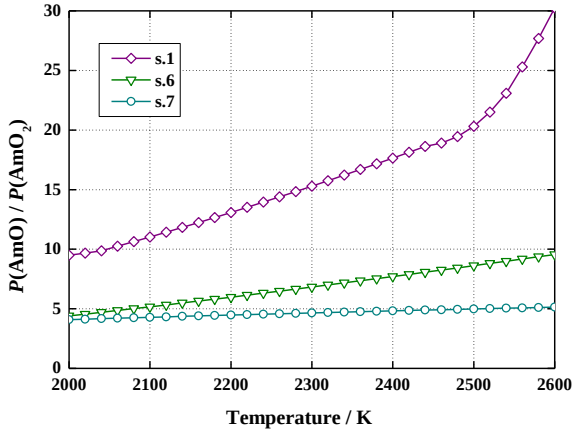

Figure 6. The partial pressures ratio of AmO over AmO_2, $P(AmO)/P(AmO_2)$, measured at 40 eV as a function of the annealing temperature for samples 6 and 7 containing Am (see Table 1) and different concentration of MgO matrix, and the reference $(Pu_{0.8}Am_{0.2})O_{2-x}$, sample 1.

To clarify this inconsistent behaviour, SEM micrographs of pieces of sample 6 were made before and after heating in the Knudsen cell at 2100 K (Figure 7). In the as-received sample the actinide-rich inclusions were clearly visible, particularly in the backscattered image (picture 2) where the bright spots are rich in actinide Pu and Am, and the dark region in Mg. In contrast, after annealing the whole surface of the sample revealed an actinide-rich phase (picture 4). A likely explanation for this might be the selective vaporisation of the matrix phase. Furthermore, Miwa *et al.* [21] observed strong growth of the actinide phase in heat treated $(Pu,Am)O_{2-x}$-MgO samples at temperatures above 2000 K, in combination with redistribution of Am.

Upon further heating also eutectic melting of the matrix and inclusions must be taken into account. We observed a decrease in the Mg pressure in all the four magnesia matrix samples between 2300 and 2400 K (Figure 3) which is close to the predicted eutectic temperatures in the $MgO\text{-}PuO_{2-x}$ and $MgO\text{-}AmO_{2-x}$ systems [22,23], in agreement with the experimental study by Miwa *et al.* [21] where the $(Pu,Am)O_{2-x}$-MgO samples were melted between 2373 and 2573 K.

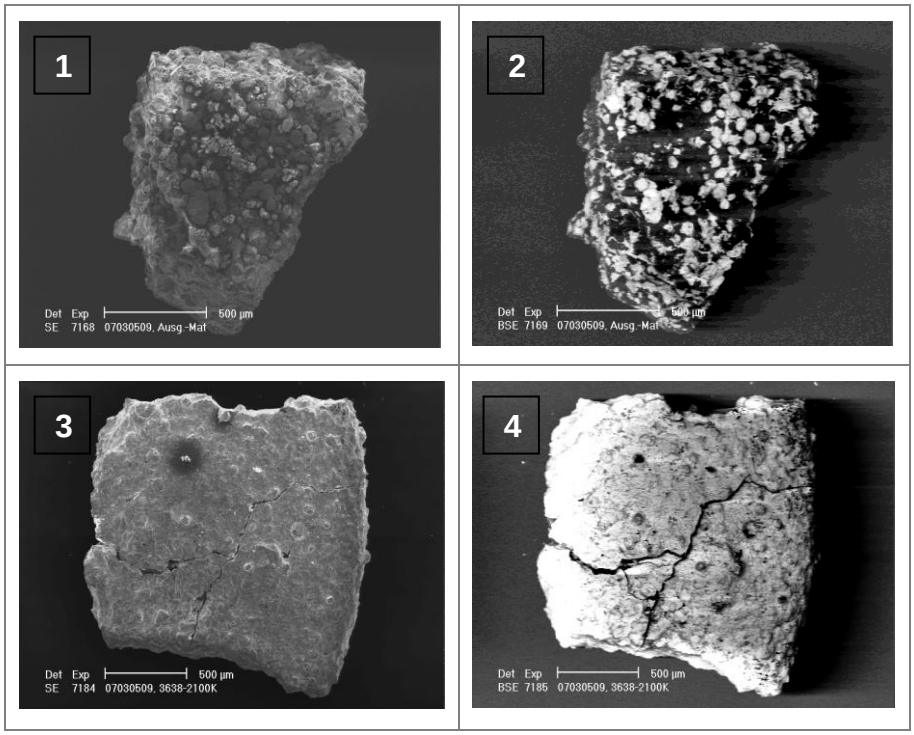

Figure 7. SEM micrographs of sample 6 (Table 1) before and after annealing at 2100 K. Pictures 1 and 2: sample as received, 3 and 4 sample after annealing. Pictures 2 and 4 are the backscattered images.

7.3.4 Molybdenum - based composites

The CERMET samples 10 and 11 in Table 1, for which the actinide containing inclusions as $(Pu,Am)O_{2-x}$ or $(Pu,Am,Zr)O_{2-x}$ phases have been mixed in a matrix of metallic molybdenum, have a somewhat different behaviour at high temperature. In sample 10 the actinides were detected above 2000 K and their pressure reached a maximum around 2370 K and subsequently decreases (Figure 8). At this temperature (T = 2370 K) molybdenum started to vaporise as well and was detected among the vapour. At about 2570 K the vaporisation of the actinides species increased again with temperature. In sample 11, the vaporisation of the actinides was much more continuous with temperature.

These observations can be explained by the differences in the vaporisation behaviour of the Mo matrix and the actinides oxides function of the

annealing temperature. Initially regular vaporisation of the actinides occurred, but only from the inclusions at the surface of the fuel fragment. Since the oxygen release from the actinide phase was affected/buffered by the presence of Mo and the congruent vaporisation was therefore not approached, the vapour pressure values are different from the reference $(Pu_{0.80}Am_{0.20})O_{2-x}$ oxide (sample 1).

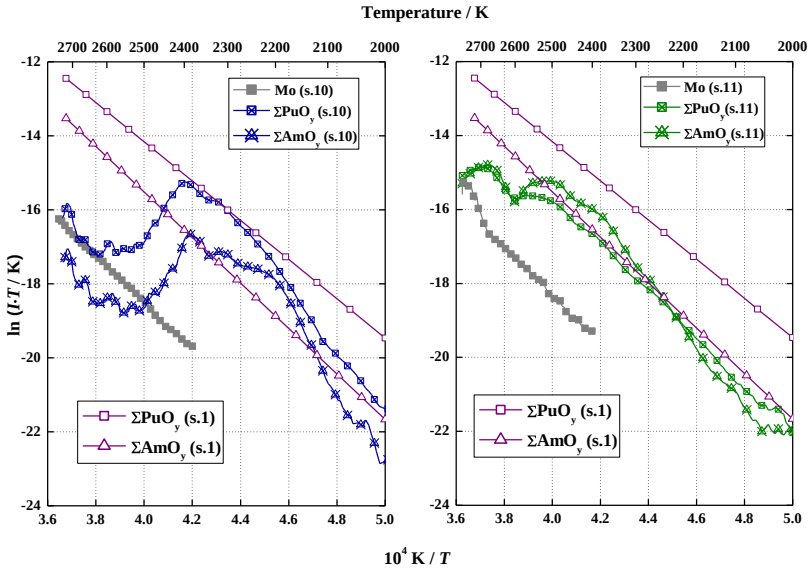

Figure 8. The mass spectrometric results of molybdenum and actinide oxides bearing species expressed in ln ($I \cdot T$/K) (represented as ΣAnO_y with An = Pu or Am and y = 0, 1, 2), measured from sample 10 and 11 and compared with the respective Mo and An oxides vapour species from sample 1 (see also Table 1).

In sample 10, which had a low volume fraction of the actinide phase (15 vol%), the inclusions at the surface became depleted in Pu and Am with further increasing of the temperature. Furthermore the vaporisation of the enclosed inclusions was inhibited by the matrix (Figure 9), and thus their vapour pressure dramatically decreased.

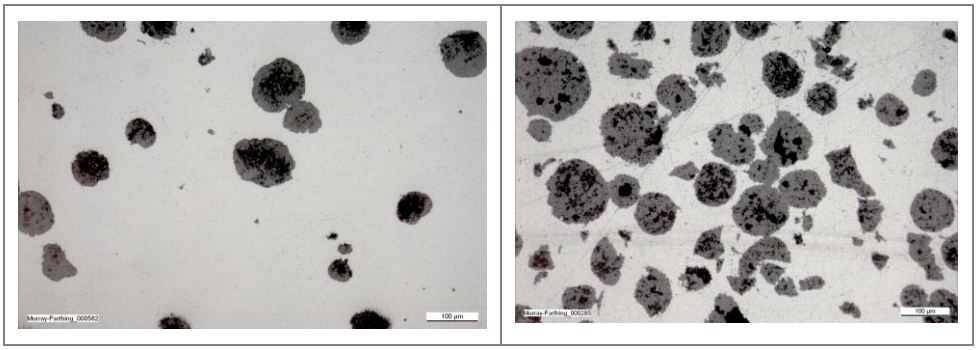

Figure 9. Ceramographies of sample 10 (left) and 11 (right) showing typical distribution of the actinide spheres in the molybdenum matrix.

Above 2570 K the vaporisation of the Mo matrix became significant and also the vaporisation of enclosed inclusions was now possible, as a result of which the vapour pressure of the actinides increased again. In sample 11, in contrast, the volume fraction of the actinide phase was higher (34 vol%), and hence the volume of the material available for vaporisation was much larger. This aspect, amplified by the fact that the included particles were not as isolated as in sample 10 but formed clusters of several particles (Figure 9), strongly contributed to a more regular vaporisation profile (Figure 8).

7.4 Conclusions

The different candidate inert matrix fuels and targets that have been studied in this work (solid solution, CERMET and CERCER composites) show distinct different vaporisation behaviour, as schematically depicted in Figure 10.

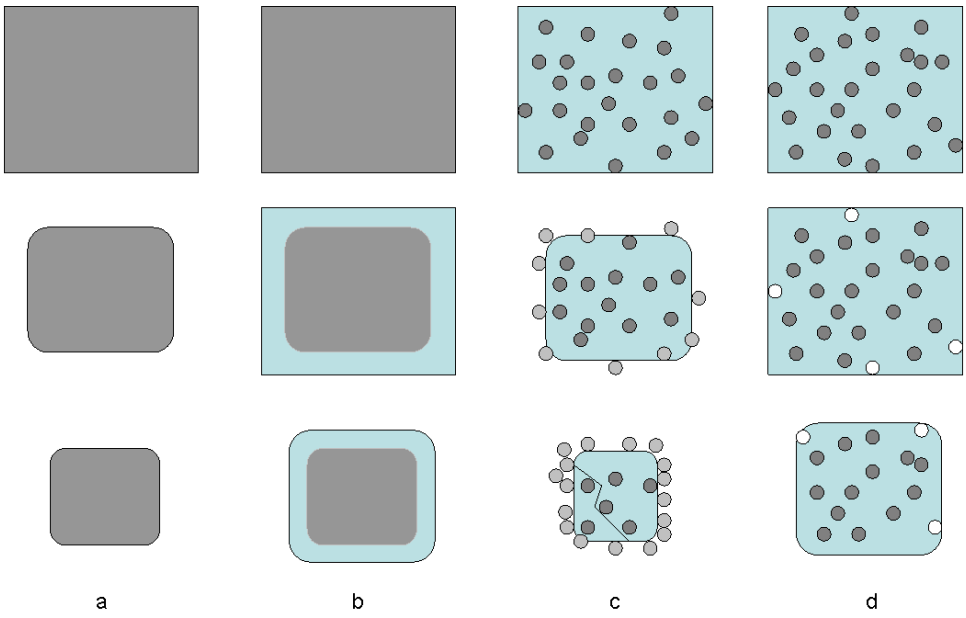

Figure 10. Schematic representation of the different vaporisation modes for the samples studied: **(a)** regular vaporisation of a solid solution; **(b)** incongruent vaporisation of a solid solution; **(c)** composite with a matrix that is more volatile than the included phase; **(d)** composite with a matrix less volatile than the included phase. Grey indicates the actinide containing phases, whereas blue the matrix phase.

We can discern the following cases:

(a) The vaporisation of the $(Pu_{0.8}Am_{0.2})O_{2-x}$ solid solutions is principally governed by the thermodynamics of the system, which behave regular.

(b) Also the vaporisation of the zirconia-based solid solutions is initially governed by the thermodynamics of the system, but due to selective vaporisation of the actinides as a result of the large difference in vapour pressure compared to zirconia, the kinetics of the diffusion of the actinides through the An-depleted outer rim of the sample must be taken into account.

(c) The magnesium oxide matrix of the composite fuels and targets reveals a strong decomposition in inert atmosphere or vacuum, producing oxygen gas that affects the thermodynamics of the vaporisation of the actinide phase (increase of oxygen potential). But

more importantly, in this case preferential vaporisation leads to an enrichment in the actinide phase in the sample, and at high temperature eutectic melting eventually occurs.

(d) The matrix of the molybdenum-based fuels and targets has a significantly lower vapour pressure compared to the included oxide phase, and selective vaporisation of the actinides inclusions at the surface occurs initially. In case the dilution is large, depletion of the inclusions at the surface occurs and the further vaporisation of the actinides is hindered by the molybdenum matrix, until the matrix vaporisation becomes significant, allowing the release of the actinides from the included phase.

Overall we conclude from our study that in addition to the thermodynamic equilibrium considerations the dynamic evolution of complex compositions and microstructures must be taken into account to explain the high temperature behaviour of inert matrix forms such as composites.

7.5 References

[1] J.P. Grouiller, S. Pillon, C. de Saint Jean, F. Varaine, L. Leyval, G. Vambenepe, B. Carlier, J. Nucl. Mater. 320 (2003) 163.
[2] IAEA, Viability of inert matrix fuel in reducing plutonium amounts in reactors, IAEA-TECDOC-1516, Austria, Vienna, August 2006.
[3] C. Ronchi, M. Sheindlin, J. Appl. Phys. 7 (2001) 3325.
[4] N. Chauvin, R.J.M. Konings, H. Matzke, J. Nucl. Mater. 274 (1999) 105.
[5] Y. Croixmarie, E. Abonneau, A. Fernández, R.J.M. Konings, F. Desmoulière, L. Donnet, J. Nucl. Mater. 320 (2003) 11.
[6] A. Fernández, R.J.M. Konings, J. Somers, D. Haas, J. Mater. Sci. Lett. 22 (2003) 119.
[7] S. Grandjean, B. Arab-Chapelet, A.C. Robisson, S. Picart, J.P. Dancausse, P. Baron, P. Brossard, D. Warin, GLOBAL 2007: Advanced Nuclear Fuel Cycles and Systems, Boise Idaho, September 2007, pp. 98–105.
[8] R.J.M. Konings, R. Conrad, G. Dassel, B. Pijlgroms, J. Somers, E. Toscano, J. Nucl. Mater. 282 (2000) 159.
[9] C. Hellwig, M. Streit, P. Blair, T. Tverberg, F.C. Klaassen, R.P.C. Schram, F. Vettraino, T. Yamashita, J. Nucl. Mater. 3452 (2006) 291.
[10] N. Kamel, H. Aït-Amar, M. Taouinet, C. Benazzouz, Z. Kamel, H. Fodil-Cherif, S. Telmoune, R. Slimani, A. Zahri, D. Sahel, Prog. Nucl. Energy 48 (2006) 70.
[11] C. Delgueldre, J. Alloy Compd. 444–445 (2007) 36.
[12] D. Staicu, J.-P. Hiernaut, J. Somers, A. Fernandez, C. Nastren, R. Konings, V.V. Rondinella, Trans. Am. Nucl. Soc. 98 (2008) 829.
[13] C. Ronchi, J.P. Ottaviani, C. Degueldre, R. Calabrese, J. Nucl. Mater. 320 (2003) 54.

[14] P. Gotcu-Freis, J.-Y. Colle, J.-P. Hiernaut, F. Naisse, C. Guéneau, R.J.M. Konings, J. Chem. Thermodyn., 43 (2011) 1164.

[15] L. Donnet, F. Jorion, N. Drin, S.L. Hayes, J.R. Kennedy, K. Pasamehmetoglu, S. L. Voit, D. Haas, A. Fernandez, Global 2005: The FUTURIX-FTA Experiment in PHENIX: Status of Fuel Fabrication, Tsukuba, Japan, 2005.

[16] P. Gotcu-Freis, J.-Y. Colle, J.-P. Hiernaut, R.J.M. Konings, J. Nucl. Mater. 409 (2011) 194.

[17] H. Kinoshita, M. Uno, S. Yamanaka, J. Alloy Compd. 354 (2003) 129.

[18] FactSage 5.5©, Developed at the Facility for the Analysis of Chemical Thermodynamics (FACT), Centre for Research in Computational Thermochemistry (CRCT), École Polytechnique de Montréal, Canada, and GTT Technologies, Herzogenrath, Germany, 2007.

[19] J. Malcom W. Chase, J. Phys. Chem. Ref. Data, NIST-JANAF Thermochemical Tables, J. Phys. Chem. Ref Data, Monograph No. 9, 1998.

[20] R.J.M. Konings, O. Benes, D. Manara, D. Sedmidubsky, L. Gorokhov, V.S. Iorish, V. Yungman, The thermodynamic properties of f-elements. Part II. The Lanthanide and Actinide Oxides, J. Phys. Chem. Ref. Data, Submitted for Publication.

[21] S. Miwa, I. Sato, K. Tanaka, T. Hirosawa, M. Osaka, J. Nucl. Mater. 400 (2010) 32.

[22] H. Zhang, R.J.M. Konings, M.E. Huntelaar, E.H.P. Cordfunke, J. Nucl. Mater. 250 (1998) 88.

[23] H. Zhang, M.E. Huntelaar, R.J.M. Konings, E.H.P. Cordfunke, J. Nucl. Mater. 249 (1997) 223.

Chapter 8

Summary, Conclusions and Outlook

Partitioning and transmutation is considered an important option for the waste management in advanced nuclear fuel cycles. Minor Actinide removal from the spent fuel and subsequent fission in fast nuclear systems are promising technologies in order to exploit the waste in a practical and valuable way and, thus, to minimise the radiotoxic inventory as well as the heat production in a geological repository.

It was the goal of this thesis to contribute to the knowledge of the thermophysical properties of advanced fuel materials containing actinides as required for analysing and predicting the behaviour of the fuel in a reactor during normal operation and accidental conditions. The results of this work were achieved by performing high temperature experiments on several actinide oxides samples, with emphasis on the mass spectrometric measurements using the Knudsen cells effusion technique. The experimental work was complemented by thermodynamic evaluations and modelling.

This chapter presents the most important aspects of this thesis.

Experimental investigation and the thermodynamic interpretation

Vapour pressure measurements

The vaporisation behaviour and phase relations of the systems studied in this thesis have been investigated using mass spectrometry. The experimental facility consisted of a Knudsen cell coupled with a quadrupole mass spectrometer, built in glove box shielded by lead bricks in order to study radioactive materials at high temperature.

The high temperature measurements have been performed generally for the binary systems in the temperature range of (2000-2200) K, and higher up to a maximum of 2300 and 2700 K for their solid solutions and inert matrix materials, respectively. The table in the Annex lists the main analysed samples, the conditions involved and the parameters which

correspond to the vapour pressure equation. The temperature recording of the Knudsen cell assembly was calibrated by measurement of the melting points of standard materials. A calibration of the Knudsen cell mass spectrometer assembly was carried out as well by vaporising a known quantity of reference material. The global calibration factor thus obtained contributed to the vapour pressure data.

Ionisation efficiency curves measurements were primarily recorded to have insight into the dissociative ionisation processes and the composition of the gaseous phase that is in equilibrium with the condensed phase under Knudsen conditions. The fragmentation patterns were thus obtained and the partial pressures of the gaseous species involved in the system were derived.

The mass spectrometric measurements have been conducted in vacuum using iridium, tungsten or tantalum cells; the latter material being known to result in reduction processes due to its affinity for oxygen. For the measurements in oxidising conditions, a new Knudsen cell assembly has been designed. Compatibility tests between oxide samples and various cell materials proposed for the oxidative conditions (e.g. Al_2O_3, ZrO_2, MgO or ThO_2) revealed that ThO_2 was the best high temperature material with non-reactive properties for oxides.

Additional physical parameter

Heat capacity is another important physical property for the reactor safety analysis. The high temperature heat capacity was derived based on new experimental data of the enthalpy increments of NpO_2 measured using a drop calorimeter [Chapter 3]. This study extended by more than 650 K the temperature range of the available measurements, which had an upper limit of 1100 K.

Thermodynamic evaluation

The mass spectrometric data have been used to provide the thermodynamic properties of the molecules in the ideal gas reference state. In this approach, the vapour pressure results were combined with known thermodynamic data for the condensed phase in order to describe

the chemical equilibrium. Using the second and third law methods the enthalpy of sublimation for the $NpO_2(g)$ and $PuO_2(g)$ have been derived.

For compositions not far from O/An = 2.00, with An = Pu or Np, the variation of NpO_2 vapour pressure with temperature is independent of the composition of the condensed phase [Chapter 2], whereas in the case of PuO_2 a dependence exists [Chapter 4]. Our results showed that the measurements in oxidative conditions can be interpreted to be close to the $AnO_2(cr) = AnO_2(g)$ equilibrium and do not need to be corrected for the AnO(g) contribution, as suggested by the literature [1,2].

The vaporisation of plutonium and neptunium oxide in vacuum revealed the dioxide as the major species in the vapour followed by the monoxide. No metallic vapour contribution has ever been observed in the temperature range studied. Compared to these actinide dioxides, the vaporisation of americium dioxide at similar temperatures showed a different behaviour [Chapter 5]. These measurements on pure americium oxide are the first partial pressure data reported to date. A substantial change occurred in the composition of the initial americium dioxide for temperatures higher than 2000 K, which is not surprising considering the high oxygen potential of AmO_{2-x}. In the actinide series the oxygen potential data indicate an important decrease of the oxide stability from thorium to americium. The oxygen potential data are the lowest for ThO_{2-x}, followed by UO_{2-x}, NpO_{2-x}, PuO_{2-x} and finally AmO_{2-x} [3]. Therefore the metal-oxygen bond is the weakest in americium dioxide.

According to the CALPHAD model developed for the Pu-Am-O system in Chapter 6, the oxygen content of the sample (initially AmO_2) could have been considerably reduced to reach Am_2O_3 at 2200 K during the time of the measurement in vacuum. Hence a O/M value significantly lower than 2 can be expected. Furthermore, considering the calculated Am-O phase diagram at atmospheric pressure and 2200 K, AmO_2 loses oxygen until reaching a O/Am ratio equal to ~1.8. Under similar experimental conditions, PuO_2 and NpO_2 do not show such a strong reduction, the PuO_2 will tend to reach the congruent vaporisation composition around O/Pu = 1.85 and O/Np = 1.93.

Since there is not a large difference between the total vapour pressures for samples of pure AmO_{2-x} and americium dioxide diluted in PuO_{2-x}, for which we infer different O/M ratios and thus oxygen potentials, it can be

concluded that the total pressure in the Am-O system does not vary strongly in the range 1.60 < O/Am < 1.83. The results for the reduced NpO_2 sample as well as for diluted neptunium oxide in americium dioxide and americium-plutonium mixed oxide assuming Raoult's law suggest that for O/Np ratios well below 1.9 the total pressure increases, similar to the behaviour of PuO_2.

Contribution to the study on candidate inert matrix materials

The mass spectrometric results on binary systems were discussed in relation with the inert matrix fuel forms such as composites [Chapter 7]. Different candidate inert matrix fuels and targets, such as solid solution, CERMET and CERCER composites, have been investigated and showed distinct vaporisation behaviour. Additionally, a plutonium americium mixed oxide sample was studied as was the included phase of several composite samples.

The vaporisation of the zirconia-based solid solutions was initially governed by the thermodynamics of the system. As a result of the large difference in vapour pressure of the actinides compared to zirconia, the kinetics of the actinides diffusion through the actinide-depleted outer rim of the sample must be taken into account subsequently.

The magnesium oxide matrix showed, in inert atmosphere or vacuum, a strong decomposition producing oxygen gas. This behaviour affected the thermodynamics of the vaporisation of the actinide phase. In such case, the preferential vaporisation of the matrix leads to enrichment of the actinide phase in the sample, and at high temperature eutectic melting eventually occurred.

The molybdenum matrix had a significantly lower vapour pressure compared to the included oxide phase. In case of low volume fraction of the actinide phase in the matrix, the vaporisation of the actinides from the inclusions occurred initially at the surface until the depletion at the surface was reached. Further vaporisation of the actinides was hindered by the molybdenum matrix until the matrix vaporisation became significant, allowing the release of the actinides from the included phase.

These candidate nuclear fuels and targets samples were used in the irradiation campaigns in the Phénix fast neutron reactor in France and in the High Flux Reactor in the Netherlands. In addition to the thermodynamic equilibrium considerations, the dynamic evolution of complex compositions and microstructures must be taken into account to explain the high temperature behaviour of inert matrix forms such as composites. This current study is therefore a complement to the ongoing R&D program directed to guaranty the reactor safety operation and fuel cycle facilities.

The need of further thermodynamic assessment

The experimental data presented in this thesis are important and necessary to understand the vaporisation and high temperature behaviour of actinide oxides and their solid solutions. However, it represents only a first contribution to the physico-chemical properties database of actinide oxides. Further measurements on pure curium oxide would be of interest since it is formed as a result of the neutron capture reactions from americium and plutonium. Due to the long half-life of some of its isotopes, curium represents the second highest radiotoxic potential, after americium, in the vitrified nuclear waste. Such vapour pressure measurements have been performed previously in ITU on a mixed curium plutonium oxide (presumably sesquioxide) sample, however, without measuring the ionisation efficiency curves and neglecting the activity in the solid phase. Furthermore, high temperature measurements on mixed oxides, foreseen as fuels for transmutation must be performed in the next future to complete the present work. This is particularly the case for the UO_2 samples with large MA content, i.e. Am, and $(U,Pu)O_2$ samples with small MA content. Currently, a study on the vaporisation of $(U,Pu)O_{2\pm x}$ mixed oxides with different Pu content is under preparation [4].

However, it is not possible to measure every composition especially when it comes to solid solutions. Therefore a practical approach was to develop a model able to predict the phase behaviour not only for binary or ternary but also for higher order systems. This work is part of the international project FUELBASE [5,6] on the modelling of nuclear fuels, dedicated to the description of the thermodynamic properties and phase equilibria of the multi-component system U, Pu, Am, Np, (C, N, Si, Ti, Zr, Mo) O. In the perspective of building the model for the multi-component system, the

data of each constituting binary had to be evaluated with the CALPHAD method. The binary models for the Am-Pu and Am-O were assessed in the frame of this thesis [Chapter 6]. The systems Pu-O and U-O systems were recently reported [5,6] and other binaries, i.e. Np-O, U-Pu, Np-Am, Np-Pu, are under preparation as part of an international collaboration [7]. They all will be combined in a consistent multi-component description of the experimental data with the CALPHAD method. Such an effort to reveal the high temperature behaviour of the ternary U-Pu-O system is ongoing [4,8]. The current model on the ternary Pu-Am-O system, provided in Chapter 6, is the first tool for a comprehensive understanding and prediction of the high temperature behaviour of transmutation fuels and targets.

The present results and the technological aspects

Studies on the behaviour of MOX fuels containing MAs (americium and/or neptunium) under irradiation have been conducted recently in the experimental fast reactor Joyo, in Japan. The redistribution of the actinides observed in the fuel under irradiation was explained by the model of pore migration employing a vaporisation-condensation mechanism [9]. In this context, vapour pressure is a crucial parameter in order to describe the behaviour under irradiation of a promising candidate fuel to transmute the MAs, i.e. MOX fuels with an initial MAs content up to 2 wt%.

The post-irradiation examinations showed no change in the Np concentration. The concentration of Pu and Am was found higher next to the pellet centre compared to the periphery. In their assessment, Maeda *et al.* [9] calculated the partial pressures of the U, Pu and Am bearing species and the vapour compositions from the enthalpies of formation of these oxides in the gaseous states taken from [2,10,11]. The thermodynamic data for these calculations were estimated based on the previous experimental results, i.e. the oxygen potential [11] and vapour pressures for the uranium and plutonium mixed oxides, and plutonium oxide with low americium content [2]. The latter data set was discussed also by us in the Chapters 4 and 5.

The calculations performed by Maeda at temperatures above 2000 K, for hyperstoichiometric $(U,Pu)O_2$ fuel with 2% Am content, indicated UO_3 as the main species in the vapour. Below the congruent composition

(O/M ≈ 1.95), the total pressure is represented by AmO. The partial pressure of UO_3 is considerably lower in this region, the pressures of PuO, UO, Pu and U increase with the decrease of the O/M ratio. The vapour pressure of AmO_2 is significantly lower than that of AmO and does not change much along the composition. The pressure of PuO_2 and UO_2 show the same behaviour.

We have shown [12] that at these high temperatures americium oxide is considerably reduced, revealing the presence of the three gaseous species, not only AmO_2 and AmO but also Am. This is not in agreement with the assessment by Maeda *et al.* [9]. In their work the vapour pressure of Am over $(U_{0.69}Pu_{0.29}Am_{0.02})O_{2-x}$ was negligible. Preliminary calculations, based on extrapolation of our results to the U-Pu-Am-O system, indicated that the Am pressure is significant in that system and must be taken into account. Therefore, the input data for the thermochemical calculation of the vapour composition for the pore migration model [9] needs revision.

References

[1] R.J. Ackermann, R.L. Faircloth, E.G. Rauh, R.J. Thorn, J. Inorg. Nucl. Chem. 28 (1966) 111.

[2] R.J. Ackermann, R.L. Faircloth, M.H. Rand, J. Phys. Chem. 70 (1966) 3698.

[3] C. Guéneau, A. Chartier, Chemistry of the Actinide and Transactinide Elements, Chapter 9, L.R. Morss, N.M. Edelstein, J. Fuger (Eds), Springer, The Netherlands, 2011.

[4] P.Gotcu-Freis, J.-Y. Colle, J.-P. Hiernaut, O. Benes, C. Guéneau, J. Somers, R.J.M. Konings, Mass spectrometric investigation of the vaporisation behaviour in $(U,Pu)O_{2\pm x}$ samples, To be submitted to the J. Nucl. Mater..

[5] C. Guéneau, M. Baichi, D. Labroche, C. Chatillon, B. Sundman, J. Nucl. Mater. 304 (2002) 161.

[6] C. Guéneau, C. Chatillon, B. Sundman, J. Nucl. Mater. 378 (2008) 257.

[7] F-BRIDGE public information: http://www.f-bridge.eu/.

[8] C. Guéneau, N. Dupin, C. Martial, J.C. Dumas, S. Gossé, S. Chatain, B. Sundman, To be submitted to the J. Nucl. Mater.

[9] K. Maeda, S. Sasaki, M. Kato, Y. Kihara, J. Nucl. Mater. 389 (2009) 78.

[10] H. Bailly, D. Menessier, C. Prunier (Eds.), The nuclear fuels of pressurized water reactors and fast reactors design and behaviour, Paris, France: Lavoisier Publishing Intercept Ltd., 1999, p.106.

[11] M.H. Rand, T.L. Markin, in: Thermodynamics of Nuclear Materials 1967, Proceedings of the IAEA Symposium, Vienna, 1968, p. 637.

[12] P. Gotcu-Freis, J.-Y. Colle, J.-P. Hiernaut, R.J.M. Konings, J. Nucl. Mater. 409 (2011) 194.

Samenvatting, Conclusies en Perspectieven

Scheiding en Transmutatie is een belangrijke optie voor behandeling van het afval van geavanceerde splijtstofketens. De afscheiding van de zogenaamde mineure actiniden (Np, Am, Cm) uit de opgebrande splijtstof en de splijting in snelle reactor systemen, zijn hoopgevende technologieën met het oog op het waardevol hergebruik van afval, en het minimaliseren van zowel de radiotoxische inhoud als de warmteproduktie in een geologische eindberging.

Het doel van dit proefschrift is het leveren van een bijdrage aan de kennis over de thermofysische eigenschappen van geavanceerde splijtstoffen die mineure actiniden (MAs) bevatten, noodzakelijk voor de analyse en voorspelling van het gedrag van splijtstof tijdens normaal gebruik en tijdens ongevalsituaties. De resultaten van dit werk werden verkregen door middel van hoge temperatuur experimenten met diverse oxiden van actiniden, met de nadruk op Knudsen-cel massaspectrometrie. Dit werk werd gecombineerd met thermodynamische evaluaties en modellering.

In dit hoofdstuk worden de belangrijkste aspecten van dit werk samengevat.

Experimentele studies en thermodynamische interpretatie

Dampspanningsmetingen

Het verdampingsgedrag en de fasenrelaties van de systemen die in het kader van dit proefschift zijn bestudeerd, werden geanalyseerd met behulp van massaspectrometrie. De apparatuur bestaat uit een Knudsen cel gecombineerd met een massaspectrometer, die in een met lood afgeschermde handschoenkast is opgesteld, daardoor geschikt voor de studie van radioactieve materialen bij hoge temperatuur.

De hoge temperatuur metingen zijn voornamelijk uitgevoerd voor binaire systemen in het temperatuurbereik (2000-2200) K, en hoger tot 2300 K en 2700 K voor vaste oplossingen en inerte matrix materialen. Een lijst met de onderzochte monsters, de experimentele condities en resultaten van de

dampspanningsmetingen zijn in de Appendix weergegeven. Voor de kalibrering van de temperatuurmeting van de Knudsen cel werden de smeltpunten van standaardmaterialen gemeten. De kalibratiefactor van de combinatie van Knudsen cel en massaspectrometer werd door middel van de verdamping van een bekende hoeveelheid referentiemateriaal verkregen.

Om inzicht te krijgen in de dissociatie reacties die tijdens ionisatie plaatsvinden en dus de werkelijke samenstelling van de gas fase die in evenwicht is met de vaste fase in de Knudsen cel, werd de ionisatie efficiëntie gemeten. Met behulp hiervan werden de fragmentatierelaties verkregen, en hiermee werden vervolgens de partiële dampdrukken van de gasvormige moleculen berekend.

De dampspanningsmetingen werden uitgevoerd in vacuüm, waarbij gebruik gemaakt werd van cellen van Iridium, Wolfraam en Tantaal. Dit laatste materiaal heeft een sterke affiniteit voor zuurstof en kan zodanig resulteren in reductie van de gasfase. Voor metingen in oxiderende omgeving werd een nieuwe Knudsen cel ontwikkeld. Door middel van experimenten met actinidenoxiden en verschillende celmaterialen (Al_2O_3, MgO, ZrO_2 en ThO_2) kon worden aangetoond dat ThO_2 het minst reactief is bij de temperaturen van de experimenten.

Aanvullende fysische eigenschap

De soortelijke warmte is een belangrijke materiaaleigenschap die bij reactor-veiligheidsanalyses van belang is. De soortelijke warmte van NpO_2 werd verkregen door middel van enthalpie-increment metingen met behulp van een valcalorimeter [Hoofdstuk 3]. Door deze resultaten werd het temperatuurbereik waarvoor experimentele metingen beschikbaar zijn (tot 1100 K) met 650 K verbreed.

Thermodynamische evaluatie

Met behulp van de massaspectrometrische metingen zijn de thermodynamische eigenschappen van de moleculen verkregen voor de "ideale gas" toestand. Hiertoe werden de resultaten voor de dampspanning gecombineerd met de thermodynamische gegevens voor de

vaste stof voor de betreffende evenwichtsreacties. Op basis van tweede en derde hoofdwet analyses werd de sublimatie-enthalpie van zowel NpO_2 als PuO_2 verkregen.

Voor samenstellingen nabij O/An = 2 (An = Np,Pu) is de dampspanning van NpO_2 onafhankelijk van de samenstelling van de vaste stof, terwijl er in het geval van PuO_2 wel een afhankelijkheid bestaat. De resultaten toonden aan dat de metingen in oxiderende omgeving zeer nauw met het evenwicht $AnO_2(cr) = AnO_2(s)$ overeenstemmen, en dat een correctie voor de bijdrage van AnO(g), zoals in de literatuur is gesuggereerd [1,2], dus overbodig is.

De verdamping van neptunium- en plutoniumoxide in vacuüm toonde aan dat het dioxide het voornaamste molecuul in de gasfase is, gevolgd door het monoxide. Geen bijdrage van de elementen is waargenomen in het bestudeerde temperatuurbereik. In vergelijking met deze twee actinidenoxiden, toonde americiumdioxide een ander gedrag [Hoofdstuk 5]. De metingen aan americiumoxide zijn de eerste die ooit zijn gerapporteerd. Een aanzienlijke verandering vond plaats in de samenstelling van het americiumdioxide startmeteriaal bij temperaturen hoger dan 2000 K, wat niet verbazingwekkend is gezien de hoge zuurstofspanning van AmO_{2-x}. De zuurstofpotentiaal gegevens voor de actinidenoxiden laten een beduidende afname van de stabiliteit gaande van thorium naar americium zien. De zuurstofpotentiaal is het laagste voor ThO_2, gevolgd door UO_{2-x}, NpO_{2-x}, PuO_{2-x} en uiteindelijk AmO_{2-x} [3]. Daarom is de metaal-zuurstof binding het zwakst in americiumdioxide.

Volgens het CALPHAD model dat voor het Pu-Am-O systeem werd ontwikkeld [Hoofdstuk 6] heeft de zuurstofinhoud van het onderzochte monster (aanvankelijk AmO_2) gedurende de meting in vacuüm een verandering/reductie ondergaan naar Am_2O_3 bij 2200 K. Verder toont het berekende Am-O fasendiagram bij atmosferische druk en 2200 K dat AmO_2 zuurstof verliest en een samenstelling met O/Am $\approx$ 1.8 bereikt. Voor experimentele vergelijkbare omstandigheden, zullen PuO_2 en NpO_2 niet zulke sterke reductie ondergaan; ze zullen de congruente verdampingssamenstelling bereiken met O/Pu = 1.85 en O/Np = 1.93, respectievelijk.

Aangezien er geen groot verschil bestaat tussen de totale dampspanning van puur AmO_{2-x} en americiumdioxide verdund in PuO_{2-x}, waarvoor we een andere O/Metaal verhouding en dus zuurstofpotentiaal kunnen

veronderstellen, kan worden geconcludeerd dat de totale dampspanning in te Am-O systeem niet sterk varieert in het bereik 1.60 < O/Am < 1.83. De resultaten voor het gereduceerde NpO_2 monster en ook voor neptuniumdioxide verdund in americium oxide and americium-plutonium mengoxide, waarvoor Rauolt's wet werd toegepast, tonen aan dat voor een O/Np verhouding lager dan 1.9 de totale dampspanning toeneemt, vergelijkbaar met het gedrag van PuO_2.

Een bijdrage aan de studie van potentiële inert matrix materialen

De massaspectrometrie resultaten voor binaire systemen werden besproken met betrekking tot inerte matrix splijtstoffen zoals composieten [Hoofdstuk 7]. Verschillende potentiële inerte matrix materialen, zoals vaste stof oplossingen, CERMET en CERCER composieten, werden bestudeerd en vertoonden duidelijk verschillend verdampingsgedrag. Bovendien werd een plutonium-americium mengoxide monster bestudeerd aangezien het de ingesloten fase is in de diverse composieten.

De verdamping van de op zirconiumoxide gebaseerde vaste-stof oplossingen werd aanvankelijk door de thermodynamica van het systeem bepaald. Als gevolg van het grote verschil in damspanning tussen de actinidenoxiden en zirconiumoxide, moet vervolgens ook de kinetische aspecten van de diffusie van de actiniden door de actiniden-verarmde rand van het monster in betracht worden genomen.

De magnesiumoxide matrix vertoonde een sterke decompositie in vacuüm en inerte atmosfeer, waarbij zuurstof gas werd gevormd. Dit proces had een invloed op de thermodynamische evenwichten die de verdamping bepalen. In dit geval, resulteerde de selectieve verdamping van de matrix in een verrijking van de actinidenfase in de monsters, en vond eventueel eutectische smelten plaats bij hoge temperaturen.

De molybdeen matrix had een beduidend lagere dampspanning in vergelijk met de oxide fase. In het geval van een lage volume concentratie van de actinidenfase in de matrix, vond verdamping van de actinidenfase aanvankelijk plaats van de insluitsels aan het oppervlak, totdat een verarming van de actiniden in deze insluitsels optrad. Daarna werd de verdere verdamping van de actinidenfase verhinderd door de molybdeen matrix, totdat de verdamping van de matrix zelf aanzienlijk werd, waardoor

het vrijkomen van de actiniden uit de insluitsels weer mogelijk werd gemaakt.

Deze potentiële inerte matrix materialen zijn benut voor bestralingsexperimenten in de Phénix snelle reactor in Frankrijk en de Hoge Flux Reactor in Nederland. Om het hoge-temperatuurgedrag tijdens bestraling te voorspellen, moet niet alleen thermodynamische overwegingen meegenomen worden maar ook de dynamische evolutie van de samenstelling en de microstructuur. Deze studie is dus een complementaire bijdrage aan de lopende R&D activiteiten die gericht zijn op het garanderen van de veiligheid van reactor bedrijf en de faciliteiten voor de splijstofketen.

De noodzaak van verdere thermodynamische evaluaties

De experimentele gegevens die in dit proefschrift werden gepresenteerd zijn van belang en noodzakelijk om het hoge-temperatuurgedrag en in het bijzonder de verdamping van actinidenoxiden en hun vaste oplossingen te begrijpen. Het betreft echter een eerste bijdrage aan de fysisch-chemische gegevens van de actinidenoxiden. Aanvullende metingen aan zuiver curiumoxide zouden van belang zijn, omdat dit element gevormd wordt als gevolg van neutronvangst in americium en plutonium. Door de lange halfwaardetijd van sommige van de isotopen draagt curium, na americium, het meest bij aan de radiotoxische inhoud van radioactief glas. Dergelijke dampspanningsmetingen zijn in het verleden in ITU uitgevoerd aan een monster van curium-plutoniumoxide, echter zonder metingen van de ionisatie efficiëntie en onder verwaarlozing van de activiteit in de vaste oplossing. Bovendien zijn metingen noodzakelijk aan mengoxiden die als splijtstof voor transmutatiereactoren voorzien zijn. Dit geldt het bijzonder voor UO_2 monsters met hoge concentraties van de mineure actiniden (Am) en $(U,Pu)O_2$ monsters met lage concentraties van de MAs. Momenteel is een studie van de verdamping van $(U,Pu)O_{2-x}$ met verschillende Pu concentraties in voorbereiding [4].

Het is echter niet mogelijk iedere samenstelling te meten, in het bijzonder voor vaste oplossingen. Daarom is het praktisch om een model te ontwikkelen dat het fasengedrag van voorspellen, niet allen voor binaire en ternaire systemen maar ook voor hogere orde systemen. Deze activiteiten

zijn onderdeel van het internationale FUELBASE project [5,6] dat is gericht op de modellering nucleaire brandstoffen, in het bijzonder van thermodynamische eigenschappen en fasenrelaties van het systeem U, Pu, Am, Np, (C, N, Si, Ti, Zr, Mo) O. Met het oog op de compilatie van een model voor dit multicomponent systeem worden de gegevens van ieder binair systeem met de CALPHAD methode geëvalueerd. De modellen Am-Pu en Am-O zijn geëvalueerd in het kader van dit proefschrift [Hoofdstuk 6]. De systemen U-O en Pu-O werden onlangs gepubliceerd [5,6] en aanvullende binaire systemen, i.e. Np-O, U-Pu, Np-Am, Np-Pu, zijn in voorbereiding als onderdeel van de internationale samenwerking [7]. Deze systemen zullen samen worden gecombineerd in een consistente multicomponent beschrijving van de experimentele gegevens met de CALPHAD methode. Een dergelijke beschrijving van het hoge temperatuurgedrag van het ternaire U-Pu-U-O systeem is in voorbereiding [4,8]. Het model voor het ternaire Pu-Am-O systeem, beschreven in Hoofdstuk 6, is een eerste hulpmiddel voor een omvattend begrip en voorspelling van het gedrag van splijtstoffen voor transmutatie van mineure actiniden.

De verkregen resultaten resultaten en de technologische toepassingen

Studies over het bestralingsgedrag van MOX splijtstof die mineure actiniden bevat (Americium, en/of Neptunium) zijn onlangs uitgevoerd in de experimentele snelle reactor Joyo in Japan. De waargenomen herverdeling van de actiniden in de bestraalde splijtstof kon worden verklaard met een poriën-migratie model gebaseerd op een verdamping/condensatie mechanisme [9]. De dampspanning is een cruciale parameter voor dit model om het gedrag tijdens bestraling van een potentiële splijtstof voor de transmutatie van mineure actiniden te beschrijven, i.e. mengoxide splijtstof met tot 2 wt% mineure actiniden.

Nabestralingsonderzoek leverde geen indicatie op voor de herdistributie van neptunium. De gemeten concentraties van Am en Pu waren hoger in het centrum van het splijtstoftablet in vergelijking met de rand. Ten behoeve van hun evaluatie hebben Maeda *et al.* [9] de dampspanningen van de U, Pu en Am moleculen in de dampfase berekend op basis van gegevens voor de vormingsenthalpie van deze gasvormige oxiden uit [2,10,11]. De thermodynamische gegevens voor deze berekeningen

werden geschat op basis van bestaande experimentele gegevens, i.e. zuurstofpotentiaal [11] en dampspanning voor uranium en plutonium mengoxide [2] en plutoniumoxide met lage americium concentraties [2]. De laatstgenoemde studie werd in Hoofdstukken 4 en 5 besproken.

De berekeningen van Meada et al. voor temperaturen boven 2000 K voor hyperstoichiometrisch $(U,Pu)O_2$ met 2% Am, leverden UO_3 als voornaamste molecuul in de dampfase. Wanneer de vaste fase de congruente verdampingssamenstelling bereikt (O/M≈1.95), wordt de totale dampspanning door AmO bepaald. De partiële druk van UO_3 is beduidend lager in dit bereik, de drukken van PuO, UO, Pu en U nemen to met de afname van de O/M verhouding. The dampspanning van AmO_2 is beduidend lager dan die van AmO en veranderd niet sterk als functie van de samenstelling. De drukken van PuO_2 en UO_2 verhouden zich vergelijkbaar.

In dit werk hebben wij aangetoond dat bij deze temperaturen americium oxide aanzienlijk gereduceerd wordt, waarbij niet alleen AmO_2 en AmO maar ook Am werd waargenomen. Dit is niet in overeenstemming met de evaluatie van Maeda *et al.* [9]. In die studie was de dampspanning van Am over $(U_{0.69}Pu_{0.29}Am_{0.02})O_{2-x}$ verwaarloosbaar. Voorlopige berekeningen gebaseerd op extrapolatie van onze resultaten naar het U-Pu-Am-O system tonen aan dat de Am dampspanning in data systeem aanzienlijk is en in betracht moet worden genomen. Daarom moeten de invoergegevens voor de thermochemische berekening van de dampsamenstelling voor poriën-migratie model worden herzien.

Referenties

[1] R.J. Ackermann, R.L. Faircloth, E.G. Rauh, R.J. Thorn, J. Inorg. Nucl. Chem. 28 (1966) 111.

[2] R.J. Ackermann, R.L. Faircloth, M.H. Rand, J. Phys. Chem. 70 (1966) 3698.

[3] C. Guéneau, A. Chartier, Chemistry of the Actinide and Transactinide Elements, Chapter 9, L.R. Morss, N.M. Edelstein, J. Fuger (Eds), Springer, The Netherlands, 2011.

[4] P.Gotcu-Freis, J.-Y. Colle, J.-P. Hiernaut, O. Benes, C. Guéneau, J. Somers, R.J.M. Konings, Mass spectrometric investigation of the vaporisation behaviour in $(U,Pu)O_{2\pm x}$ samples, To be submitted to the J. Nucl. Mater..

[5] C. Guéneau, M. Baichi, D. Labroche, C. Chatillon, B. Sundman, J. Nucl. Mater. 304 (2002) 161.

[6] C. Guéneau, C. Chatillon, B. Sundman, J. Nucl. Mater. 378 (2008) 257.

[7] F-BRIDGE public information: http://www.f-bridge.eu/.
[8] C. Guéneau, N. Dupin, C. Martial, J.C. Dumas, S. Gossé, S. Chatain, B. Sundman, To be submitted to the J. Nucl. Mater.
[9] K. Maeda, S. Sasaki, M. Kato, Y. Kihara, J. Nucl. Mater. 389 (2009) 78.
[10] H. Bailly, D. Menessier, C. Prunier (Eds.), The nuclear fuels of pressurized water reactors and fast reactors design and behaviour, Paris, France: Lavoisier Publishing Intercept Ltd., 1999, p.106.
[11] M.H. Rand, T.L. Markin, in: Thermodynamics of Nuclear Materials 1967, Proceedings of the IAEA Symposium, Vienna, 1968, p. 637.
[12] P. Gotcu-Freis, J.-Y. Colle, J.-P. Hiernaut, R.J.M. Konings, J. Nucl. Mater. 409 (2011) 194.

Annexed table. Overview to the samples studied in the chapters of this thesis, using the Knudsen cell mass spectrometry, the conditions applied and the parameters which correspond to the equation:

$$\ln (P/\mathrm{Pa}) = A - B \cdot (T/\mathrm{K})^{-1},$$

characteristic to each vaporisation process.

Sample	Conditions	A	B
NpO_{2-x}	(2000-2300) K W cell, vacuum	26.05 ± 0.06	60534 ± 139
NpO_{2-x}	(2000-2300) K W/Ir cell, vacuum	26.08 ± 0.14	60704 ± 307
NpO_{2-x}	(2000-2500) K W cell, vacuum	33.05 ± 0.20	73971±318
NpO_{2-x} *in* AmO_{2-x}	(2000-2400) K W cell, vacuum	30.13 ± 0.35	69664 ± 431
NpO_{2-x} *in* $(Pu_{0.76}Am_{0.24})O_{2-x}$	(2000-2400) K W cell, vacuum	29.65 ± 0.51	66718 ± 118
NpO_{2-x} *in* $(Pu_{0.80}Am_{0.20})O_{2-x}$	(2000-2400) K W cell, vacuum	30.16 ± 0.27	67681 ± 521
PuO_{2-x}	(2000-2230) K W cell, vacuum	27.76 ± 0.65	64440 ± 332
PuO_{2-x}	(2000-2230) K Ir cell, vacuum	27.61 ± 0.60	64264 ± 380
PuO_{2-x} $(Pu_2O_3 - PuO_{2-x})$	(2000-2250) K Ta cell, vacuum	30.98 ± 0.17	66138 ± 370
PuO_{2-x}	(2000-2230) K ThO_2 cell, O_2	30.48 ± 0.09	67985 ± 195
PuO_{2-x} *in* $(Pu_{0.756}Am_{0.244})O_{2-x}$	(2000 to 2300) K W/Ir cells	26.30 ± 0.50	62453 ± 1023
AmO_{2-x}	(2000-2200) K W cell, vacuum	27.56 ± 0.14	66011 ± 310
AmO_{2-x}	(2000-2200) K Ir cell, vacuum	29.15 ± 0.74	69655 ± 634

AmO_{2-x} *in* $Pu_{0.939}Am_{0.061}O_{2-x}$	(2270 to 2400) K W/Ir cell, vacuum	30.93 ± 0.25	72737 ± 820
AmO_{2-x} *in* $(Pu_{0.756}Am_{0.244})O_{2-x}$	(2000 to 2300) K W/Ir cells	29.01 ± 0.40	70052 ± 857

Acknowledgements

This thesis presents the results on the high temperature thermodynamics of transuranium oxides and their solid solutions; the experimental work was carried out at the Institute for Transuranium Elements (ITU) of the European Commission's Joint Research Centre in Karlsruhe, Germany, in the Materials Research (MR) group under the supervision of Dr. Rudy Konings. My first contact with the group was in 2005 during the traineeship in the frame of the Master studies. Thereafter, positively impressed of the scientific environment, experimental facilities and the warm multicultural community I decided to continue with a PhD work. In the frame of the program "Training and Mobility of Researchers" I would like to acknowledge the European Commission (and the European citizens) for support given along the three-year fellowship. Part of this research has been performed within the F-BRIDGE project, financed by the 7th Framework Program of the European Commission (Grant agreement No. 211690).

I would like to express my gratitude to Rudy for giving me the opportunity to work in the MR unit, the continuous assistance and the constructive critics. I am grateful for the support and advices received and for the time spent together in ITU as well. My thanks go also to my first supervisor, Dr. Jean-Pol Hiernaut, for his advices in approaches of data interpretations. They opened the path towards high scientific quality of the experimental results in this thesis.

The PhD project was performed in collaboration with Delft University of Technology (TU Delft). My special thanks go to Professor Bert Wolterbeek, my promoter, for the valuable discussions, suggestions and help in improving the quality and consistency of this thesis and the accompanied propositions.

During my thesis, a lot of people gave me support for the theoretical background, in performing experiments and handling the highly radioactive samples, and reviewing the publications and this thesis. Big thanks to Jean-Yves Colle for valuable assistance in performing the measurements and discussions regarding the experimental setup and processing the measured

data. Thank you Jean-Yves also for the friendship on the time I have spent in ITU. I wish to thank Thierry Wiss for the scientific discussions and the pleasant lunches. Many thanks to Joe Somers for the constructive discussions we had and comments on the publications; Ondrej Benes for the help in performing the drop calorimetric measurements and analysis of the measured data.

I am deeply indebted to Christine Guéneau for introducing and assistance on Thermo-Calc, advices and much more. Thank you, Christine, I will always remember with pleasure the time I spent in Saclay during my internship. I am also grateful to the group who hosted me at CEA Saclay: DEN/DANS/DPC/SCP/LM2T (Sylvie, Stephane, Jean-Louis, Philipe, Martine, Alain, …) who made my stay there very pleasant.

A warm thank you to Nathalie Dupin and Bo Sundman for discussions, contribution and help given on modelling with Thermo-Calc.

Many thanks to Dr. Christian Chatillon and Dr. Ioana Nuta of CNRS Grenoble, France for the useful discussions we had together regarding the experimental facilities and the results of the measured data.

I am thankful to Franco Capone for the inspiring discussions which supported the vaporisation studies and the Knudsen cell mass spectrometric measurements; to Vincenzo Rondinella, David Bottomley for the good conversations during coffee breaks.

A warm thank you to the secretaries of the two departments, Petra Strube (MR, ITU) and Yvonne Weijgertse-Janssen (RIH, TU Delft) for the help and assistance concerning all the administrative issues.

Many samples used in this work were fabricated and provided from different groups and units within the ITU, where pre-/post- measurement characterisation was performed. Therefore I thank Joe Somers for providing the plutonium and mixed oxide samples, Patrick Lajarge and Stephane Gardeur for performing the heat treatment analysis. I wish to thank Rachel Eloirdi, Jean-Christophe Griveau and Jean Rebizant for providing the plutonium metal, neptunium dioxide and AmO_2 powder, respectively; the microscopy group (and Mr. Thiele) for the SEM analysis, Giorgio Pagliosa and Daniel Bouexiere for performing the XRD measurements, Rachel Eloirdi and Philippe Raison for the help in analysis and interpreting the XRD results; Markus Ernstberger for the TGA post

mass spectrometric measurement; Jozsef Zsigrai and the Analytical Services group for the alpha-, gamma- analysis.

I wish to thank a lot to Frederic Naisse and the people from the ITU Werkstatt for the work done (cells, crucibles, shields).

I am grateful to Karin Popa, who put me in contact for the first time with the ITU environment. Thank you Karin for encouraging applying at the ITU Summer School 2005.

I always appreciated the PhD Progress meetings held within the MR unit and the fruitful discussions afterwards. I therefore thank to all the people who took part, Thierry, Paul, Dario, Dragoş, Philippe, Dinos, Arndt, … , and all the MR unit members.

I had a great time taking part in the Copas meetings; thank you Jacques for giving me this opportunity.

Also many thanks to all the people that have made part of my daily life at ITU: Ernesto Fontana (I always enjoyed the fruitful discussions we had together), Franck de Bruycker (my office mate for ~three years), Mike, Zsolt, Zeynep, Emilio, Phil, Ilaria, Ra, Steffi (and the Research Fellows group), Markus, Teya, Anna-Isabel, Nicole, Răzvan, Ştefan, Mark, Bradu, Dimitri, Rachid, John, Wim, Ramil, Gégé, and many, many others.

Finally, but most importantly, my very special thanks go to my family. To my parents and my sister for their unconditioned love and support, even when miles apart. A warm thank you to my husband Daniel, for all his support, care and attention.

Curriculum Vitae

Petronela Gotcu was born on the 12th of March, 1982 in Iaşi, Romania. After attending the secondary school, Colegiul Național "Emil Racoviță" Iaşi, she took up the study of general chemistry at the "Alexandru Ioan Cuza" University of Iaşi, Faculty of Chemistry in 2001. In 2005 she received her BSc and thereafter she continued with two years Master studies at the same university. In the frame of her Master studies she had an in-service training at the Institute for Transuranium Elements of the European Commission's Joint Research Centre in Karlsruhe, Germany and at the French Atomic and Alternative Energies Commission (CEA) - Saclay, France, during which she was involved in experimental work and modelling dedicated to the advanced nuclear fuels. In 2007 she started the PhD work at the Institute for Transuranium Elements. This was performed in collaboration with Delft University of Technology, The Netherlands, where the defence of this thesis takes place. The PhD study comprised the high temperature thermodynamics of the transuranium oxides and their solid solutions, knowledge important for the development of the advanced fuels for the next generation nuclear reactors. The experimental work was focussed on high temperature vaporisation studies carried out on oxides of plutonium and minor actinides like neptunium and americium, which will be used for predicting the possible behaviour of the (fast) reactor fuel under normal operation and accidental conditions.